Landslide Susceptibility Mapping using GIS-based Frequency Ratio, Shannon Entropy, Information Value and Weight-of-Evidence approaches in part of Kullu district, Himachal Pradesh, India

A DISSERTATION

SUBMITTED IN PARTIAL FULFILLMENT OF THE
REQUIREMENT FOR THE AWARD OF THE DEGREE OF

MASTER OF TECHNOLOGY

IN

GEOTECHNICAL ENGINEERING

Submitted by:

SUJEEWON BABOO CHOORESHWARSINGH

(2K19/GTE/23)

Under the Supervision of

PROF. RAJU SARKAR

DEPARTMENT OF CIVIL ENGINEERING

DELHI TECHNOLOGICAL UNIVERSITY

(Formerly Delhi College of Engineering)

Bawana Road, Delhi-110042

JUNE 2021

DEPARTMENT OF CIVIL ENGINEERING

DELHI TECHNOLOGICAL UNIVERSITY

(Formerly Delhi College of Engineering)

Bawana Road, Delhi-110042

CANDIDATE'S DECLARATION

I, SUJEEWON Baboo Chooreshwarsingh, Roll No – 2K19/GTE/23, student of M.Tech. (Geotechnical Engineering), hereby declare that the project Dissertation titled "Landslide susceptibility mapping using GIS-based Frequency Ratio (FR), Shannon Entropy, Information Value (IV) and Weight-of-Evidence (WofE) approaches in part of Kullu district, Himachal Pradesh, India" which is submitted by me to the Department of Civil Engineering, Delhi Technological University, Delhi in partial fulfillment of the requirement for the award of the degree of Master of Technology, is original and not copied from any source without proper citation. This work has not previously formed the basis for the award of any Degree, Diploma Associateship, Fellowship or other similar title or recognition.

Place: Delhi **SUJEEWON BABOO CHOORESHWARSINGH**

Date: 25.06.2021

DEPARTMENT OF CIVIL ENGINEERING

DELHI TECHNOLOGICAL UNIVERSITY

(Formerly Delhi College of Engineering)

Bawana Road, Delhi-110042

CERTIFICATE

I hereby certify that the Project Dissertation titled "Landslide susceptibility mapping using GIS-based Frequency Ratio, Shannon Entropy, Information Value and Weight-of-Evidence approaches in part of Kullu district, Himachal Pradesh, India" which is submitted by Sujeewon Baboo Chooreshwarsingh; Roll No – 2K19/GTE/23; Department of Civil Engineering, Delhi Technological University, Delhi in partial fulfillment of the requirement for the award of the degree of Bachelor of Technology, is a record of the project work carried out by the student under my supervision. To the best of my knowledge, this work has not been submitted in part or full for any Degree or Diploma to this University or elsewhere.

Raju Sarkar

Place: Delhi

Date: 25.06.2021

PROF. RAJU SARKAR

SUPERVISOR

ABSTRACT

Landslides are serious geological hazards that cause significant damage and casualties in India, creating a high need to identify landslide-prone areas and their associated causative factors, for efficient risk reduction strategies by authorities. This study aims at evaluating the effectiveness of four GIS-based statistical approaches namely, Frequency ratio (FR), Shannon Entropy (SE), Information Value (IV) and Weight-of-Evidence (WofE) for the landslide susceptibility mapping of a region in Kullu district, situated in the state of Himachal Pradesh, where a high surge in tourism and development since the past decade has been witnessed. The causative factors considered as input in this study are slope, aspect, curvature, lithology, distance to roads, distance to faults/lineaments, distance to drainage, land use/land cover and elevation. Since the existing landslide inventory maps from Geological Survey of India and past literatures do not cover the whole study area, an updated inventory has been prepared from visual interpretation of Google Earth Images (2001-2019) and use of a Scarp Identification and Contour Connection method (SICCM) ArcGIS toolbox. The compiled landslide inventory data was randomly divided into training (70%) and validation (30%) datasets. The correlation between past landslide locations and each landslide-influencing parameter has been carefully evaluated using the statistical models. Four landslide susceptibility maps resulted from this research work which were then validated and compared using the three different metrics namely, Landslide Density Index (LDI), Relative Landslide Density Index (R_{index}) and Area Under Curve (AUC) of Receiver Operator Characteristics (ROC) to find out the most suitable methods for susceptibility mapping in this geographical extent. FR and SE depicted highest fitness and predictive ability respectively. The resultant maps can be useful for future land use planning and disaster mitigation measures.

ACKNOWLEDGEMENTS

This research work is the final output of my two years master's degree in Geotechnical Engineering at the Delhi Technological University (DTU), New Delhi, India. I would therefore like to express my very great appreciation to the staff of Delhi Technological University (DTU) for their steadfast academic and administrative support, without which this work would not have been successful.

I would like to express my gratitude towards the Indian Council for Cultural Relations (ICCR), Delhi, India for the second opportunity given at studying in India and for financial support provided throughout the course duration under the Africa Scholarship Scheme (2019-2021). I am sincerely grateful to my thesis supervisor, Prof. Raju Sarkar for his invaluable guidance and constructive scholarly advice during the planning and implementation of my project work and in the publishing of my conference paper.

I extend my appreciation to my family members for their incessant encouragement and support to complete this course abroad during the Covid-19 pandemic situation. I am also very much thankful to the wonderful moments and experiences shared with all the friends that I met throughout this study programme. These acknowledgements would be incomplete without mentioning my heartfelt appreciation to Janice for her love, support and understanding. This gratitude extends to two more friends, Prithivee and Adriano for making the good times even better and the hard times a whole lot smoother.

SUJEEWON BABOO CHOORESHWARSINGH

TABLE OF CONTENTS

LIST OF TABLES

LIST OF FIGURES

CHAPTER 1
INTRODUCTION

1.1 Background and motivation of research

Landslides are among the most-devastating natural disasters causing immense damage to life and property. The complex nature of landslide has made it a challenging subject of study involving different fields to work collaboratively for more efficient and holistic solutions formulation.

India has witnessed a long history of disastrous events, most particularly landslides in the Himalayan and Ghats mountainous regions. The Himalayan orogeny is comparatively younger characterized by unstable geology and presence of major faults. Anthropogenic factors along with other triggering factors such as flash-floods, heavy rainfall, earthquakes among others, further aggravated the situation since the last decade.

Himachal Pradesh, one of the 22 states vulnerable to landslide hazard in India, has been receiving an increasing number of tourists every year leading to an increase in developmental activities such as guest house construction, road widening/construction, hydro-power generation. These development works have definitely been a way of socio-economic upliftment for rural mountain areas, but at the risk of further increasing the vulnerability of slopes in the form of un-scientific dumping of materials along drainage channels, un-engineered road cuts, etc. Despite the immense efforts by stakeholders in mapping landslides in the area, the influencing factors for slope failures in some areas have not well been evaluated nor have many susceptibility studies been conducted at this scale using four probabilistic approaches along the Parvati valley, situated in the district of Kullu.

Risk assessment and mitigation of these disasters is possible only after a complete understanding of the causative factors, the methods employed and their relative accuracy as well as a detailed updated database of past landslide incidents for the study area. As a result, a comparative study on different approaches to landslide susceptibility mapping has been chosen for a better grasp on the present landslide scenario in this area.

1.2 Aims of research work

This study aims at classifying a study area into different landslide susceptibility classes using four statistical methods and at analysing the direct relationships between the different selected landslide causative factors to landslide occurrences in a GIS environment. The goal of this investigation is to reveal the applicability of the different probabilistic methods in the mountainous region of Kullu.

This work also sets sights on further fuelling the drive for more sustainable and ecologically sound development in the area by creating awareness of the contrasting effects of un-planned development on the vulnerability of slopes.

1.3 Objectives

The main research objectives formulated for this research work has been outlined as:

- To have a more detailed insight on the study area, the surrounding landslide-prone areas, the causative factors considered by other authors and the different landslide susceptibility evaluation methods employed in India and other countries through peer-reviewed journals, conference papers and reports.
- To generate an inventory for past landslides in the area from available sources and creation of a new incidence map to cater for landslides previously un-mapped or un-reported.
- To create thematic maps for each landslide causative factor considered in this research using Geographic Information Systems (GIS) platform.
- Usage of four bi-variate statistical approaches; Frequency Ratio (FR), Shannon Entropy (SE), Information Value (IV) and Weight-of-Evidence (WofE) to find out the level of correlation between the factors and 75% of occurrences and using these ratios to reclassify the thematic layers.
- Creation of landslide susceptibility maps for the study area for the four different approaches and their classification into areas of low and high susceptibilities.

- Validation of prepared final maps using the testing (25%) datasets is to be carried out using the different metrics to assess both model fitness and predictive capacity of models.
- This research is a product from months of consultation of peer-reviewed research papers, government reports and manuals on landslide-related studies in the Indian Himalayan region and around the world.

The backbone of the study is the landslide incidence map, where each past slide has been carefully identified, examined and recorded, since the main assumption of the probabilistic approaches is that past landslides give valuable indication for future slides. This led to the creation of a new landslide incidence map that covers the whole research area for a better and updated representation of the real scenario along the Parvati valley of the Kullu district.

1.4 Outline of thesis

A brief description of the major chapters/parts with key points has been outlined below as the blueprint of this research work.

CHAPTER 1: INTRODUCTION

This opening chapter is an overview of the motivation and background of research carried out. The various objectives are here-in discussed as well as the outline of the thesis is presented as a summary.

CHAPTER 2: LITERATURE REVIEW

This chapter contains a compendium of various findings from past landslide-related investigations as well as a brief introduction to various approaches adopted for landslide susceptibility mapping, both locally and globally.

CHAPTER 3: RESEARCH AREA

This chapter gives a description of the various characteristics of the research area as well as the district it lies in. The description is not limited to the physical attributes only but incorporates the socio-economic aspects of the region.

CHAPTER 4: METHODOLOGY AND DATABASE PREPARATION

This chapter goes through the methodology adopted for this work, the acquisition process for all the data used and the preparation of thematic layers for further analysis, including the compilation of the landslide incidence map followed by its random splitting process into validation and testing datasets.

CHAPTER 5: ADOPTED PROBABILISTIC APPROACHES: CONCEPT AND COMPUTATION RESULTS

The chapter explains about the concepts behind the four GIS-based statistical methods (FR, SE, IV and WofE) employed for data analysis. The computation process using each approach for every category of the factor maps is presented and the direct relationships between the factors and past landslide events here-in discussed.

CHAPTER 6: LANDSLIDE SUSCEPTIBILITY ANALYSIS: RESULTS AND DISCUSSIONS

This chapter describes the processing of the final landslide susceptibility maps through data integration after reclassification of thematic maps. The validation and accuracy assessment for the four models have been presented and compared here-in.

CHAPTER 7: CONCLUSION, LIMITATIONS AND RECOMMENDATIONS.

This chapter concludes the research work and highlights the limitations, recommendations as well as future scope of work.

CHAPTER 2
LITERATURE REVIEW

2.1 Overview of research carried out

The review of literature provides a summary of information gathered through consultation of various publications, articles, manuals, reports and tools employed by previous researchers and stakeholders, forming the basis of desk study in any investigation as well as devising appropriate problem-solving methodologies.

The main reasons behind many scientists, researchers and other stakeholders mobilizing more and more time and resources in landslide-related studies are to evaluate, quantify and potentially reduce the immense socio-economic losses resulting from landslide events. This has led to an exponential increase in the number of publications nationally and internationally in the past decade whereby several methods have been explored, employed, compared and validated.

However, the complex multi-facetted nature of these disastrous events makes it almost impossible to devise a general 'reasonable' solution, with some of the major hurdles being the selection of causative factors specific to an area, followed by selection of appropriate data analysing and predictive modelling techniques. These solutions are in turn highly dependent on other external factors such as data availability, location remoteness, etc. Landslide-related investigations in the form of susceptibility and hazard mapping, early warning systems, etc. are thereby being encouraged at all levels in countries facing losses from such disasters. Likewise, this investigation is a contribution to the ongoing efforts by other practitioners in better understanding landslide mechanisms in the Indian Himalayan region and attempting to delineate areas vulnerable to future slope failures through various methods.

The final intent of this study is to prepare landslide susceptibility maps for the area investigated by employing and comparing different statistical methods as well as analyse the spatial relationships between different causative factors and past land sliding events.

2.2 Landslides: Definitions, types and causes

One of the earliest definitions for landslides as proposed by Terzaghi [1] was the sudden outward or downslope movement of slope-forming materials (rock, sediments or residual soil) adjoining a slope due to the action of gravitation force. Numerous definitions have since then emerged in several books, articles, papers and theses due to the difficulty in formulating a global definition for such a complicated event. The different terminologies used to define the various landslide features, are outlined in Fig. 2.1.

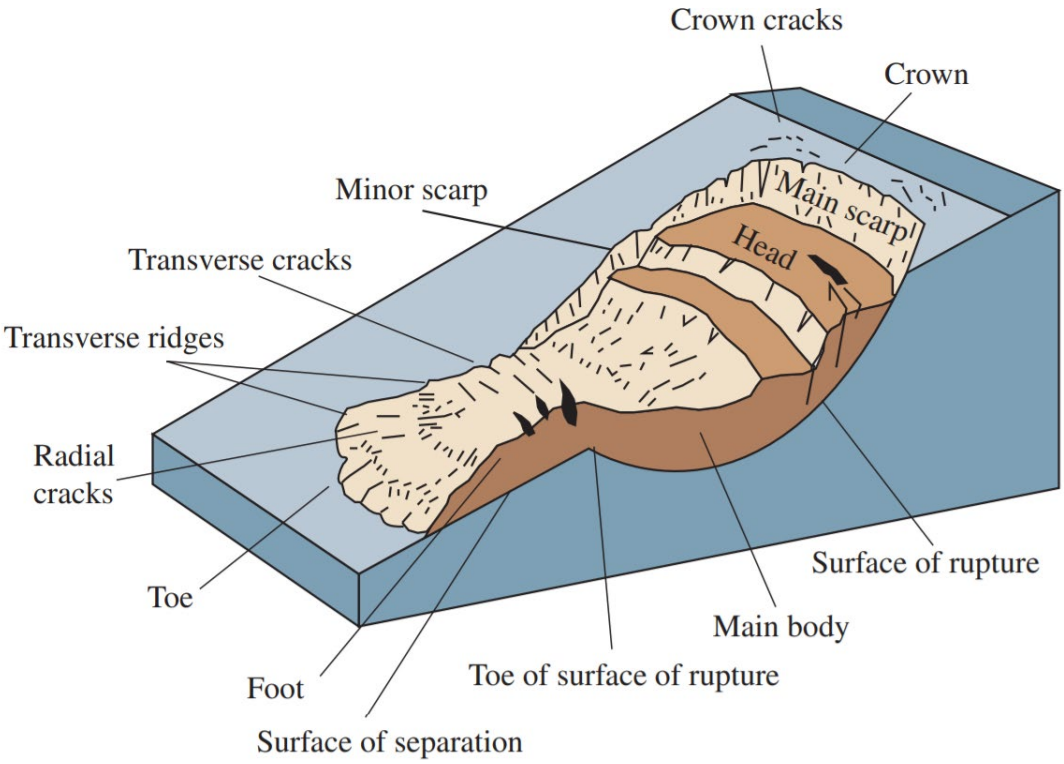

Fig. 2.1 . Schematic diagram of a rotational landslide (*Source: Landslide types and processes, USGS (2004)*)

Similarly, various detailed classification systems were developed over the years addressing all the types of mass wasting event as a result of different material and movement type, most of which are based on the Cruden and Varnes (1996) classification system [2]. A detailed classification as outlined by Lee and Jones [3], is given in Table 2.1.

Table 2.1 Classification of landslides

			Material type		
			Rock	**Debris**	**Soil**
Movement type	**Falls**	**Falls**	Rock fall	Debris fall	Soil fall
		Topples	Rock topple	Debris topple	Soil topple
	Flows		Rock avalanche	Debris flow	Mud flow
	Slides	**Rotational**	Single rotational slide	Multiple rotational slides	Successive rotational slides
		Non-rotational	Block slide	Slab slide	Spreading failure
		Planar	Rock slide	Debris slide	Mudslide

The classification of the causes of landslides as external and internal one has been done by Terzaghi [1]. He further explained the external causes as those attributed to shear stress increase (changes in slope material characteristics, pore water pressure, drawdown, etc.) at constant shear resistance while the internal causes as those attributed to shear resistance decrease at unaltered shear stress (weathering, creep, etc). Cruden and Varnes [2] further classified the landslide causes into geologic, anthropogenic and morphological and physical causes. Some of these factors have been selected on the basis of their availability as well as relevancy and have been used to assess their contribution to past land sliding events later in this study.

2.3 Remote sensing and Geographic Information System (GIS) applications

The advent of Geographic Information System (GIS) and remote sensing techniques have brought to surface their wide range of applicability to different fields namely natural sciences, disaster management, urban planning and design, exploration programmes, etc. The relationship between GIS technologies and remote sensing techniques can be defined in three plausible ways as outlined by Wilkinson [4] :

- The usage of remote sensing for data collection to be used in GIS platforms.
- The usage of GIS datasets for improved data processing of products from remote sensing techniques.
- The combined operation of GIS and remote sensing techniques for modelling purposes, etc.

GIS and remote sensing have been applied and validated successfully by many researchers in many engineering studies; namely transportation analysis, site-selection studies, potential zone mapping, mineral exploration programmes, change detection analysis and many more. However, only its relevancy and popularity amidst landslide-related studies has been reviewed in this study.

The growth of geo-informatics users can be mostly attributed to the ease in data entry, handling and modelling using the various tools and resources available. GIS software packages nowadays come with specialised tools such as data conversion, spatial analyst, geoprocessing, overlaying, cartographic manipulation and image processing among others along with possibility of using external plug-ins/toolboxes by the use of python-based scripts. Availability of more flexible open-source software and better-quality datasets made the usage of GIS and remote sensing indispensable to data scientists, coupled with the immense processing capacity of today's hard-drives.

Nonetheless, some researchers highlighted the misconceptions behind usage of GIS and its validity since the requirement of 'experts' in specific areas has reduced with its inception and that the focus was mostly shifting towards data scientists and statisticians for development of more robust models [5]. Some difficulties still

encountered by GIS users nowadays are unavailability of data freely, difficulty in data acquisition, powerful hardware requirement for the huge data handling ability, etc.

Remote sensing techniques, through the usage of specialised sensors, have enabled several researchers detect, map and monitor objects or events without being physically present in the area under investigation. This has set the basis of many studies conducted in remote locations with hurdles like decreased personnel accessibility and increased cost of investigations/exploration. To be more specific, a detailed geotechnical exploration programme in mountainous/remote areas might have huge costs in the form of transportation of special testing apparatus due to inaccessibility, unpredictable climatic conditions hampering testing procedures, etc.

The increased operability and accessibility of satellite products along with the immense data analysing techniques available to researchers has fuelled a growing body of literature in the field of GIS and remote sensing and this rapid evolution along with its extended grasp in many other streams has made it really difficult to keep track of the developments and breakthroughs.

Remote sensing and GIS-based technologies have been gaining popularity amidst landslide researchers for the simple reason that they have a role to play at every link of landslide investigation and those links may be broadly categorized as:

- Landslide detection
- Landslide mapping
- Landslide monitoring
- Landslide prediction
- Landslide mitigation
- Landslide preparedness

Some researchers [6] extracted several landslide inducing factors such as slope, lineaments, aspect, curvature, land cover and NDVI from satellite imagery and the mapping of landslide was carried out through aerial photograph interpretation. Frequency ratio and logistic regression models were used to formulate and validate the final landslide

susceptibility map. The difficulty in carrying out field surveys in mountainous areas and in predicting the time of land sliding events were highlighted by the authors.

2.4 Landslide identification and mapping

The basis of any landslide susceptibility/hazard/risk analysis is the process of identifying and mapping previous landslides in the form of landslide inventory/incidence maps, and the approaches for this process are diverse and still expanding. The main objective of this task is to gather as much information about past slope failures in order to properly assess and evaluate the possible underlying causative factors, to identify patterns/hotspots, to aid in predicting future slides with similar characteristics/causes [7].

A broad classification of the various types of landslide inventory maps has been presented by some researchers [8] as:

1. Archival maps comprising of landslide information retrieved from newspapers, government archives and literatures.
2. Geomorphological historical maps (the most widely adopted) compiling information about sliding incidents over a certain period of time with not much emphasis on the date of occurrences.
3. Event-driven maps prepared from compiling slope failure incidents during and following an event (earthquake, rainfall, flood, dam-break, etc.).
4. Multi-temporal maps are derived from interpretation of multiple datasets over a longer period of time, generally comprising of more than a single event.

There is a need to distinguish between detection and classification of landslides, with the latter requiring higher resolution imagery for generation while the former relies on identifying scarred features left behind by landslide events through visual interpretation of optical imagery.

Traditional landslide field mapping/delineation is not a given task with many difficulties arising. Some of them has been outlined as:

i. Local perspective of expert not enough to perceive the whole extent of the slide under investigation

ii. Landslide boundaries may have been obscured by vegetation or debris.
iii. Rapid remediation by local services may change landslide features such as removal of debris/flows without estimating the flow extent and volume.

Advancements in the field of geomatics, geodetics and surveying brought forward various novel technologies and techniques to identify and map landslides. Some methods of mapping landslides that have been previously employed are:

- Direct geomorphological mapping [9]
- Visual interpretation of various aerial imageries [10] [6]
- Remote sensing products interpretation (SAR images, multi-spectral images, etc.) [11]
- Semi-automated methods of mapping techniques [12]

Rabby and Li [13] utilized Google Earth software to identify and mapped 230 landslides from 2001 to 2016 in the Chittagong area in Bangladesh and after field verification determined that the accuracy of the remotely mapped landslides varied between 69-88%. This indicates the potential of using very high-resolution (VHR) imagery in Google Earth to map landslides with reasonable accuracy. Other researchers [14] applied an integrated landslide mapping approach using Sentinel-1 satellite data, Google Earth VHR and field survey in Pahang, Malaysia, validated 20% of mapped events through field survey despite inaccessibility.

A detailed review on the different remote sensing techniques adopted in nineteen recent studies was made by Zhao and Lu [15], explaining the usage of optical imagery, spaceborne/ground-based synthetic aperture radar (SAR) and light detection and ranging (LiDAR), field surveys along with monitoring techniques.

The final landslide inventory map, used for landslide susceptibility analysis for the western part of Crete Island, was created by Psomiadis out of a combination of historical landslides information, events detected using Google Earth VHR and Sentinel-2 data along with field mapping of recent slides [16].

Semi-automated novel methods for landslide mapping such as the Scarp Identification and Contour Connection Method (SICCM), was developed and tested in western Oregon, USA [17] as an ArcGIS external python script toolbox to aid the mapper to automatically, semi-automatically or even manually map landslide scars (as polylines) along with the deposits in a separate algorithm; all of which is dependent on the spatial resolution of the input DEM from which factors such as slope and curvature layers were derived.

Despite the diversity in satellite data available both freely and commercially, the difficulty in acquisition of particular earth observation datasets, the dependency on image processing and data handling capacity of the hardware, satellite data along with new geoprocessing tools are proving to be powerful landslide detection and monitoring gadgets.

2.5 Methods for landslide susceptibility analysis in India

India has been the focus of several disaster-related studies; among which, landslides form part of the most disastrous events that are still being investigated in the hilly and mountainous areas. The areas that have been broadly identified as landslide prone areas in the Indian peninsula are the 22 states and 2 union territories housing the North-eastern and North-western Himalayas, the Eastern and Western Ghats [18].

The National Remote Sensing Center (NRSC) under the Indian Space Research Organisation (ISRO) and the Geological Survey of India (GSI), are the agencies designated for local and national landslide inventorying and susceptibility assessment using datasets from Indian satellites [19]. In an attempt towards disaster mitigation measures, the Building Materials and Technology Promotion Council (BMPTC) under the Ministry of Housing and Urban Affairs, Government of India (GOI) prepared a national as well as a state-wise vulnerability atlas for the natural disasters (cyclone, earthquake, flood and landslide) in India [20].

The North-western Himalayan region in question comprises mainly of the states of Jammu & Kashmir, Himachal Pradesh and Uttarakhand while the states of Assam, Arunachal Pradesh, Sikkim as well as North Bengal constitute the lower North-

eastern Himalayan region. The reason for frequent happening of these catastrophic phenomena can be linked to other triggering events such as heavy rainfall (during the monsoon season), glacial lake outburst flood (GLOF) events, earthquakes, etc. The ever-growing population in these regions along with ever-expanding tourism activities, led to an increase in road construction/widening and building construction, consequently bearing huge environmental impacts.

Landslide susceptibility zonation, defined as the delineation process of an area based on its level of propensity to sliding events, is an important pre-hazard management tool [21] that has been applied across the world.

A detailed review made by Lee [22], based on 776 articles from 1999 to 2018 spanning across 65 countries, revealed that the most common research areas for landslide susceptibility mapping (found in 143 articles) were located in China (18.5%) with the second (89 articles) most common in India (11.5%).

The Bureau of Indian Standard (BIS) published guidelines for the generation of landslide hazard zonation maps as IS 14496 (Part 2): 1998 which is an expert-based heuristic approach for factor weight assignment, used for map generation with scales up to 1:50,000.

Van Westen et al. [19] presented four case studies from different parts of India (Uttarakhand, West Bengal, Tamil Nadu and Kerala) regarding usage of various methods for landslide mapping and susceptibility/hazard/risk evaluation depending on terrain characteristics and availability of data. This research collaboration resulted in the publishing of five PhD theses and over 20 journals.

The most commonly adopted approaches to landslide susceptibility mapping can be broadly classified as per Fig. 2.2.

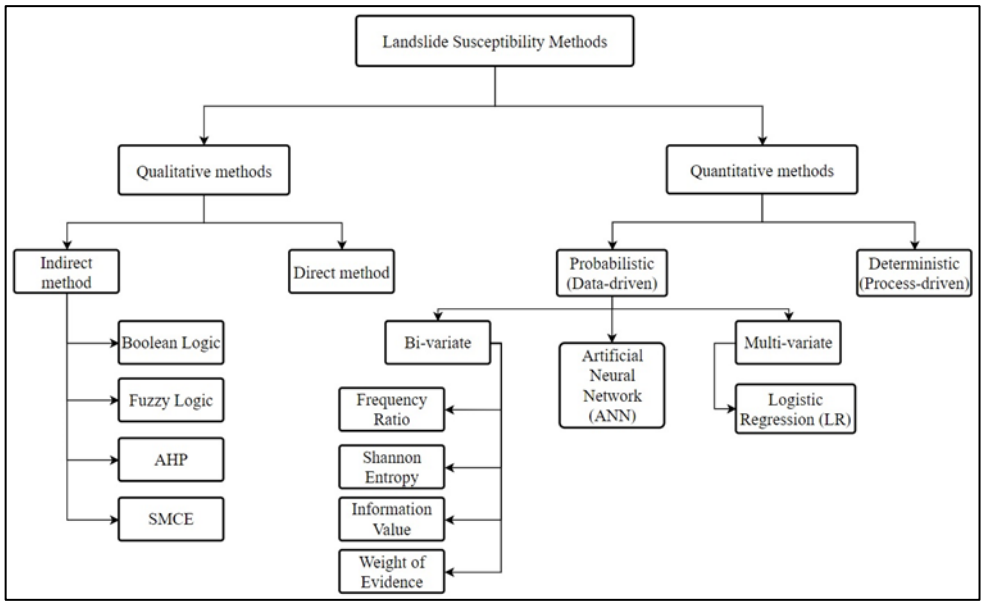

Fig. 2.2 Methods adopted for LSM

2.6 Heuristic methods

Heuristic approach, otherwise known as knowledge-driven, empirical or qualitative approach can be direct or indirect in nature. The direct method relies on the knowledge on experts for geomorphological mapping [23] while the indirect method constitutes expert-based procedures of weight assignment for landslide causative factors [24].

A detailed geomorphological mapping was carried out for a part of eastern Cuba by Abella and Westen [25] to determine the different landslide causative factors and landforms. Then, a three-level heuristic expert-based model of weight assignment was applied for landslide hazard and risk assessment.

These methods have been believed to introduce a high degree of subjectivity due to their reliance on expertise rather than reliance on data or process. Albeit, heuristic approaches have been the basis of many studies, guidelines and manuals despite their dependency on the expert's knowledge.

The advent of GIS has brought about the opportunity of assigning expert-based weights to factor maps/classes for the creation of LSM, giving rise to indirect methods. These indirect empirical approaches can be broadly classified [26] into:

i. Boolean logic method
ii. Fuzzy logic method
iii. Multi-class overlay method
iv. Spatial Multi-Criteria Evaluation (SMCE) method

The research work of Panchal and Shrivastava [27] consisted of using the Analytical Hierarchy Process (AHP) to generate landslide susceptibility map for the whole district Kullu of Himachal Pradesh. Meena et al. [28] applied a hybrid SMCE method involving the integration of the AHP and Frequency Ratio (FR) approaches in a GIS environment, to delineate landslide susceptible areas in the entire Kullu district. The output results of the models demonstrated the superior accuracy rate of the hybrid SMCE (91.0%) over the FR (90.7%) and AHP (79.7%) approaches.

Veerappan et al. [29] concluded that FR (81.57%) method had better prediction capability over heuristic AHP approach (67.80%) from comparing the prediction results of two landslide susceptibility models along a 52 km stretch of NH-58 in the state of Uttarakhand.

2.7 Probabilistic methods

Probabilistic methods are also known as data-driven methods since they rely on past landslide information for future slide prediction. They can be largely grouped as:

- Bi-variate approaches
- Multi-variate approaches

Both these approaches rely on the assumption that the combination of past landslide events and contributing factors will aid in predicting future slides under same conditions [30]. Bi-variate models focus on the relationship between each parameter class to past slope failure events [31] whereas multi-variate models account for the relative weight determination between the factors as well [32]. Since they do not rely on

knowledge of experts for any weight determination, they are less subjective in nature than qualitative methods.

Some of the bi-variate approaches that have been adopted globally to map landslide susceptibility are:

i. Frequency ratio (FR)
ii. Certainty factor (CF)
iii. Statistical Index (SI)/Information value (IV)
iv. Weight of evidence (WofE)
v. Evidence belief function (EBF)
vi. Index of Entropy (IOE)/Shannon entropy (SE)

Some of the multi-variate approaches are Logistic Regression Analysis, Multiple Regression Analysis, Discriminant Analysis, etc. Artificial Neural Network (ANN) models are non-linear data-driven models that require lesser training data but still give accurate results [33]. Probabilistic approaches and physically-based approaches are both termed as quantitative methods for landslide susceptibility mapping. A hybrid of qualitative and quantitative methods also has been employed and validated by several researchers.

Logistic Regression, Frequency Ratio and Artificial Neural Network were the three most adopted approaches to landslide susceptibility mapping around the world as revealed in a detailed review of 776 articles carried out by Lee [22] for the year 1999-2018.

In recent studies, it is quite common to come across a comparison of two or more different landslide susceptibility models applied to the same geographical extent using two or more validation methods. The need for validation of output results of probabilistic models is the innate spatial variability in input data and uncertainty in data handling procedures, etc.

Bi-variate approaches has been successfully applied and validated to the four most vulnerable mountainous regions of India. Sujatha et al. [34] evaluated LSM for the

Tevankarai watershed using Certainty Factor (CF) probabilistic method while Banshtu et al. [35] employed FR approach for landslide hazard zonation and Fuzzy Logic approach for risk estimation in the Kullu district. Other applied probabilistic models are the Index of Entropy (IoE) model that was applied to the Darjeeling area by Mondal and Mandal [36] and the Statistical Index (SI) model that was applied in part of the state of Himachal Pradesh by Kumar et al. [37]. Keeping in mind the immense literature present in India concerning landslide susceptibility mapping, it can be observed that recent research works are more oriented towards comparison of different models to opt for the most accurate one for a specific area before proceeding with more detailed analysis.

The present study attempts at preparing and comparing four landslide susceptibility maps using the four probabilistic methods FR, SE, IV and WofE. The concepts behind each of these applied methods are presented in Chapter 5 Adopted Probabilistic Approaches: Concepts and Computation Results.

CHAPTER 3
RESEARCH AREA

The purpose of this chapter is to highlights the different characteristics of the study area as well as the district it lies within for a better understanding of the present scenario for selection of landslide causative factors.

3.1 Himachal Pradesh (An Intro)

One of the twelve states along the Indian Himalayan Region, stretching about 2,500 kilometres, Himachal Pradesh (HP) is situated between the states of Uttarakhand (south-east), Punjab and Haryana (south and south-west) and Jammu & Kashmir (north and north-east) as depicted in Fig. 3.1. It has elevation ranging from 350 metres to nearly 7,000 metres, through the Outer, Lesser and Greater Himalayas, defined broadly as the three-prevailing physio-graphic regions.

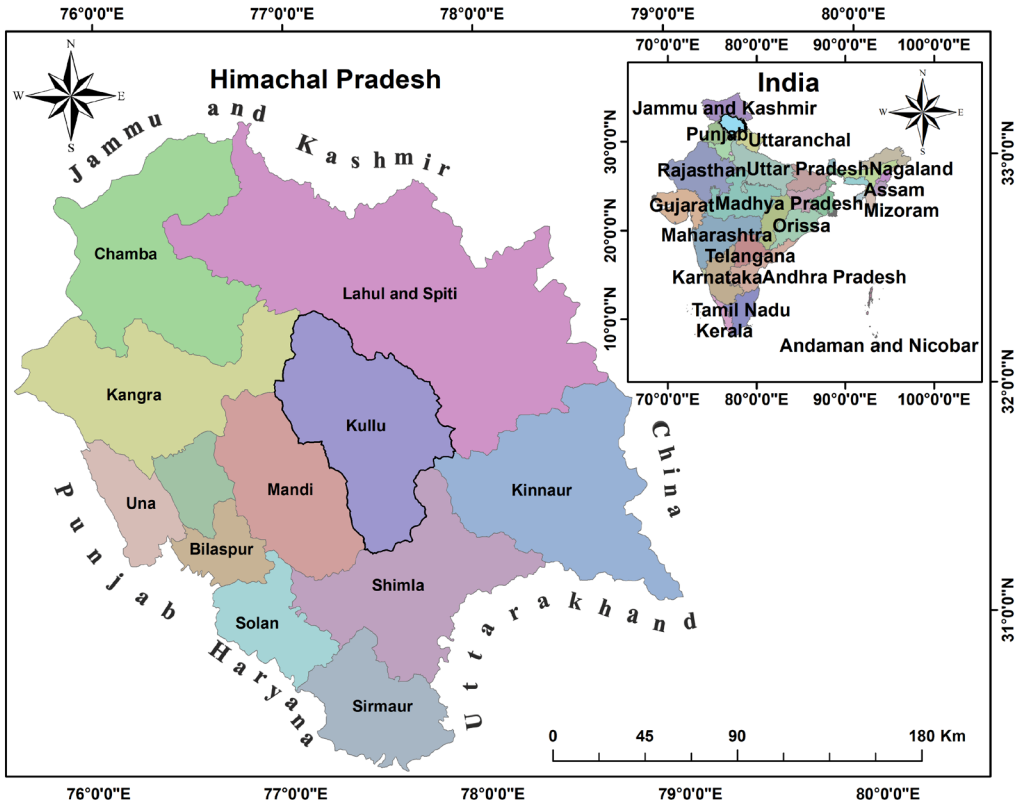

Fig. 3.1 Himachal Pradesh map

The hilly and mountainous terrains experience variations in climate from hot, sub-humid tropical climate to cold due to the rise in altitude towards the easterly and northern direction. The coldest, driest and largest district are Kinnaur and Lahaul & Spiti, situated on the north-eastern end while the warmest and wettest districts are situated on the lower south-western end. The five rivers namely Beas, Ravi, Chenab, Sutlej and Yamuna form the main drainage network.

Home to picturesque places like Khajjiar (known as 'Mini-Switzerland' of India) and Kasol (known as 'Mini-Israel' of India), the state of Himachal Pradesh is administratively divided into twelve districts which experience three seasons around the year namely rainy(monsoon), winter and summer. The winter season is known for snowfall and snow-clad peaks in the higher elevated places.

The inherent fragility of the Himalayan mountain areas and unpredictability of its hydro-meteorological conditions coupled with rise in man-made activities, have made Himachal Pradesh even more vulnerable to disasters [38] like landslides, soil erosion, heavy rainfalls, floods, etc.

3.2 District Kullu (A glance)

Out of the twelve districts of Himachal Pradesh, Kullu was selected as a focus for this study due to the recent surge in tourism, rise in anthropogenic activities, change in crop pattern; ultimately increasing the area's vulnerability to climate change. The district houses four tehsils (sub-divisions) Kullu, Manali, Nirmand and Banjar and two sub-tehsils Anni and Sainj as shown in Fig. 3.2. The main drainage networks are mostly fed by melting snow/glaciers and rainfall in the region and consist of the Beas, Parvati and Satluj rivers and other tributaries.

Around 325 villages and 5 towns are connected and depend on a road network of approximately 1,900 km road length. Approaching Kullu through Bhuntar gives a traveller the option to choose between following the National Highway through the beautiful Beas valley to Manali as a popular honeymoon destination or one may choose to go for a more serene and peaceful trip along the lush Parvati valley.

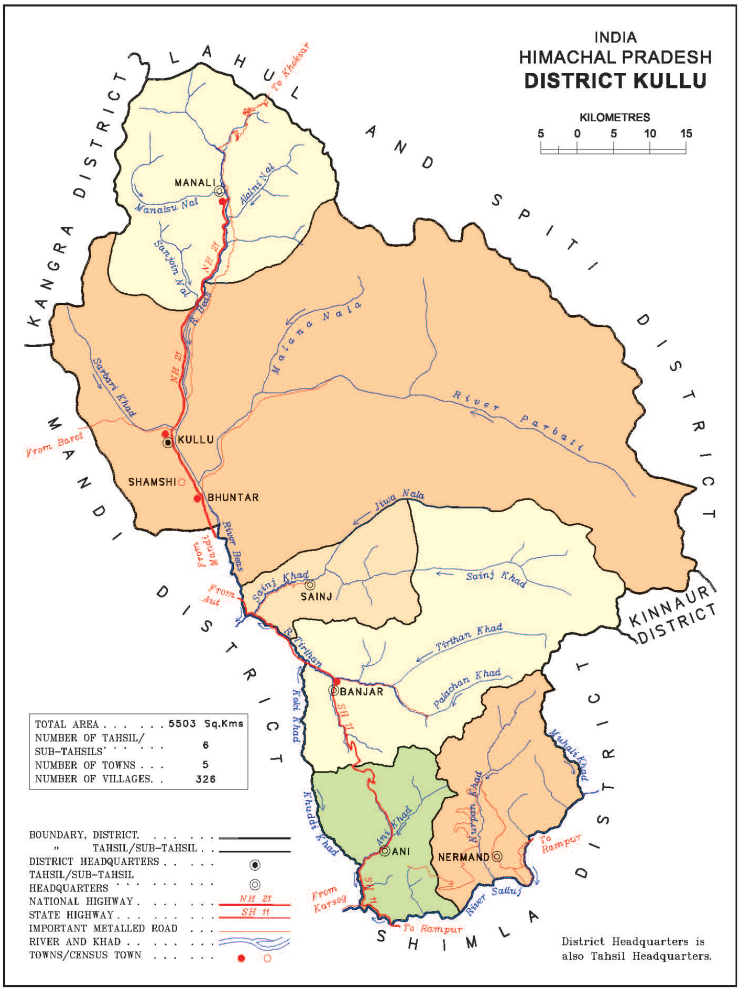

Fig. 3.2 Kullu district map (*Source: Census of India, 2011*)

3.3 Study area

Before proceeding with the data preparation and processing part of this work, some aspects of the research area were explored to better understand the area's vulnerability to natural disasters, which is of increasing concern to local authorities and residents. Specific characteristics of the study area can be found in next chapter of this thesis where the parameters that have been identified as potential landslide-inducing factors, have been prepared as thematic maps for better visualisation and analysis.

3.3.1 Administrative setting

The research area investigated is located at the heart of the district of Kullu in the Kullu tehsil as in Fig. 3.3 and covers an area of around 1,000 km^2 with elevation ranging from 1,050 to 4,900 metres.

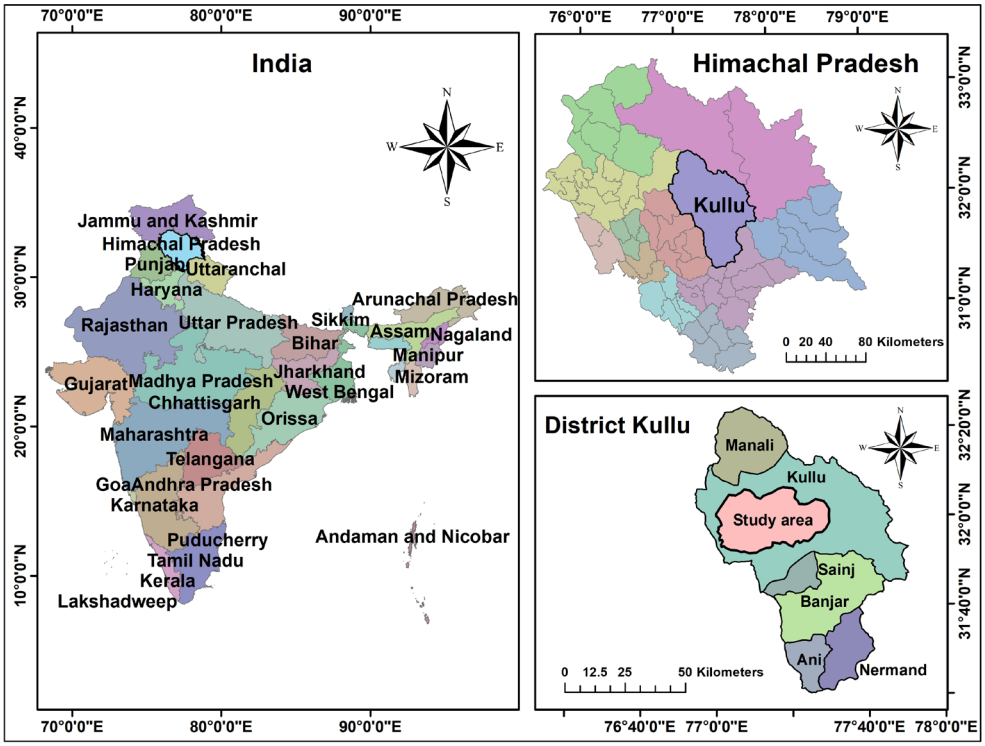

Fig. 3.3 Location map of study area

The two valleys in the study area are the Kullu valley along the Beas River and the Parvati/Manikaran valley along the Parvati River. The source of Parvati river is from Beli (about 4,100 m altitude) beyond the study area's boundary but flows north-westerly until Manikaran and takes a south-westerly course to meet the Beas river near Bhuntar. The tributaties of the Parbati river are Tosh Nala intersecting near the Barshaini hydro-electric dam project and Malana Nala finally joining near Jari hydro-electric dam project.

Kullu is accessible by road through the national highway NH-3 or the major district roads Kullu-Nagar-Manali and Jia-Manikaran, and by air through the nearest airport in Bhuntar which is approximately 10 kilometres away. The rise in tourism and

development activities has made this area easily accessible with frequent bus and taxi services in the recent years.

3.3.2 Tourism

The study area covers part of the Kullu tehsil housing villages such as Bhuntar, Jari, Malana, Kasol, Manikaran, Tosh, Kalgha, etc which are far-flung villages from the main Kullu valley area as seen in Fig. 3.4. The concept of tourism changed over the last decades with more and more tourists, whether local or foreign, shifting towards exploring far-flung villages in search for serenity, inner-peace and minimalistic living rather than mainstream tourist attractions.

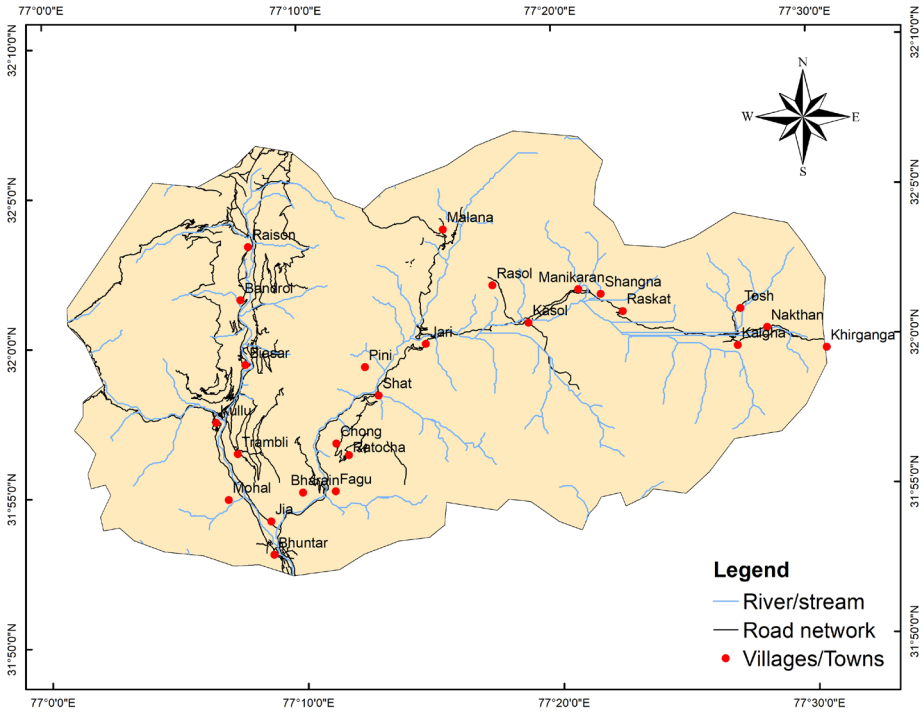

Fig. 3.4 Research area

The Parvati valley is also known for famous treks like Pin Parvati pass, Khirganga and Chanderkhani, taking one from lush green valley, through dense alpine forests, to snow-capped peaks. Geothermal activity due to presence of structural faults gave rise to hot springs in places notably Kullu, Kasol, Manikaran and Khirganga. In short, the area provides a combination of eco, adventure, and culture tourism with

accommodation facilities ranging from expensive hotels, cottages, homestays, guest houses and camping tent sites.

The Parvati valley is becoming more and more famous and is facing a huge rise in development activities such as construction of guest houses, road widening and hydroelectric projects rise, all of which is adversely impacting the environment one way or another.

3.3.3 Climate and rainfall

Climatic conditions mainly depend on elevation, rainfall, moisture, temperature, etc. Kullu is found at the heart of Himachal Pradesh with climatic zones sub-tropical monsoon without dry winter, with warm summer near the Manali area and moderate hot summer for the rest for the district.

However, regionally, these climatic zones further subdivide into micro zones namely arid, semi-arid, glaciers and sub-tropical. The two predominant agro-ecological zones in this area are sub-temperate mid hills and wet-temperate high hills. The temperature falls to approximately -1.5°C in cold months of December-January and rises to approximately 37°C in the hot month of July. High altitude village areas like Khirganga, Malana and Tosh receive snowfall in the month of December-January, sometimes causing road blockages and economic disruptions.

Rainfall is fairly well-distributed in the lower plains with an average annual rainfall of 1,405.7 mm and maximum recorded intensity during the monsoon season (July-August) as seen from Table 3.1.

Table 3.1 Variation of average montly rainfall intensity for 2014-2018 (*Source: IMD*)

	MONTH											
	JAN	FEB	MAR	APR	MAY	JUN	JUL	AUG	SEP	OCT	NOV	DEC
YEAR	***Rainfall intensity (mm)***											
2014	83.1	150.7	204.9	88.3	114.6	50	181	114.2	70.8	21.3	5.1	72.6
2015	110.8	212.2	195	113.3	47.1	91.6	235.8	108.9	62.2	15.3	26.5	34.9
2016	37.9	74.1	186.6	92.5	57.5	58.6	185.9	282.6	36.4	4.9	0	0.1
2017	186.8	77.6	106.9	109.2	96.5	146.1	218.9	106.2	106.4	1	19	44.9
2018	12.4	56.8	67.5	91.9	43.3	100.1	204.9	194.4	273.8	10.7	88	10.9

The trends in the average monthly rainfall intensity (mm) for the year 2014-2018 can be interpreted from Fig. 3.5 below. For the years 2014, 2015 and 2016, rainfall intensities were at peak during the first months of Feb and Mar as well as the mid-calendar months of July and August. The year 2016 experienced the highest downpour during the month of August compared to the two previous years that received maximum rainfall intensity during July. The anomalies observed for the year 2017 were the low rainfall intensity in the months February and March compared to previous year rainfall trends, and for the year 2018, the maximum rainfall intensity was in September compared to previous years which was in July.

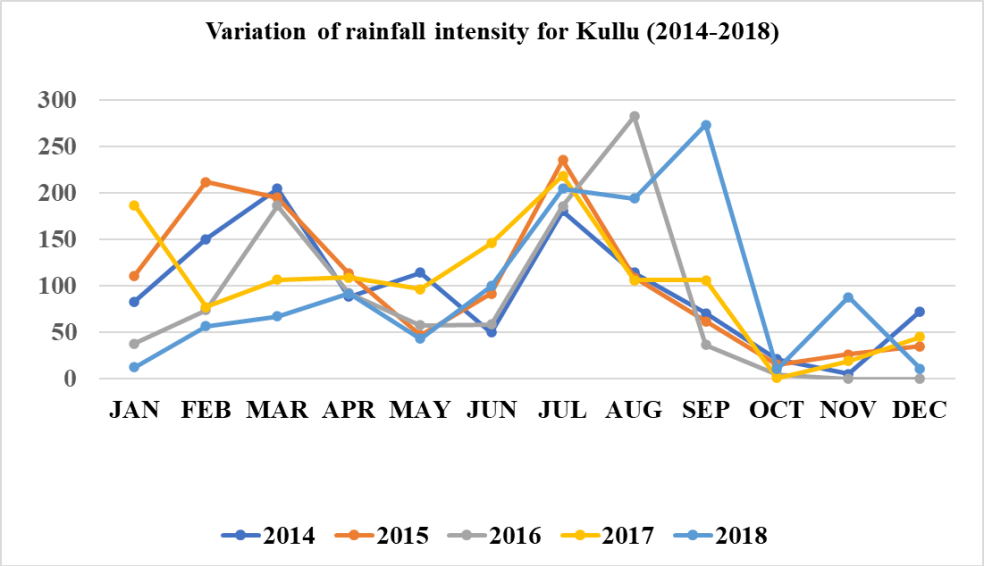

Fig. 3.5 Average monthly rainfall trend (2014-2018) (*Source: IMD*)

Annual global rise in temperature has caused major irregularities in the Indian Himalayan climatic conditions with some resulting visible changes like reducing extent of snow cover, increasing extent of denuded land, and visible changes in crop pattern with respect to elevation and temperature [38]. All these climate-driven changes have made the research area more vulnerable to natural disasters.

3.3.4 Physical characteristics

The area can be hydro-geologically divided into unconsolidated sediments (porous formations) as valley and fluvial channel deposits and semi-consolidated to consolidated sediments (fissured formations of sedimentary, metamorphic and igneous

origin) forming the hill ranges [39]. This region falls under the landform classification of the Lesser Himalayan Hills which spans in other districts of HP such as Solan, Shimla, Kinnaur, Chamba and northern parts of Kangra.

The major soil types, though very distinct in nature, in the district Kullu [35] can be identified as:

- Coarse loamy
- Fine loamy
- Loamy skeletal
- Sandy skeletal

Characterized as having high to very high organic carbon content, these soils find their depth ranging from shallow to deep [40]. Some compiled soil data has been presented in Table 3.2 below.

Table 3.2 Soil characteristics of the study area (*Compiled from WRIS website)*

Soil texture	Sandy loam to clay loam
Soil depth	50 - 100 cm
Soil pH	Acidic
Soil colour	Brown to dark brown

Geologically, metamorphic rocks are prevalent along the steep slopes while crystalline rocks occupy the valley areas. The geomorphic units in the district of Kullu have been categorized [41] as:

- Active flood plain
- Younger alluvial plain
- River
- Channel island
- Piedmont slope
- Dissected terrain:
    - Low

    - Moderate
    - High
- Glaciated terrain

The rivers in the study region are perennial in nature; fed by melting snow/glaciers and rainfall. The major source of water is from springs and open wells for domestic and irrigation purposes, making the area also rich in both hydropower generation and ground water harnessing potential [39].

3.4 Hazard scenario in the region

Some notable works by previous researchers in the district of Kullu have been mentioned below to better understand the types of disasters and their underlying causes/mechanisms affecting the region under investigation.

Chandel [42] explored the different dimensions of disasters in Himachal Pradesh such as landslides, earthquakes, flash-flood and avalanches and the major causes for slope failures were found to be immature topography coupled with tectonically active structures; geologically weak and highly fractured. The rise in hydropower projects as well as other man-made related activities have contributed to more frequent mass movement occurrences in the area since the past decades.

Sah and Mazari [43] conducted an in-depth analysis of the factors and mechanisms behind some major landslides in the Kullu area. Some past major slides and their extensive damage in the area have been critically analysed and some of the key factors responsible have been identified as being oversaturation of unconsolidated material due to high rain infiltration, seepage in slopes, and bank erosion owing to overflow conditions. Some landslide mitigation measures have also been suggested by the authors.

Vaidya et al. [44] used change detection techniques using satellite imageries for 27 years to gather valuable information about the land use changes in the Kullu Valley. The land use classification was executed using Maximum Likelihood Classification algorithm and validation was carried out through field surveys. Surveying through questionnaires was done to identify underlying causes of land use changes in the area.

Results revealed changes in crop patterns, rise in anthropogenic activities and impact of climate change on crop growth among others, all pointing towards the increasing vulnerability of this region.

The types of hazards affecting the lesser Himalayan region of the Kullu Valley such as soil erosion and landslides were discussed by Prasad et al. [45] and some of the underlying causes found were increasing population, human development on slopes and road construction. Several suggestions have been made with much emphasis on more ecologically and environmentally friendly development strategies.

An in-depth analysis of the lithological, structural and terrain slope interactions using morpho-tectonic parameters and their relation to landslide occurrences in the Kullu area was carried out by Mishra et al. [46]. Mass movements were found to mostly occur in the southern and southwestern facing slopes and the rocks in the area were found to be affected by joint-sets and fractures, facilitating water infiltration and accelerating weathering.

Meena and Nachappa [41] used the frequency-ratio approach to evaluate the impact of three DEMs of different spatial resolutions (ALOS-PALSAR 12.5 m, ASTER 30 m, SRTM 90 m) on the quality and prediction accuracy of the prepared landslide susceptibility map. The chosen area of interest, Kullu district has been portrayed by the authors as being highly susceptible to mass movements due to its highly dissected topography and heavy rainfall presence. The 30 m resolution DEM was found best-suited for the Kullu district since it had the highest accuracy (0.910) compared to the 12.5 m (0.839) and the 90 m (0.824) resolution DEM. The study concluded that usage of higher resolution DEM data might not compulsorily have the most accurate results for an area.

A field visit to the study area revealed some small slides along transportation corridors with presence of construction materials as well as sliding debris on the hard-shoulder of these mountain roads making road users more and more susceptible. Moreover, un-scientific dumping of materials including construction and debris materials alongside road changes drainage pattern; even going to the extent of completely blocking road gully networks causing huge stresses on the slope-forming materials. Fig. 3.6 and Fig. 3.7 shows the different parts of the study area susceptible to mass movements.

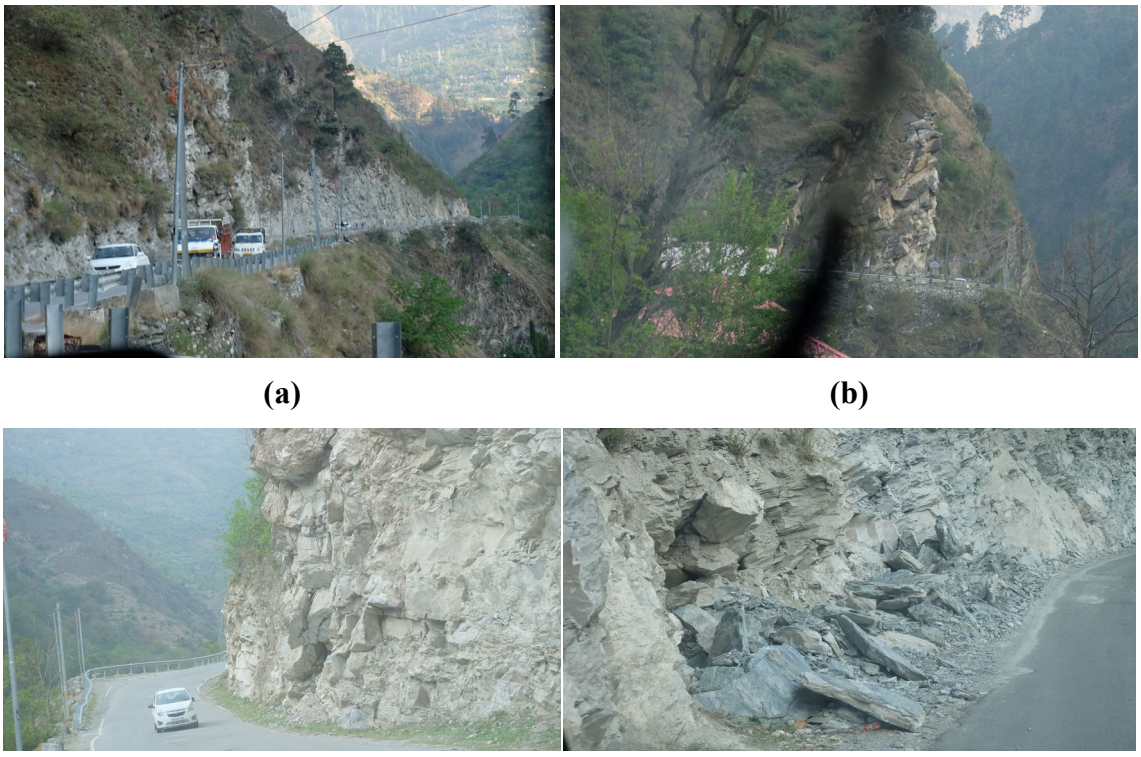

(a) **(b)**

(c) **(d)**

Fig. 3.6 Transportation corridors susceptible to landslides (a) Road cuts along Kasol-Manikaran road stretch (b) Steep road cut along a section of Bhuntar-Kasol road (c) over-hanging rock at-risk of falling over road users (d) rock debris on side of road along a stretch of Bhuntar-Kasol road

Fig. 3.7 Sliding events observed during the site visit near Kasol, Manikaran and Barshaini

CHAPTER 4
METHODOLOGY AND DATABASE PREPARATION

4.1 Methodology adopted

The present research adopted a rather simple and straight-forward methodology to evaluate the applicability of four statistical methods (Frequency Ratio (FR), Shannon Entropy (SE), Information Value (IV) and Weight of Evidence (WofE)) to map landslide susceptibility in part of the Kullu tehsil of the Kullu district using a compiled landslide inventory from acquired historical data and newly mapped landslide using remote sensing and earth observation techniques. Fig. 4.1 gives an outline of the adopted methodology.

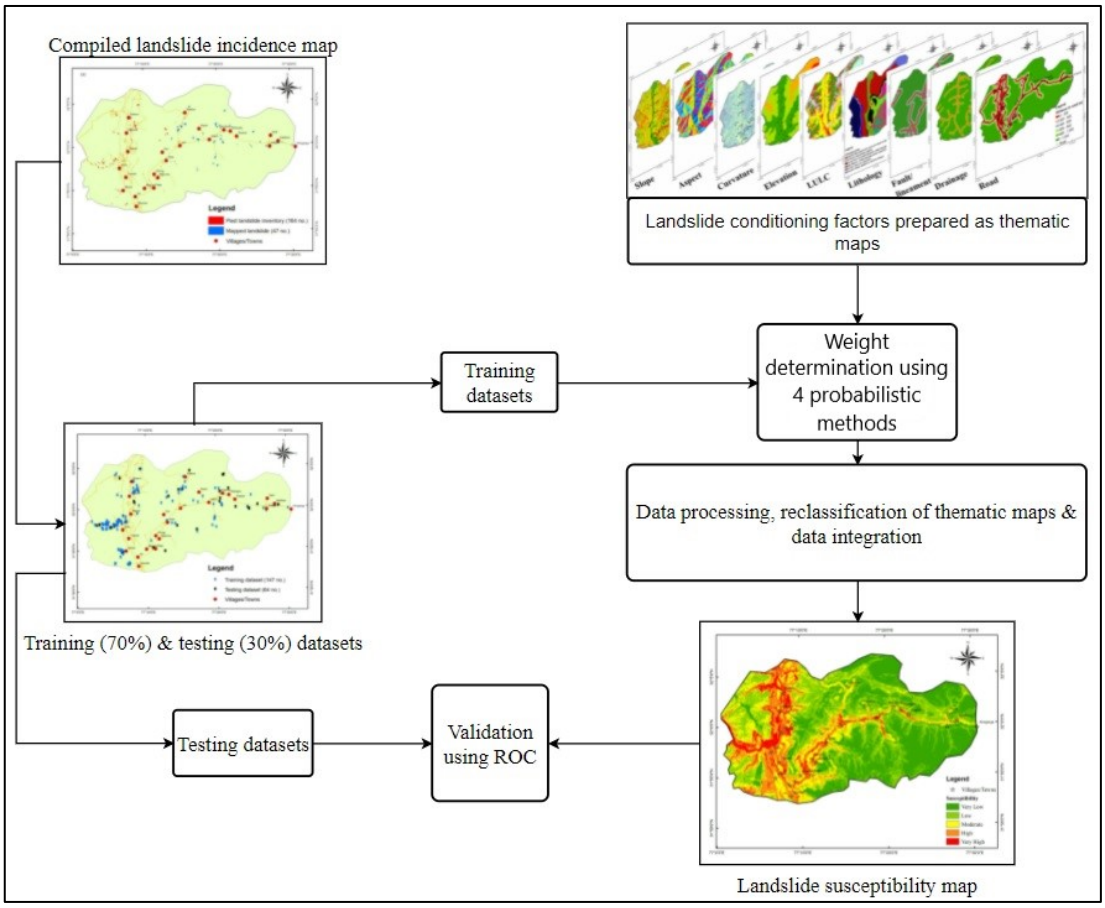

Fig. 4.1 General research methodology

The main pillar for a data-driven landslide susceptibility evaluation model is a landslide incidence map depicting the past and most recent sliding events in the area. Inadequacy or incompleteness of landslide inventory may cause serious setbacks in terms of model fitness and may also influence the model's prediction accuracy. Susceptibility analysis is incomplete without the identification and processing of the factors responsible for sliding events in the area under investigation. The review of literature allowed the author to carefully analyse, compare, evaluate and choose the proper sets of methods and causative factors most applicable to the region beforehand. The correlation between each factor and past sliding events can give an indication on the causality of landslides and to better understand the mechanisms of those slope failures. Fitness and accuracy evaluation are needed to validate the model from data-related uncertainties and errors.

The adopted landslide susceptibility evaluation procedure can be classified as:

a) Selection of landslide-inducing factors for the area
b) Generation of thematic layers for the chosen factors
c) Preparation of a new landslide incidence map
d) Compilation of newly mapped and historical landslide data
e) Application of the bi-variate probabilistic FR, SE, IV and WofE methods to calculate ratios for every factor classes and factor maps.
f) Landslide Susceptibility Maps (LSM) creation and classification
g) Model validation and comparison through:
    i. Landslide Density Index (LDI) evaluation
    ii. Area Under Curve (AUC) of ROC

4.2 Data used

The various data used for this research were collected from various departments/organisations and processed in a Geographic Information System (GIS) environment for further analysis. The main software used were ESRI ArcGIS platform, Microsoft Word and Microsoft Excel. The primary data required for statistical analysis were the landslide incidence map and thematic maps for the chosen causative factors. The underlying principle was to gather as much information available for the study area, both

for analysis and for better understanding of localised landslide scenarios. Nine landslide-inducing parameters were therefore selected based on past literatures, author's understanding of the region and data availability. These factors (Slope, lithology, aspect, elevation, curvature, roads, drainage, faults/lineaments, land use/land cover) were all assumed to have an association to past sliding activity, in turn contributing to prediction of future slides in the region.

The data used and their respective sources are given in Table 4.1 below:

Table 4.1 Data used and their various sources

Data used	Source
CartoSAT-1 DEM (30m resolution)	Bhuvan web-platform, Indian Space Research Organisation (ISRO), National Remote Sensing Centre (NRSC), Hyderabad
Landsat-8 OLI/TRS images (Cloud cover <10%)	Earth Explorer web-platform, United States Geological Survey (USGS)
Road map	Open Street Map website
Faults/lineaments	Bhukosh web-platform, Geological Survey of India (GSI)
Lithology	
Historical landslide data	

The Digital Elevation Model (DEM) acquired freely as CartoSAT-1 DEM from Indian Space Research Organisation (ISRO) is a raster file (TIFF) having 1 arc-second (30 m) spatial resolution, which was used to derive several topographical factor maps such as slope, aspect, curvature and elevation for further processing. The preparation of the various thematic maps derived from the DEM as well as other sources were described in the sections below.

4.3 DEM pre-processing

The study area falls at the intersection of two DEM layers namely, 'i43x' and 'h43f'. The adopted technique was using the Data Management tool, 'Mosaic To New Raster' to merge the two raster datasets into one merged raster file. One of the advantages of using this tool is the availability of a 'Mosaic Operator' which allows the user to opt

for the method of handling overlapping of raster datasets such as the First, Min, Max, Blend or Mean options for tackling overlapping cell values. Additionally, pixel type/cell size and number of bands can be optionally chosen based on the user's criteria and the input data properties.

The next step consisted of generating a shape file for the study area which could be in turn used to clip the DEM to the required extent. The area was mapped on Google Earth Pro software and exported as a Keyhole Markup Language (KML) file and later converted to the required shapefile (SHP) format in ArcMap using the Conversion tools. The shapefile is then imported for the clipping procedure.

'Extract by mask' tool was used to clip the shapefile extent to the processed DEM. This process preserves the 'NoData' values if any, and care should be taken as to that the two files are in the same geographically projected coordinated systems which in this case was the Universal Transverse Mercator (UTM) projection with spheroid WGS 84 North Zone 43.

4.4 DEM derivatives

A digital elevation model is usually created from known cell elevation points for terrain relief variation representation, for derivation of several topographical factors explaining those variations and for elevation-related calculations/operations. Some popularly DEM derived relief-defining factors are slope, aspect and curvature which have been considered for analysis by various researchers as landslide inducing factors [47].

4.4.1 Slope

A slope map depicts the inclination angles of prevalent slopes in an area and directly relates to slope instability [48]. A rise in slope angle will generally result in a decrease in stability of slopes. Slope steepness is expressed in percent rise or degrees and has some effect on surface runoff [10]. The slope factor map was derived from the CartoSAT-1 DEM using spatial analyst surface tool of the GIS software. The resulting map was reclassified using the reclassifying tool into five distinct categories namely, 0° - 14°, 15° - 24°, 25° - 33°, 34° - 45° and > 45° as in Fig. 4.2.

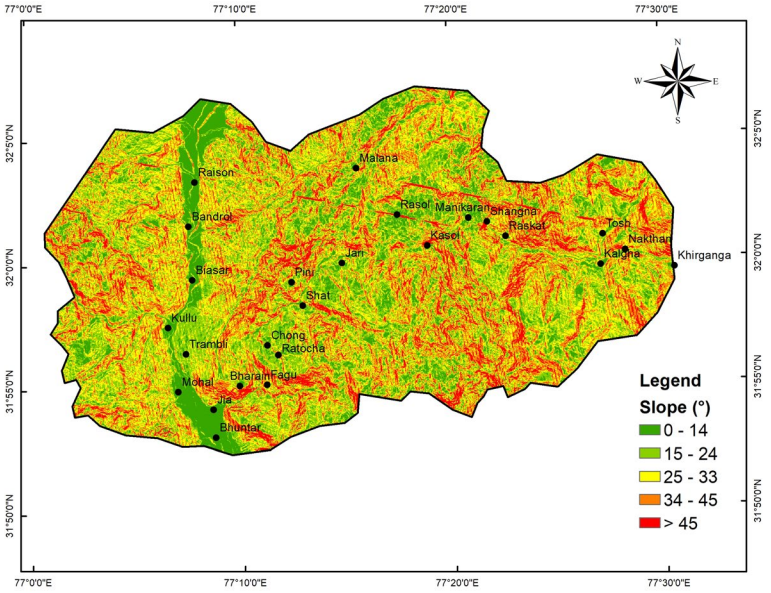

Fig. 4.2 Slope map

4.4.2 Aspect

The directions of slopes are calculated and classified from the DEM clockwise starting North at 0° back to North at 360° using the spatial analyst aspect tool in the GIS software. The flat areas have no aspect since they have negligible (< 5°) slopes and they are denoted by grey cells having value -1 as in Fig. 4.3.

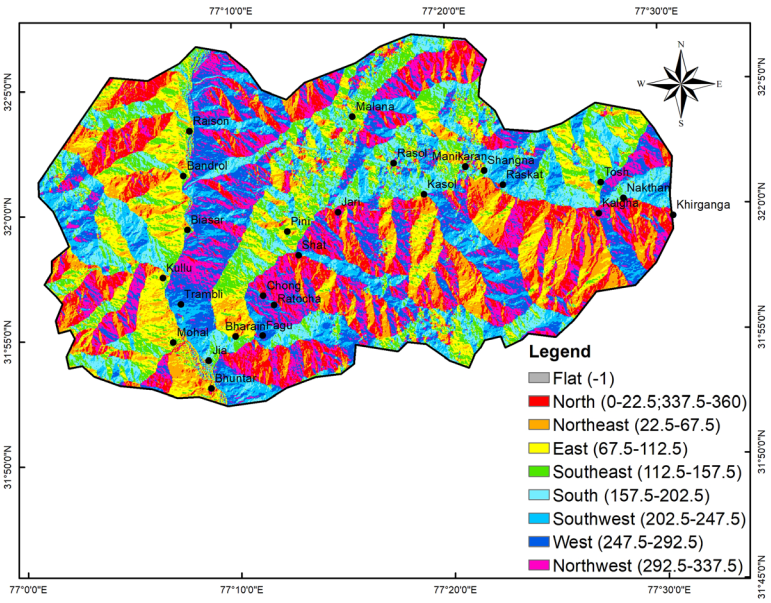

Fig. 4.3 Aspect map

The orientation that a slope faces, has an impact on many processes along that particular slope; most importantly, the amount of sunlight, rainfall and wind exposure which in turn affects vegetation type, vegetation growth and soil moisture index among others [49].

4.4.3 Curvature

The curvature map was derived from the DEM using the spatial analyst curvature tool to determine the degree of convexity/concavity/recti-linearity of surfaces, defined as the geometries of a sloping face [10] which in turn influences the acceleration/deceleration rate of surficial flows.

The resulting map has three distinct classes with negative values (< -0.05) for convex surfaces, positive values (> 0.05) for concave surfaces and near zero values (-0.05 – 0.05) for rectilinear surfaces as in Fig. 4.4.

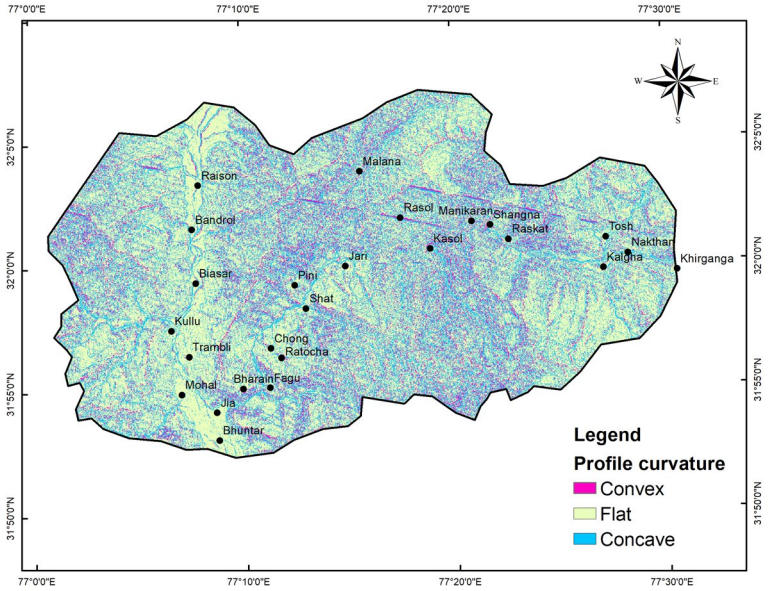

Fig. 4.4 Profile curvature map

The reason for concavity/convexity being attributed to higher landslide occurrences is the simple reason that rainfall infiltration takes longer, thereby having a more profound effect on slope instability [50].

4.4.4 Elevation

For the preparation of elevation map, contour lines were first generated from the DEM which were then used to create Triangulated Irregular Networks (TIN) through triangulation of vertices by employing 3D analyst conversion tools in the GIS platform before being reclassified into the final elevation raster layer. The four classes of the raster were 1,050 – 2,000 m, 2,000 – 3,000 m, 3,000 – 4,000 m and 4,000 – 4,900 m as in Fig. 4.5.

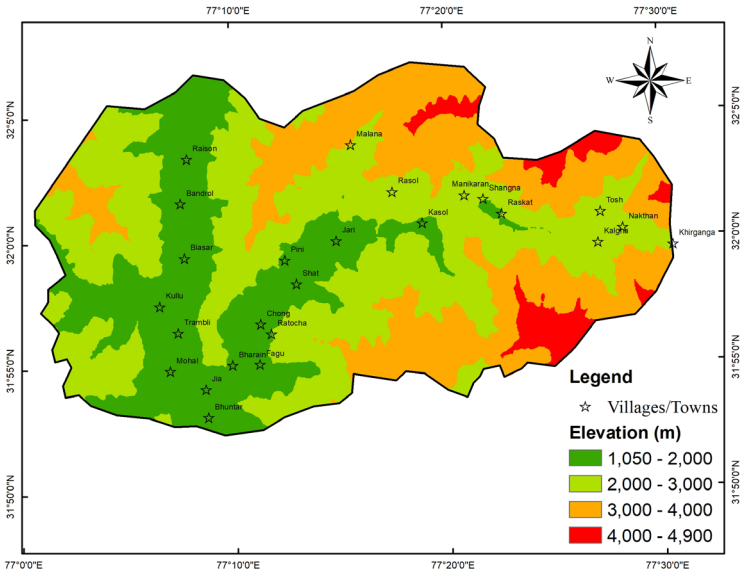

Fig. 4.5 Elevation map

Upon viewing of the elevation classes and the villages/towns in the area, it can be noticed that most human settlement are restricted to lesser elevated areas (< 4,000 m). Also, the all-year presence of snow/glaciers, lesser vegetation extent, unavailability of fertile land and harsh climatic conditions discouraged human intervention in the most elevated class (> 4,000 m).

Though the elevation factor does not directly contribute to slope instability occurrences, it does affect other processes and factors such as vegetation type, soil moisture, rainfall intensity, temperature, wind exposure, etc which in turn can be related to mass movements.

4.4.5 Distance to drainage

Drainage has been identified as being a factor responsible for mass movements due to toe under-cutting and bank erosion in overflow conditions [43]. Most of the road network in the area is concentrated along the main rivers/streams in the area, turning transportation corridors along the mountainous areas of Himachal Pradesh into landslide hotspots. The influence of the drainage on slope instability must hence be evaluated in terms of their closeness to past slope failure events.

The river/stream networks in the area were derived from the DEM using the hydrology tools in the GIS platform. The basis of this toolset is to model waterflow across a surface and comprises of several tools that can be collectively utilized to determine river networks in an area as well as delineating watersheds. Flow direction tool is used to determine water outflow orientation from individual cells of the DEM, followed by filling of imperfections using Fill tool after their identification using Sink tool for appropriate mapping process. This output is then processed using Flow Accumulation tool before determining the stream networks in the study area by using the Stream Order tool by selecting the appropriate threshold value and ordering method as in Fig 4.6.

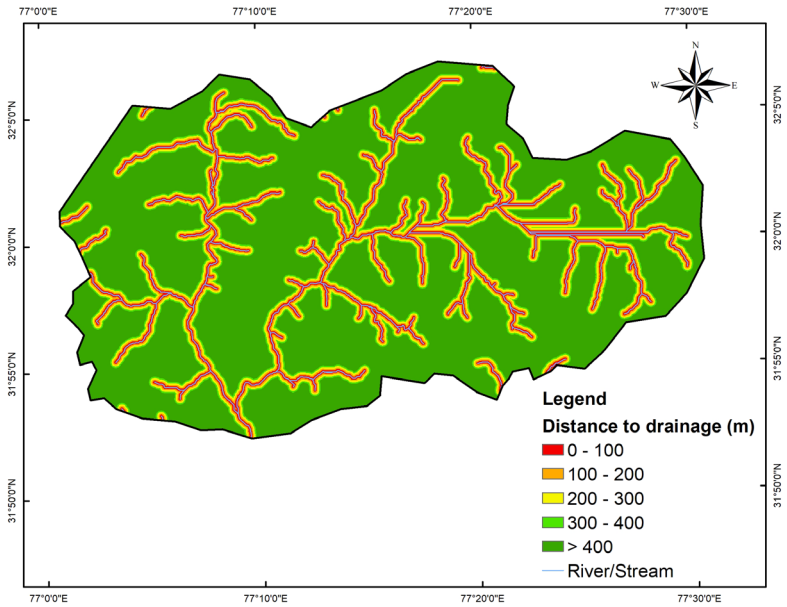

Fig. 4.6 Distance to drainage map

4.5 Other prepared thematic layers

The following thematic layers were extracted using data from other sources. They were also chosen to evaluate their relationship to slope instability in the region.

4.5.1 Distance to roads

Himachal Pradesh has witnessed several slope failures along road corridors since most of the roads in hilly/mountainous terrains need to be built by face cutting, blasting methods, etc. Several factors complicate the process of road construction and widening such as presence of steep gradients along road alignment, geological structure anomalies, presence of faults, presence of drainage sources. The very action of altering a slope profile de-stabilises both the stable slopes and slopes on the verge of failure in the area. Additionally, changing of drainage patterns due to road construction is one issue which cause future slope instabilities in neighbouring areas since the changed pattern now affects another area maybe un-exposed to such drainage patterns [34]. Therefore, the influence of distance to roads to landslide occurrences needed to be investigated.

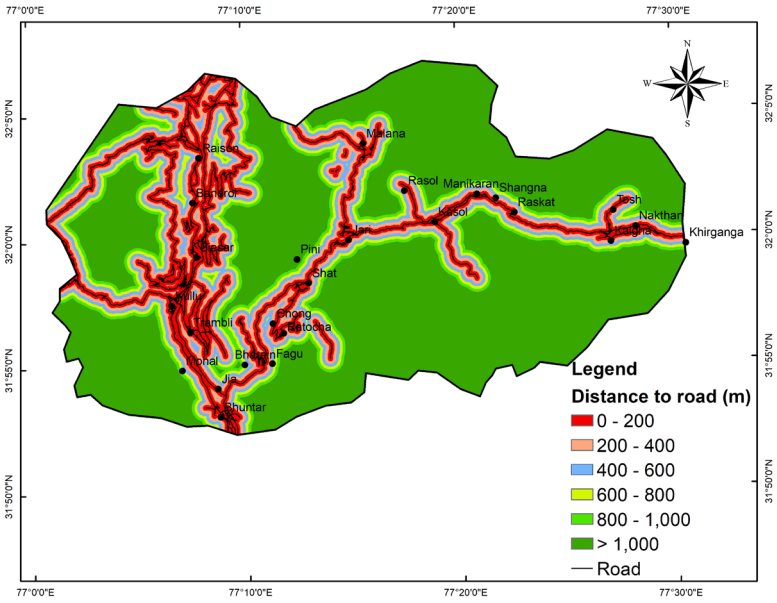

Fig. 4.7 Distance to road map

The major roads in the area consist of national highway, major district roads and local distributary roads. The road shape file was downloaded from the Open Streets Map website and verified before rasterizing into 30 m cell resolution and reclassified with

200 metres buffering intervals resulting into six categories namely 0 – 200 m, 200 – 400 m, 400 – 600 m, 600 – 800 m, 800 – 1,000 m and >1,000 m as in Fig. 4.7.

4.5.2 Distance to faults/lineaments

The inhomogeneities and discontinuities encountered in faulted and fractured regions might reduce the stability and strength of slopes, and as a result, increase the likeliness of having landslide events in those neighbourhoods [51]. The relationship between these structural elements and landslide distribution needs to be assessed to find out whether this geo-mechanical relationship increases the vulnerability of slopes.

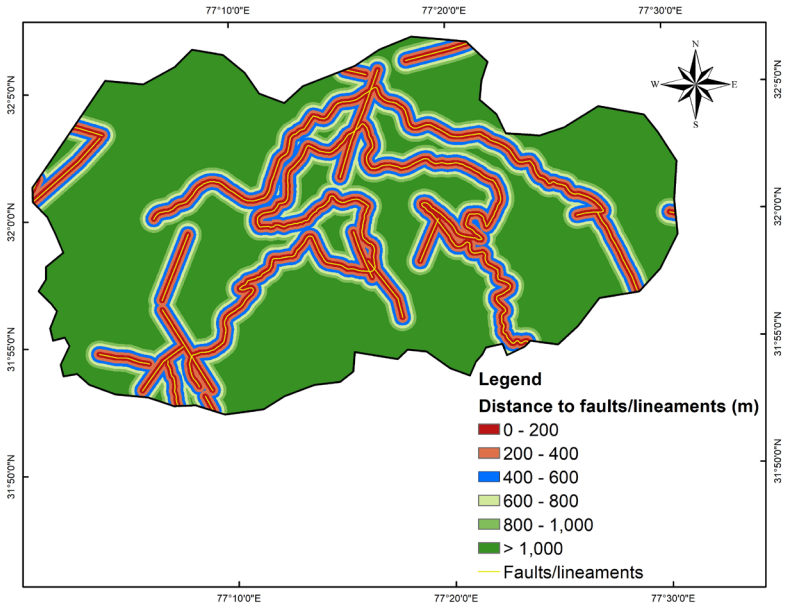

Fig. 4.8 Distance to faults/lineaments map

The shape files for faults and lineaments were individually obtained from Bhukosh web-platform of the Geological Survey of India (GSI) and later merged into one shape file containing both structural discontinuities since this study considered assessing both their influence on mass movements. The buffer tool of the GIS platform was used to delineate the area into 200 metres intervals from faults and lineaments and the resulting layer was rasterized in 30 m cell resolution. Reclassification of this layer gave six sub-categories namely 0 – 200 m, 200 – 400 m, 400 – 600 m, 600 – 800 m, 800 – 1,000 m and > 1,000 m as shown in Fig. 4.8.

4.5.3 Lithology

The difference in structure, strength, composition and plasticity potential of each litho-stratigraphic units [37] is the main reason behind evaluating the relationship between the various lithological components in a study area and past land sliding events.

The lithology shape file was acquired from the Bhukosh web-platform of the Geological Survey of India (GSI), extracted to fit the study area, rasterized and resampled to 30 m cell resolution featuring a total of thirteen units as shown in Fig. 4.9.

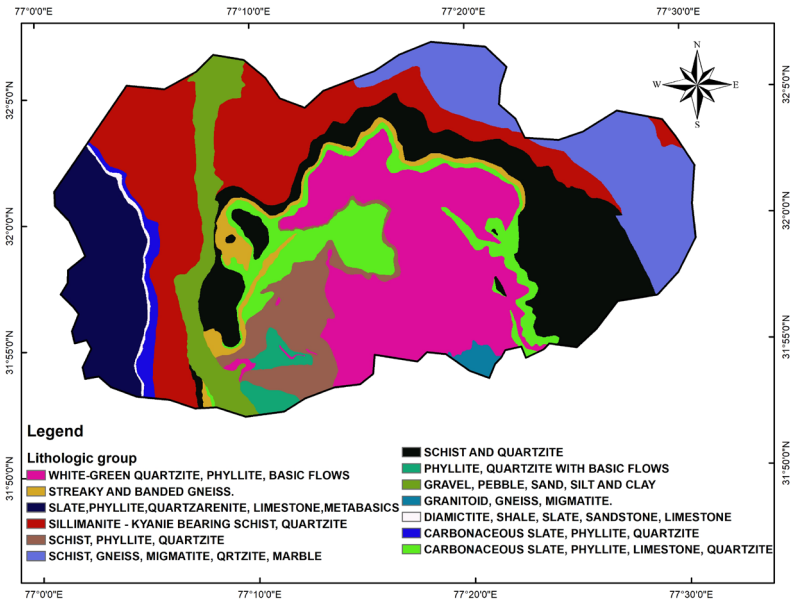

Fig. 4.9 Lithology map

4.5.4 Land Use/Land Cover (LULC)

Land use/land cover (LULC) is basically used to depict the various natural land surface types along with the various anthropogenic uses of these land types [44]. For the purpose of preparing the LULC map, Landsat 8 Operational Land Imager (OLI)/Thermal Infrared Sensor (TRS) images taken in October 2017 with cloud cover less than 10% were acquired from the Earth Explorer web-platform of the United States Geological Survey (USGS) Earth Explorer. Landsat 8 images are multi-band raster files, comprising of nine bands, the various combinations of which, result in visualizing relevant information (vegetation analysis, hydrological and settlement analysis among others) according to user's requirements and can be classified mainly by either supervised

or unsupervised classification. The main difference between the two classification methods is the absence/presence of the analyst's intervention in providing spectral signatures.

Firstly, training of samples using the 'Training sample manager tool' from the Image Classification toolbar was necessary in case of supervised classification, as was chosen in this case; involving selection of areas with specific reflectance values as training samples to be later merged and used for better delineation of the different land uses by the algorithm chosen. The interactive supervised classification tool was used to check classification result for each category. An average of 10-15 samples were selected, analysed using scatterplots for distinct patterns, merged for each category and saved as signature files which was then fed into the Maximum Likelihood Supervised Classification algorithm for final map production. The five resulting classes of the LULC are Built-up area, Agricultural Land, Barren Land, Forest (Evergreen, Deciduous), Snow/Glaciers and Water bodies as depicted in Fig. 4.10 below.

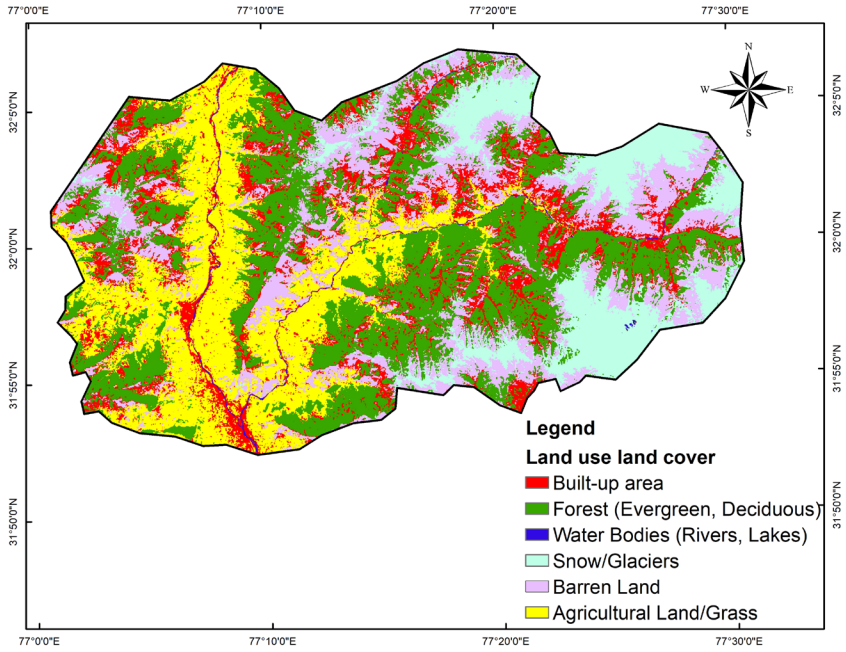

Fig. 4.10 Land Use/Land Cover (LULC) map

4.6 Landslide Inventory map

The basis of any landslide susceptibility/hazard/risk analysis is the process of identifying and mapping previous landslides in the form of landslide inventory/incidence maps, and the approaches for this process are diverse and still expanding. For the purpose of this study, a compilation of both historical incidence map and a newly created inventory has been carried out for a better depiction of the actual landslide distribution in the area. A detailed breakdown of these processes has been presented in the following sections.

4.6.1 Historical landslide incidence map

The historical data for past sliding events for the state of Himachal Pradesh was acquired from Geological Survey of India (GSI) as polygon shape file, which was later clipped to cover the Area of Interest (AOI). The compiled data contains detailed information about past slides such as geographical coordinates, sliding dates, types of slide, land use/land cover associations, etc. Five main types of slides mapped in the region before were rotational, translational, falls, topples and debris flows. The adopted methodology in this study does not account for specific types of slide occurrences in the area and their specific causes, but rather encloses all landslide types in one group to be analysed with the inducing factors using the frequency ratio approach. However, the types of sliding events and their characteristics gave insight behind mechanisms of past events and the selection of causative factors for susceptibility analysis in this region specifically.

4.6.2 Landslide Mapping

The basic mapping of landslide scars in the study area was done through visual interpretation of high-resolution satellite imageries from Google Earth Pro software for the years 2002-2019. The idea behind creating a new inventory was the lack of historical data in the Parvati valley side, instead, clustering of data was observed around the Kullu-Bhuntar area. The Parvati valley has been victim of an increasing number of slope failure incidents, especially in the road corridors and riverbanks, with many of those events unreported or unmapped. Identification and mapping of landslide scars through visual interpretation of Google Earth historical images is done through

mainly identification of change in vegetation cover, presence of debris material and other scarped features [52].

Landslide scars can be rapidly lost or obscured with time due to several reasons such as excess vegetation veiling the scarred features, rapid remediation works after an event, etc. Use of the Scarp Identification and Contour Connection Method (SICCM) toolbox extension of the GIS platform was done to aid in semi-automatically delineating some obscured landslide scarred features [17] before proceeding with final mapping as landslide polygons in Google Earth Pro software.

The module uses as input the area's high-resolution DEM and progresses into creating hill-shade, slope, resampled DEM, stream order and other factor maps with chosen cell size for better demarcation and interpretation of scarps. The tool has also been a great aid in identifying rocky outcrops and to delineate non-scarps from scarped features. Unavailability of higher resolution DEM limits the user in generating better and more accurate results. Hence, this method was employed as an indication of potential landslide sites where the scarped features were not clearly delineated due to vegetation and quick remediation works after slide event by local authoririties.

The final mapping of landslide polygons on Google Earth pro was done using the polygon drawing tool and the mapping was done as such, as to cover the head, toe and the lateral extent (spread) of every landslide event to ensure proper analysis as shown below in in Fig. 4.11 and Fig. 4.12 for the identification and mapping of two landslide incidents near Tosh and Manikaran respectively. Landslide mapping process is time consuming and requires usage of other tools from the Google Earth Pro software such as consultation of multi-temporal images, usage of sun exposure settings among others for better image interpretation and contrasting purposes.

The polygons were then exported as a Keyhole Markup Language (KML) file, converted to shape file (SHP) in the GIS environment before resampling them to a 30 x 30 m cell resolution for overlaying process.

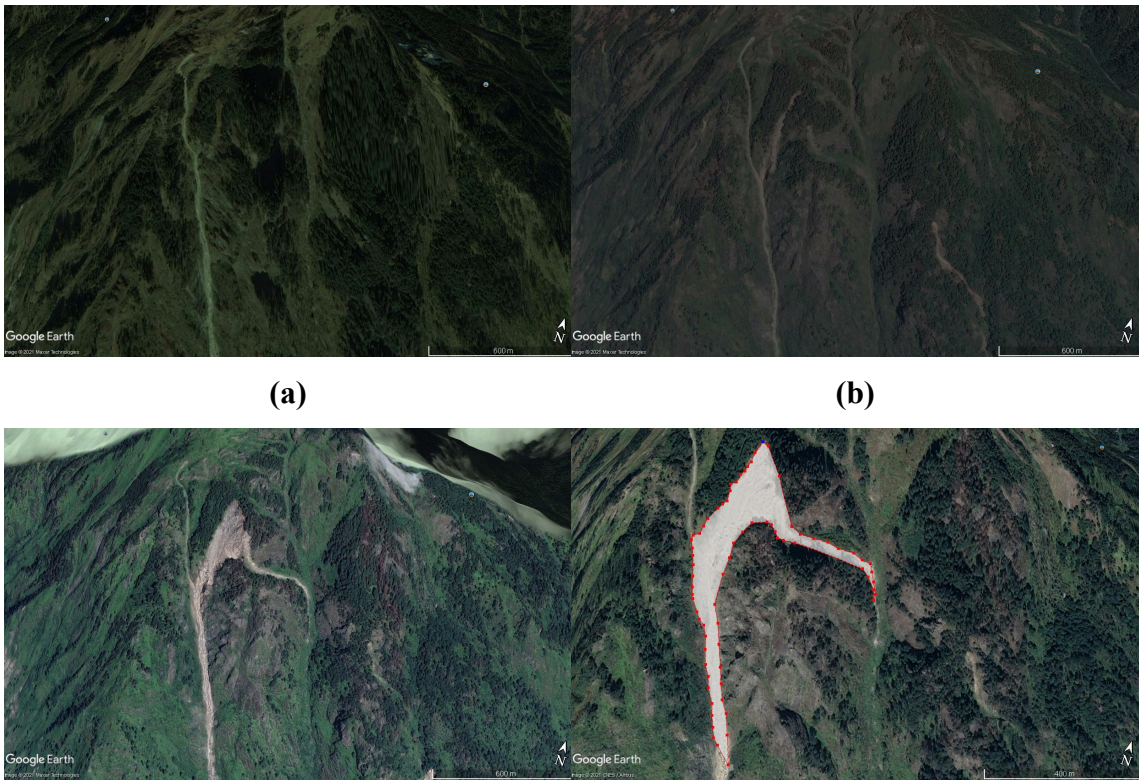

Fig. 4.11 Landslide identification and mapping near Tosh (a) before slide (11.2010) (b) landslide initiation (06.2014) (c) Identification of sliding (09.2017) (d) Final mapping of landslide features carried out in Google Earth Pro

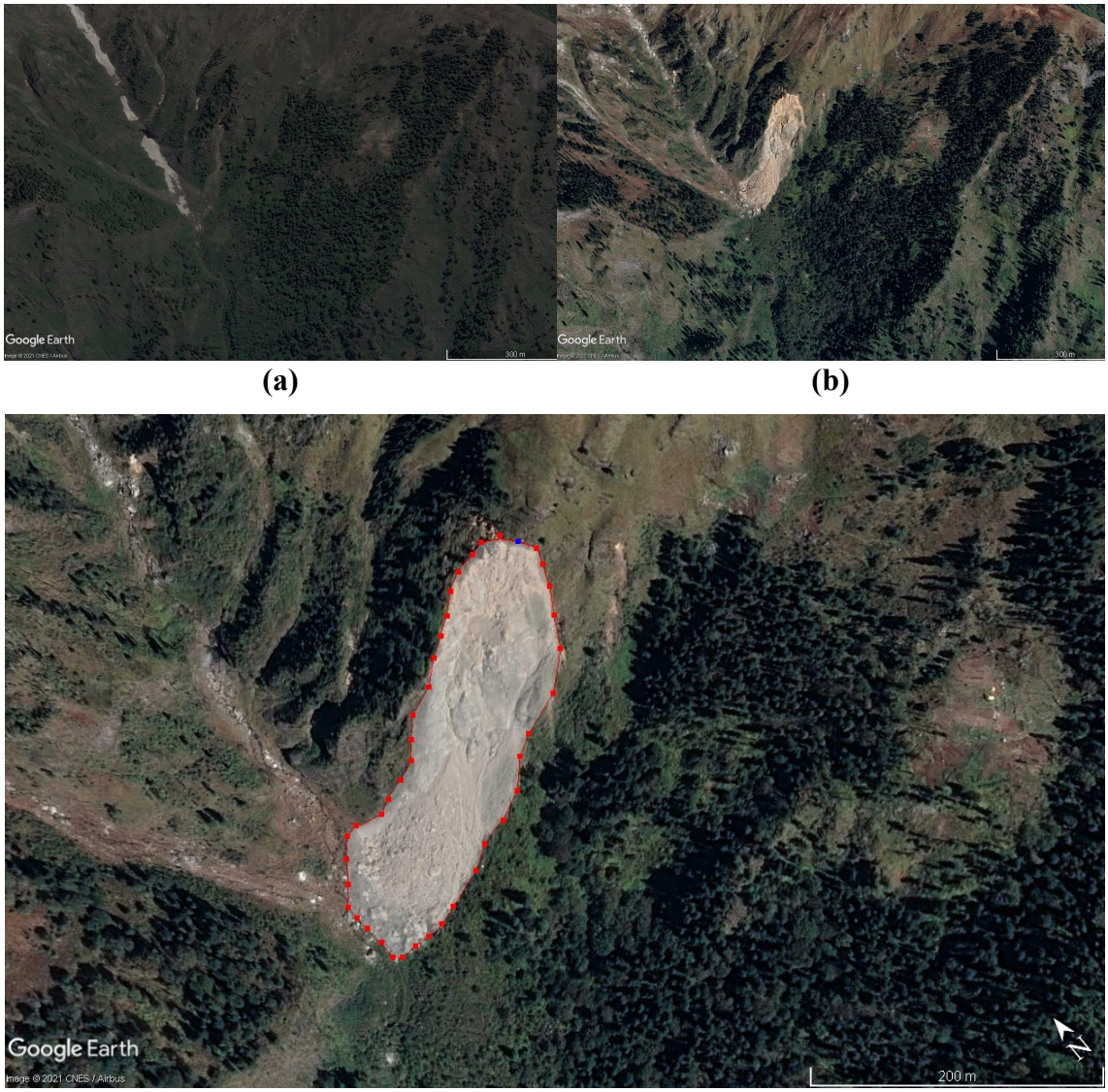

Fig. 4.12 Landslide identification and mapping near Manikaran (a) before slide event (06.2014) (b) identification of landslide (10.2017) (c) final mapping of landslide features (head,side scarps and debris run-out)

The 30 x 30 m cell resolution was the adopted cell size for all thematic map layers generation as well as the landslide incidence data for statistical and overlaying analysis. The total number of mapped landslides were 47 whereas the acquired historical landslide data contained 164 mapped polygons, resulting in a total of 211 total polygons for the study area as in Fig. 4.11.

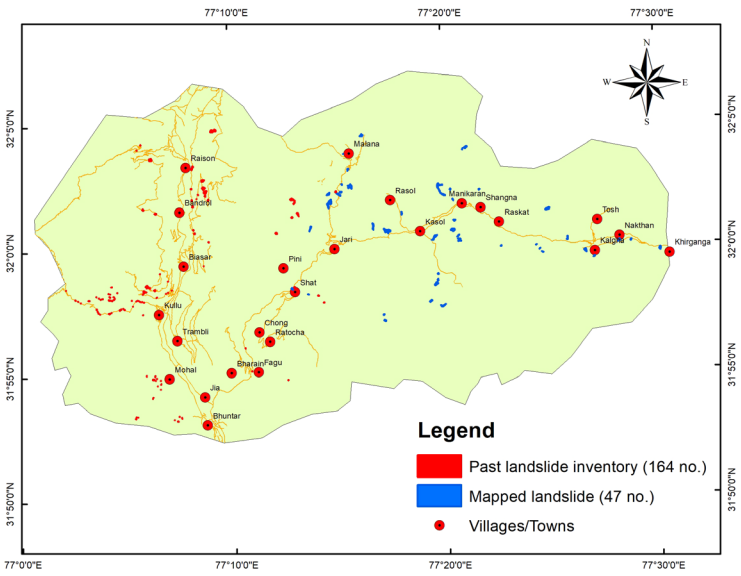

Fig. 4.13 Compiled landslide inventory map

4.6.3 Random splitting of samples

Random splitting of past landslide samples was carried out mainly because of missing multi-temporal incidence data. The geostatistical analyst tool of the GIS platform was used to randomly split the 211 samples into 70% (147 nos.) as training samples and 30% (64 nos.) as validating samples as shown in Fig. 4.12.

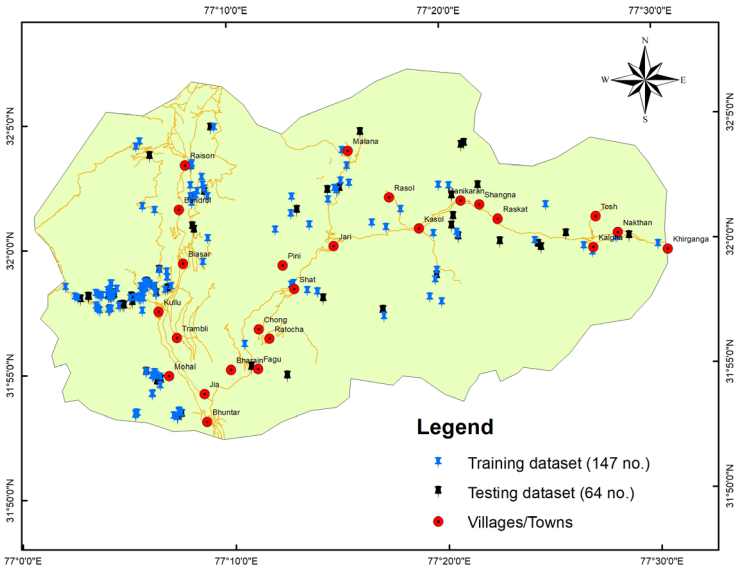

Fig. 4.14 Training and testing datasets

Ground truthing of newly mapped landslide locations were not carried out due to location remoteness and travel limitation. However, images of some recent landslide events along and around the road corridors were taken during a recent trip to the study area. Many slides were noticed along the road corridor between Manirakan and Barshaini, and with recent rise in tourism in the area, the region is only like to become more and more vulnerable to slope failures.

CHAPTER 5
ADOPTED PROBABILITY APPROACHES: CONCEPTS AND COMPUTATION RESULTS

5.1 Concepts behind adopted probabilistic methods

One of the key components of this research work involved the usage of different statistical methods along with past landslide incidence dataset to evaluate the area's propensity to land sliding with nine selected influencing parameters. The algorithm and data analysis procedures of all the four models differ from one another; a deeper insight of which, enable the user to extract valuable information between variables involved and to establish relevant relationships between the causes and effect of landslides. The final part of this work consisted of using these established relationships to better explore the underlying mechanisms behind the different factors responsible for slope instability as well as to better predict these disastrous events.

For this purpose, the concepts behind the four adopted quantitative methods have been presented in the sections below.

5.1.1 Frequency Ratio (FR) concept

The FR method is an observation-driven bi-variate probabilistic approach that is directly based on the association of past data to considered factors for weight evaluation. This method has been effectively employed and validated by several researchers directly associating past landslide data to selected causative factors [50]. Their high dependency on past landslide data for accurate predictive capability made them less popular in areas having poor landslide data, or few past landslide events data.

Nevertheless, it remains one of the simplest and most popular data-driven approaches adopted widely in landslide susceptibility mapping and has been successfully put into practice, compared with other models and validated by various researchers [29] [30] [35] [37] [41] [53].

Bi-variate approaches such as FR do not account for the relative weights between causative factors unlike multi-variate approaches but rely on direct spatial association of each factor to landslide occurrences [21].

The FR values were computed using the Equation 5.1.

$$FR = \frac{P_L \Big/ \sum_{i=1}^{n} P_L}{P_C \Big/ \sum_{i=1}^{n} P_C} \tag{5.1}$$

Following this calculation, the factor maps were reclassified using the resulting FR values for data integration purposes as outlined in Chapter 6. The final landslide susceptibility index (LSI) for this approach was computed through the Raster Calculator tool using Equation 5.2.

$$LSI_{FR} = \Big(FR_{Slope} + FR_{Aspect} + FR_{Curvature} + FR_{LULC} + FR_{Lithology} + FR_{Elevation} + FR_{D_{Road}} + FR_{D_{Drainage}} + FR_{D_{Faults\ /lineaments}}\Big) \tag{5.2}$$

5.1.2 Shannon Entropy (SE)

Originally developed based on the Boltzmann principle for statistical thermodynamic entropy evaluation, Shannon further developed an entropy model for information theory application [54]. It can be used for imbalance, disorderliness and uncertainty quantification of landslide events [48] which due to their complex nature, can be taken as entropy values under factor classes [55].

This method has been used and validated in several landslide susceptibility analyses for weight calculation [51] [56] [36] using the following equations.

P_{ij} in Equation 5.3 represents the frequency ratio value for each class whereas (P_{ij}) in Equation 5.4 denotes the probability density for each class.

$$P_{ij} = \frac{\%\ landslide\ pixels}{\%\ class\ pixels} \tag{5.3}$$

$$(P_{ij}) = \frac{P_{ij}}{\sum_{j=1}^{n_j} P_{ij}} \tag{5.4}$$

H_j and $H_{j_{max}}$ represent the entropy values for each class with n_j denoting the number of classes in each selected parameter.

$$H_j = -\sum_{i=1}^{n_j} (P_{ij}) \log_2 (P_{ij}) \tag{5.5}$$

$$H_{j_{max}} = \log_2 n_j \tag{5.6}$$

The information coefficient, defined by I_j, is then determined using Equation 5.7.

$$I_j = \frac{H_{j_{max}} - H_j}{H_{j_{max}}} \tag{5.7}$$

The final weight indexes, W_j for each of the nine parameters were calculated as per Equation 5.8.

$$W_j = I_j \times P_j \tag{5.8}$$

The final landslide susceptibility index (LSI) for this approach was computed through the Raster Calculator tool using Equation 5.9.

$$\begin{aligned} LSI_{SE} = \big(&P_{ij} * W_{Slope} + P_{ij} * W_{Aspect} + P_{ij} * W_{Curvature} + P_{ij} * W_{LULC} + P_{ij} * W_{Lithology} \\ &+ P_{ij} * W_{Elevation} + P_{ij} * W_{D_{Road}} + P_{ij} * W_{D_{Drainage}} \\ &+ P_{ij} * W_{D_{Faults\ /lineaments}} \big) \end{aligned} \tag{5.9}$$

5.1.3 Information Value (IV)

The Statistical Index or Information Value method also known as the InfoVal approach is a widely adopted Bayes conditional probability model applied by many researchers like Singh et al. [55], Kumar et al. [37], Versain [57], Sharma and Mahajan [58], in landslide susceptibility mapping studies.

It can be defined as the natural logarithm of the ratio of landslide occurrence in a particular class to the ratio of landslide occurrences in the whole study area [59]. Equation 5.12 is used to evaluate the information values as the natural logarithm of the ratio of conditional probability (computed as per Equation 5.10) to prior probabilities (computed as per Equation 5.11).

$$P_{Conditional} = \frac{N_{Landslide\ pixels}}{N_{Class\ pixels}} \tag{5.10}$$

$$P_{Prior} = \frac{N_{Total\ landslide\ pixels}}{N_{Total\ class\ pixels}} \tag{5.11}$$

$$Information\ Value, IV = \log_e \left[\frac{P_{Conditional}}{P_{Prior}}\right] \tag{5.12}$$

Positive information values (IV > 0) indicate high correlation to landslide occurrences while negative information values (IV < 0) indicate the contrary. The final landslide susceptibility index (LSI) for this approach was eventually computed through the Raster Calculator tool using Equation 5.13.

$$LSI_{IV} = \left(IV_{Slope} + IV_{Aspect} + IV_{Curvature} + IV_{LULC} + IV_{Lithology} + IV_{Elevation} + IV_{D_{Road}} + IV_{D_{Drainage}} + IV_{D_{Faults\ /lineaments}}\right) \quad (5.13)$$

5.1.4 Weight of Evidence (WofE)

Originally developed as a Bayesian conditional probability model for medical diagnosis, the Weight of Evidence (WofE) method found its way to spatial applications like mineral potential mapping [60], [61]. This approach has been applied and validated by several researchers in mapping landslide susceptibility as well [62]- [63], [12].

The positive and negative weights for each influencing factor are evaluated based on the presence (S) or absence ($\bar{S}$) of landslide events as per Equations 5.14 and 5.15 respectively with the presence or absence of factor class denoted as B and $\bar{B}$.

$$W_i^+ = \log_e\left[\frac{P(B|S)}{P(B|\bar{S})}\right] \quad (5.14)$$

$$W_i^- = \log_e\left[\frac{P(\bar{B}|S)}{P(\bar{B}|\bar{S})}\right] \quad (5.15)$$

After re-writting the equations in terms of pixel contributions, the Equations 5.16 and 5.17 were used for weights evaluation.

$$W_i^+ = \log_e \left[\frac{\left(\frac{N_p^1}{N_p^1 + N_p^2} \right)}{\left(\frac{N_p^3}{N_p^3 + N_p^4} \right)} \right] \quad (5.16)$$

$$W_i^- = \log_e \left[\frac{\left(\frac{N_p^2}{N_p^1 + N_p^2} \right)}{\left(\frac{N_p^4}{N_p^3 + N_p^4} \right)} \right] \quad (5.17)$$

Where,

N_p^1 = number of pixels with landslides in the factor class

N_p^2 = number of pixels with landslides outside factor class

N_p^3 = number of pixels without landslides in the factor class

N_p^4 =number of pixels without landslides outside factor class

The significance of the calculated positive and negative weights can be further evaluated by their variances $S^2(W^+)$ and $S^2(W^-)$ using the Equations 5.18 and 5.19 respectively.

$$s^2(W^+) = \frac{1}{N\{B \cap S\}} + \frac{1}{N\{B \cap \bar{S}\}} \quad (5.18)$$

$$s^2(W^-) = \frac{1}{N\{\bar{B} \cap S\}} + \frac{1}{N\{\bar{B} \cap \bar{S}\}} \quad (5.19)$$

The degree of correlation between each factor class and slide events is better represented by the contrast values, C which is computed as per Equation 5.20.

$$C = W^+ - W^- \quad (5.20)$$

While zero values obtained for C denote zero or unidentified correlation with any slide events, positive and negative contrast values signify favourable and unfavourable spatial correlations respectively [64]. The standard deviation for the calculated contrast values can be evaluated from the variances of the obtained weights using the Equation 5.21 below.

$$s(C) = \sqrt{s^2(W^+) + s^2(W^-)} \tag{5.21}$$

The studentized contrast value, C_s is finally calculated as a ratio of a contrast value (C) to its respective standard deviation S(C) as per Equation 5.23 [34].

$$C_s = \frac{C}{s(C)} \tag{5.22}$$

It is used as a means to signify the relative certainty of the obtained posterior probability [65]. The final landslide susceptibility index (LSI) for this approach was computed through the Raster Calculator tool using Equation 5.23.

$$LSI_{WofE} = \left(C_{Slope} + C_{Aspect} + C_{Curvature} + C_{LULC} + C_{Lithology} + C_{Elevation} + C_{D_{Road}} + C_{D_{Drainage}} + C_{D_{Faults\ /lineaments}}\right) \tag{5.23}$$

5.2 Computation results

The computation of weight values for every class of every factor map gives an insight about the landslide distribution and about the degree of correlation of each class to landslide occurrences. The results from the Frequency Ratio (FR), Shannon Entropy (SE), Information Value (IV) and Weight-of-Evidence (WofE) probabilistic methods have been presented in tabular form as Table 5.1 to Table 5.4 respectively below. The variation in these weights was then interpreted in graphical formats in the upcoming sections of this chapter.

Table 5.1 FR computation results

Land Use Land Cover	Class pixels	% Class pixels	Landslide pixels	% Landslide pixels	FR
Built up	146846	0.14516	23400	0.17687	1.21842
Forest	308834	0.3053	9900	0.07483	0.24511
Water Body	4629	0.00458	900	0.0068	1.48662
Snow/Glaciers	123809	0.12239	1800	0.01361	0.11116
Barren Land	203861	0.20153	15300	0.11565	0.57385
Agricultural Land/Grass	223609	0.22105	81000	0.61224	2.76974
Slope (°)	**Class pixels**	**% Class pixels**	**Landslide pixels**	**% Landslide pixels**	**FR**
0 – 14	137223	0.12973	5400	0.04082	0.31462
15 – 24	261701	0.24741	18900	0.14286	0.57741
25 – 33	321808	0.30424	44100	0.33333	1.09564
34 – 45	241211	0.22804	49500	0.37415	1.64071
> 45	95810	0.09058	14400	0.10884	1.20164
Aspect	**Class pixels**	**% Class pixels**	**Landslide pixels**	**% Landslide pixels**	**FR**
Flat	87	0.00008	0	0	0
North	64632	0.06111	8100	0.06122	1.00184
Northeast	125781	0.11893	17100	0.12925	1.08678
East	132831	0.1256	20700	0.15646	1.24576
Southeast	121512	0.11489	19800	0.14966	1.30259
South	121435	0.1153	29700	0.22449	1.94696
Southwest	156412	0.11482	14400	0.10884	0.94794
West	156412	0.14789	14400	0.10884	0.73596
Northwest	146739	0.13875	4500	0.03401	0.24515
North	66228	0.06262	3600	0.02721	0.43453
Profile Curvature	**Class pixels**	**% Class pixels**	**Landslide pixels**	**% Landslide pixels**	**FR**
Convex	113351	0.10555	16200	0.12245	1.16009
Flat	669252	0.6232	72900	0.55102	0.88418
Concave	291289	0.27125	43200	0.32653	1.20382
Distance to road (m)	**Class pixels**	**% Class pixels**	**Landslide pixels**	**% Landslide pixels**	**FR**
0 – 200	138618	0.13702	67500	0.5102	3.72347
200 – 400	87959	0.08695	6300	0.04762	0.54768
400 – 600	71444	0.07062	3600	0.02721	0.3853
600 – 800	59745	0.05906	5400	0.04082	0.69112
800 – 1,000	54078	0.05346	11700	0.08844	1.65435
> 1,000	599789	0.59289	37800	0.28571	0.4819
Distance to faults/lineaments (m)	**Class pixels**	**% Class pixels**	**Landslide pixels**	**% Landslide pixels**	**FR**
0 – 200	95610	0.09451	8100	0.06122	0.64781
200 – 400	87818	0.08681	12600	0.09524	1.09711
400 – 600	82262	0.08132	9900	0.07483	0.92024
600 – 800	72002	0.07117	4500	0.03401	0.47789
800 – 1,000	68400	0.06761	11700	0.08844	1.30796
> 1,000	605541	0.59858	85500	0.64626	1.07966
Distance to drainage (m)	**Class pixels**	**% Class pixels**	**Landslide pixels**	**% Landslide pixels**	**FR**
0 – 100	82554	0.0861	15300	0.11565	1.41715
100 – 200	69486	0.06869	18900	0.14286	2.07983
200 – 300	74861	0.074	7200	0.05442	0.73543
300 – 400	61776	0.06107	8100	0.06122	1.0026
> 400	722956	0.71464	82800	0.62585	0.87575
Elevation (m)	**Class pixels**	**% Class pixels**	**Landslide pixels**	**% Landslide pixels**	**FR**
1,050 – 2,000	264717	0.2603	101700	0.76871	0.83979
2,000 – 3,000	430533	0.42335	28800	0.21769	0.14622
3,000 – 4,000	281431	0.27674	1800	0.01361	0.05916
4,000 – 4,900	40277	0.03961	0	0	0
Lithology	**Class pixels**	**% Class pixels**	**Landslide pixels**	**% Landslide pixels**	**FR**
SCHIST AND QUARTZITE	159066	0.15724	8100	0.06122	0.38938
CARBONACEOUS SLATE, PHYLLITE, LIMESTONE, QUARTZITE	74580	0.07372	1800	0.01361	0.18455
CARBONACEOUS SLATE, PHYLLITE, QUARTZITE	13122	0.01297	0	0	0
DIAMICTITE, SHALE, SLATE, SANDSTONE, LIMESTONE	4463	0.00441	0	0	0
SILLIMANITE - KYANIE BEARING SCHIST, QUARTZITE	204013	0.20167	60300	0.45578	2.26007
WHITE-GREEN QUARTZITE, PHYLLITE, BASIC FLOWS	197575	0.1953	18900	0.14286	0.73146
STREAKY AND BANDED GNEISS	23534	0.02326	3600	0.02721	1.16969
PHYLLITE, QUARTZITE WITH BASIC FLOWS	13721	0.01356	0	0	0
SCHIST, GNEISS, MIGMATITE, QUARTZITE, MARBLE	116964	0.11562	2700	0.02041	0.17651
SCHIST, PHYLLITE, QUARTZITE	57587	0.05692	4500	0.03401	0.59752
SLATE, PHYLLITE, QUARTZARENITE, LIMESTONE, METABASICS	87693	0.08668	28800	0.21769	2.51125
GRANITOID, GNEISS, MIGMATITE	5695	0.00563	0	0	0
GRAVEL, PEBBLE, SAND, SILT AND CLAY	53620	0.053	3600	0.02721	0.51338

Table 5.2 SE computation results

							Shannon Entropy (SE)			
LULC	**Class pixels**	**% Class pixels**	**Landslide pixels**	**% Landslide pixels**	P_{ij}	(P_{ij})	H_j	H_{jmax}	I_j	W_j
Built up	146846	0.145164	23400	0.176871	1.21842	0.19023	2.06103	2.58496	0.20269	0.21636
Forest	308834	0.305296	9900	0.074830	0.24511	0.03827				
Water Body	4629	0.004576	900	0.006803	1.48662	0.23211				
Snow/Glaciers	123809	0.122391	1800	0.013605	0.11116	0.01736				
Barren Land	203861	0.201526	15300	0.115646	0.57385	0.0896				
Agricultural Land/Grass	223609	0.221048	81000	0.612245	2.76974	0.43244				
Distance to faults/lineaments (m)	**Class pixels**	**% Class pixels**	**Landslide pixels**	**% Landslide pixels**	P_{ij}	(P_{ij})	H_j	H_{jmax}	I_j	W_j
0 - 200	95610	0.094511	8100	0.061224	0.64781	0.11713	2.51311	2.58496	0.0278	0.02562
200 - 400	87818	0.086808	12600	0.095238	1.09711	0.19837				
400 - 600	82262	0.081316	9900	0.074830	0.92024	0.16639				
600 - 800	72002	0.071174	4500	0.034014	0.47789	0.08641				
800 - 1000	68400	0.067613	11700	0.088435	1.30796	0.23649				
> 1000	605541	0.598578	85500	0.646259	1.07966	0.19521				
Distance to roads (m)	**Class pixels**	**% Class pixels**	**Landslide pixels**	**% Landslide pixels**	P_{ij}	(P_{ij})	H_j	H_{jmax}	I_j	W_j
0 - 200	138618	0.137024	67500	0.510204	3.72347	0.49754	2.05102	2.58496	0.20656	0.25764
200 - 400	87959	0.086948	6300	0.047619	0.54768	0.07318				
400 - 600	71444	0.070622	3600	0.027211	0.3853	0.05148				
600 - 800	59745	0.059058	5400	0.040816	0.69112	0.09235				
800 - 1000	54078	0.053456	11700	0.088435	1.65435	0.22106				
> 1000	599789	0.592892	37800	0.285714	0.4819	0.06439				
Distance to drainage (m)	**Class pixels**	**% Class pixels**	**Landslide pixels**	**% Landslide pixels**	P_{ij}	(P_{ij})	H_j	H_{jmax}	I_j	W_j
0 - 100	82554	0.081605	15300	0.115646	1.41715	0.23191	2.2153	2.32193	0.04592	0.05612
100 - 200	69486	0.068687	18900	0.142857	2.07983	0.34036				
200 - 300	74861	0.074000	7200	0.054422	0.73543	0.12035				
300 - 400	61776	0.061066	8100	0.061224	1.0026	0.16407				
> 400	722956	0.714643	82800	0.625850	0.87575	0.14331				
Slope (°)	**Class pixels**	**% Class pixels**	**Landslide pixels**	**% Landslide pixels**	P_{ij}	(P_{ij})	H_j	H_{jmax}	I_j	W_j
0 - 14	137223	0.129731	5400	0.040816	0.31462	0.06514	2.13695	2.32193	0.07966	0.07696
15 - 24	261701	0.247412	18900	0.142857	0.57741	0.11955				
25 - 33	321808	0.304237	44100	0.333333	1.09564	0.22684				
34 - 45	241211	0.228041	49500	0.374150	1.64071	0.33969				
> 45	95810	0.090579	14400	0.108844	1.20164	0.24879				

Table 5.3 SE computation results (*continued*)

Shannon Entropy (SE)											
Aspect	**Class pixels**	**% Class pixels**	**Landslide pixels**	**% Landslide pixels**	**P_{ij}**	**(P_{ij})**	**H_j**	**H_{max}**	**I_j**	**W_j**
Flat	87	0.000082	0	0	0	0				
North	64632	0.061112	8100	0.061224	1.00184	0.11197				
Northeast	125781	0.118930	17100	0.129252	1.08678	0.12146				
East	132831	0.125597	20700	0.156463	1.24576	0.13923				
Southeast	121512	0.114894	19800	0.149660	1.30259	0.14558	2.99631	3.32193	0.09802	0.14618
South	121944	0.115302	29700	0.224490	1.94696	0.2176				
Southwest	121435	0.114821	14400	0.108844	0.94794	0.10594				
West	156412	0.147893	14400	0.108844	0.73596	0.08225				
Northwest	146739	0.138747	4500	0.034014	0.24515	0.0274				
North	66228	0.062621	3600	0.027211	0.43453	0.04856				
Profile Curvature	**Class pixels**	**% Class pixels**	**Landslide pixels**	**% Landslide pixels**	**P_{ij}**	**(P_{ij})**	**H_j**	**H_{max}**	**I_j**	**W_j**
Convex	113351	0.105552	16200	0.122449	1.16009	0.35716				
Flat	669252	0.623202	72900	0.551020	0.88418	0.27221	1.57223	1.58496	0.00803	0.00522
Concave	291289	0.271246	43200	0.326531	1.20382	0.37062				
LITHOLOGIC GROUP	**Class pixels**	**% Class pixels**	**Landslide pixels**	**% Landslide pixels**	**P_{ij}**	**(P_{ij})**	**H_j**	**H_{max}**	**I_j**	**W_j**
SCHIST AND QUARTZITE	159066	0.157237	8100	0.061224	0.38938	0.04563				
CARBONACEOUS SLATE, PHYLLITE, LIMESTONE, QUARTZITE	74580	0.073722	1800	0.013605	0.18455	0.02163				
CARBONACEOUS SLATE, PHYLLITE, QUARTZITE	13122	0.012971	0	0	0	0				
DIAMICTITE, SHALE, SLATE, SANDSTONE, LIMESTONE	4463	0.004412	0	0	0	0				
SILLIMANITE - KYANITE BEARING SCHIST, QUARTZITE	204013	0.201667	60300	0.455782	2.26007	0.26484				
WHITE-GREEN QUARTZITE, PHYLLITE, BASIC FLOWS	197575	0.195303	18900	0.142857	0.73146	0.08571				
STREAKY AND BANDED GNEISS	23534	0.023263	3600	0.027211	1.16969	0.13706	2.67486	3.70044	0.27715	0.39419
PHYLLITE, QUARTZITE WITH BASIC FLOWS	13721	0.013563	0	0	0	0				
SCHIST, GNEISS, MIGMATITE, QUARTZITE, MARBLE	116964	0.115619	2700	0.020408	0.17651	0.02068				
SCHIST, PHYLLITE, QUARTZITE	57587	0.056925	4500	0.034014	0.59752	0.07002				
SLATE, PHYLLITE, QUARTZARENITE, LIMESTONE, METABASICS	87693	0.086685	28800	0.217687	2.51125	0.29427				
GRANITOID, GNEISS, MIGMATITE	5695	0.005630	0	0	0	0				
GRAVEL, PEBBLE, SAND, SILT AND CLAY	53620	0.053003	3600	0.027211	0.51338	0.06016				
Elevation (m)	**Class pixels**	**% Class pixels**	**Landslide pixels**	**% Landslide pixels**	**P_{ij}**	**(P_{ij})**	**H_j**	**H_{max}**	**I_j**	**W_j**
1,050 - 2,000	264717	0.260303	101700	0.768707	2.95313	0.83979				
2,000 - 3,000	430533	0.423354	28800	0.217687	0.5142	0.14622	0.70325	2	0.64837	0.456
3,000 - 4,000	281431	0.276738	1800	0.013605	0.04916	0.01398				
4,000 - 4,900	40277	0.039605	0	0	0	0				

Table 5.3 IV computation results

					Information Value (IV)			
LULC	**Class pixels**	**% Class pixels**	**Landslide pixels**	**% Landslide pixels**	**Conditional Probability**	**Prior Probability**	**Conditional/Prior probability**	**IV**
Built up	146846	0.145164	23400	0.176871	0.15935	0.13078	1.21842	0.1976
Forest	308834	0.305296	9900	0.074830	0.03206	0.13078	0.24511	-1.4061
Water Body	4629	0.004576	900	0.006803	0.19443	0.13078	1.48662	0.3965
Snow/Glaciers	123809	0.122391	1800	0.013605	0.01454	0.13078	0.11116	-2.1967
Barren Land	203861	0.201526	15300	0.115646	0.07505	0.13078	0.57385	-0.5554
Agricultural Land/Grass	223609	0.221048	81000	0.612245	0.36224	0.13078	2.76974	1.0188
Distance to faults/lineaments (m)	**Class pixels**	**% Class pixels**	**Landslide pixels**	**% Landslide pixels**	**Conditional Probability**	**Prior Probability**	**Conditional/Prior probability**	**IV**
0 - 200	95610	0.094511	8100	0.061224	0.08472	0.13078	0.64781	-0.4342
200 - 400	87818	0.086808	12600	0.095238	0.14348	0.13078	1.09711	0.0927
400 - 600	82262	0.081316	9900	0.074830	0.12035	0.13078	0.92024	-0.0831
600 - 800	72002	0.071174	4500	0.034014	0.06250	0.13078	0.47789	-0.7384
800 - 1000	68400	0.067613	11700	0.088435	0.17105	0.13078	1.30796	0.2685
> 1000	605541	0.598578	85500	0.646259	0.14120	0.13078	1.07966	0.0766
Distance to roads (m)	**Class pixels**	**% Class pixels**	**Landslide pixels**	**% Landslide pixels**	**Conditional Probability**	**Prior Probability**	**Conditional/Prior probability**	**IV**
0 - 200	138618	0.137024	67500	0.510204	0.48695	0.13078	3.72347	1.3147
200 - 400	87959	0.086948	6300	0.047619	0.07162	0.13078	0.54768	-0.6021
400 - 600	71444	0.070622	3600	0.027211	0.05039	0.13078	0.38530	-0.9537
600 - 800	59745	0.059058	5400	0.040816	0.09038	0.13078	0.69112	-0.3694
800 - 1000	54078	0.053456	11700	0.088435	0.21635	0.13078	1.65435	0.5034
> 1000	599789	0.592892	37800	0.285714	0.06302	0.13078	0.48190	-0.7300
Distance to drainage (m)	**Class pixels**	**% Class pixels**	**Landslide pixels**	**% Landslide pixels**	**Conditional Probability**	**Prior Probability**	**Conditional/Prior probability**	**IV**
0 - 100	82554	0.081605	15300	0.115646	0.18533	0.13078	1.41715	0.3486
100 - 200	69486	0.068687	18900	0.142857	0.27200	0.13078	2.07983	0.7323
200 - 300	74861	0.074000	7200	0.054422	0.09618	0.13078	0.73543	-0.3073
300 - 400	61776	0.061066	8100	0.061224	0.13112	0.13078	1.00260	0.0026
> 400	722956	0.714643	82800	0.625850	0.11453	0.13078	0.87575	-0.1327
Slope (°)	**Class pixels**	**% Class pixels**	**Landslide pixels**	**% Landslide pixels**	**Conditional Probability**	**Prior Probability**	**Conditional/Prior probability**	**IV**
0 - 14	137223	0.129731	5400	0.040816	0.03935	0.13078	0.30091	-1.2010
15 - 24	261701	0.247412	18900	0.142857	0.07222	0.13078	0.55223	-0.5938
25 - 33	321808	0.304237	44100	0.333333	0.13704	0.13078	1.04786	0.0468
34 - 45	241211	0.228041	49500	0.374150	0.20521	0.13078	1.56917	0.4505
> 45	95810	0.090579	14400	0.108844	0.15030	0.13078	1.14925	0.1391

Table 5.3 IV computation results (*continued*)

					Information Value (IV)			
Aspect	**Class pixels**	**% Class pixels**	**Landslide pixels**	**% Landslide pixels**	**Conditional Probability**	**Prior Probability**	**Conditional/Prior probability**	**IV**
Flat	87	0.000082	0	0	0	0.13078	0	0
North	64632	0.061112	8100	0.061224	0.12532	0.13078	0.95830	-0.0426
Northeast	125781	0.118930	17100	0.129252	0.13595	0.13078	1.03955	0.0388
East	132831	0.125597	20700	0.156463	0.15584	0.13078	1.19161	0.1753
Southeast	121512	0.114894	19800	0.149660	0.16295	0.13078	1.24597	0.2199
South	121944	0.115302	29700	0.224490	0.24355	0.13078	1.86234	0.6218
Southwest	121435	0.114821	14400	0.108844	0.11858	0.13078	0.90674	-0.0979
West	156412	0.147893	14400	0.108844	0.09206	0.13078	0.70397	-0.3510
Northwest	146739	0.138747	4500	0.034014	0.03067	0.13078	0.23449	-1.4503
North	66228	0.062621	3600	0.027211	0.05436	0.13078	0.41565	-0.8779
Profile Curvature	**Class pixels**	**% Class pixels**	**Landslide pixels**	**% Landslide pixels**	**Conditional Probability**	**Prior Probability**	**Conditional/Prior probability**	**IV**
Convex	113351	0.105552	16200	0.122449	0.14292	0.13078	1.09283	0.0888
Flat	669252	0.623202	72900	0.551020	0.10893	0.13078	0.83292	-0.1828
Concave	291289	0.271246	43200	0.326531	0.14831	0.13078	1.13403	0.1258
LITHOLOGIC GROUP	**Class pixels**	**% Class pixels**	**Landslide pixels**	**% Landslide pixels**	**Conditional Probability**	**Prior Probability**	**Conditional/Prior probability**	**IV**
SCHIST AND QUARTZITE	159066	0.157237	8100	0.061224	0.05092	0.13078	0.38938	-0.9432
CARBONACEOUS SLATE, PHYLLITE, LIMESTONE, QUARTZITE	74580	0.073722	1800	0.013605	0.02414	0.13078	0.18455	-1.6898
CARBONACEOUS SLATE, PHYLLITE, QUARTZITE	13122	0.012971	0	0	0	0.13078	0	0
DIAMICTITE, SHALE, SLATE, SANDSTONE, LIMESTONE	4463	0.004412	0	0	0	0.13078	0	0
SILLIMANITE - KYANITE BEARING SCHIST, QUARTZITE	204013	0.201667	60300	0.455782	0.29557	0.13078	2.26007	0.8154
WHITE-GREEN QUARTZITE, PHYLLITE, BASIC FLOWS	197575	0.195303	18900	0.142857	0.09566	0.13078	0.73146	-0.3127
STREAKY AND BANDED GNEISS	23534	0.023263	3600	0.027211	0.15297	0.13078	1.16969	0.1567
PHYLLITE, QUARTZITE WITH BASIC FLOWS	13721	0.013563	0	0	0	0.13078	0	0
SCHIST, GNEISS, MIGMATITE, QUARTZITE, MARBLE	116964	0.115619	2700	0.020408	0.02308	0.13078	0.17651	-1.7344
SCHIST, PHYLLITE, QUARTZITE	57587	0.056925	4500	0.034014	0.07814	0.13078	0.59752	-0.5150
SLATE, PHYLLITE, QUARTZARENITE, LIMESTONE, METABASICS	87693	0.086685	28800	0.217687	0.32842	0.13078	2.51125	0.9208
GRANITOID, GNEISS, MIGMATITE	5695	0.005630	0	0	0	0.13078	0	0
GRAVEL, PEBBLE, SAND, SILT AND CLAY	53620	0.053003	3600	0.027211	0.06714	0.13078	0.51338	-0.6667
Elevation (m)	**Class pixels**	**% Class pixels**	**Landslide pixels**	**% Landslide pixels**	**Conditional Probability**	**Prior Probability**	**Conditional/Prior probability**	**IV**
1,050 - 2,000	264717	0.260303	101700	0.768707	0.38418	0.13078	2.93766	1.0776
2,000 - 3,000	430533	0.423354	28800	0.217687	0.06689	0.13078	0.51150	-0.6704
3,000 - 4,000	281431	0.276738	1800	0.013605	0.00640	0.13078	0.04891	-3.0179
4,000 - 4,900	40277	0.039605	0	0	0	0.13078	0	0

Table 5.4 WofE computation results

					Weight of Evidence (WofE)					
LULC	**Class pixels**	**% Class pixels**	**Landslide pixels**	**% Landslide pixels**	W^+	W^-	**C**	$S^2(W^+)$	$S^2(W^-)$	**S(C)**	C_s
Built up	146846	0.145164	23400	0.176871	0.2310	-0.0434	0.2743	0.0467	0.0085	0.2350	1.1676
Forest	308834	0.305296	9900	0.074830	-1.5136	0.3377	-1.8513	0.0983	0.0046	0.3207	-5.7735
Water Body	4629	0.004576	900	0.006803	0.4725	-0.0026	0.4751	1.0068	0.2424	1.1177	0.4251
Snow/Glaciers	123809	0.122391	1800	0.013605	-2.3223	0.1357	-2.4579	0.5069	0.0086	0.7180	-3.4235
Barren Land	203861	0.201526	15300	0.115646	-0.6175	0.1185	-0.7360	0.0665	0.0061	0.2694	-2.7317
Agricultural Land/Grass	223609	0.221048	81000	0.612245	1.3284	-0.7704	2.0988	0.0287	0.0075	0.1902	11.0330
Distance to faults/lineaments (m)	**Class pixels**	**% Class pixels**	**Landslide pixels**	**% Landslide pixels**	W^+	W^-	**C**	$S^2(W^+)$	$S^2(W^-)$	**S(C)**	C_s
0 - 200	95610	0.094511	8100	0.061224	-0.4858	0.0416	-0.5274	0.1184	0.0114	0.3602	-1.4641
200 - 400	87818	0.086808	12600	0.095238	0.1074	-0.0107	0.1181	0.0789	0.0131	0.3034	0.3892
400 - 600	82262	0.081316	9900	0.074830	-0.0951	0.0081	-0.1032	0.0983	0.0136	0.3344	-0.3085
600 - 800	72002	0.071174	4500	0.034014	-0.8140	0.0453	-0.8593	0.2070	0.0144	0.4706	-1.8258
800 - 1000	68400	0.067613	11700	0.088435	0.3159	-0.0259	0.3418	0.0844	0.0170	0.3184	1.0738
> 1000	605541	0.598578	85500	0.646259	0.0887	-0.1442	0.2329	0.0298	0.0042	0.1844	1.2630
Distance to roads (m)	**Class pixels**	**% Class pixels**	**Landslide pixels**	**% Landslide pixels**	W^+	W^-	**C**	$S^2(W^+)$	$S^2(W^-)$	**S(C)**	C_s
0 - 200	138618	0.137024	67500	0.510204	1.8419	-0.6294	2.4713	0.0272	0.0138	0.2025	12.2063
200 - 400	87959	0.086948	6300	0.047619	-0.6679	0.0487	-0.7166	0.1500	0.0121	0.4027	-1.7795
400 - 600	71444	0.070622	3600	0.027211	-1.0422	0.0527	-1.0949	0.2570	0.0144	0.5209	-2.1018
600 - 800	59745	0.059058	5400	0.040816	-0.4149	0.0221	-0.4370	0.1738	0.0177	0.4375	-0.9988
800 - 1000	54078	0.053456	11700	0.088435	0.6071	-0.0432	0.6503	0.0844	0.0223	0.3266	1.9907
> 1000	599789	0.592892	37800	0.285714	-0.8051	0.6827	-1.4878	0.0333	0.0044	0.1943	-7.6553
Distance to drainage (m)	**Class pixels**	**% Class pixels**	**Landslide pixels**	**% Landslide pixels**	W^+	W^-	**C**	$S^2(W^+)$	$S^2(W^-)$	**S(C)**	C_s
0 - 100	82554	0.081605	15300	0.115646	0.4135	-0.0433	0.4568	0.0665	0.0145	0.2846	1.6050
100 - 200	69486	0.068687	18900	0.142857	0.9096	-0.0949	1.0045	0.0556	0.0189	0.2728	3.6818
200 - 300	74861	0.074000	7200	0.054422	-0.3463	0.0241	-0.3704	0.1322	0.0144	0.3829	-0.9675
300 - 400	61776	0.061066	8100	0.061224	0.0030	-0.0002	0.0032	0.1184	0.0179	0.3691	0.0086
> 400	722956	0.714643	82800	0.625850	-0.1512	0.3189	-0.4701	0.0291	0.0052	0.1850	-2.5410
Slope (°)	**Class pixels**	**% Class pixels**	**Landslide pixels**	**% Landslide pixels**	W^+	W^-	**C**	$S^2(W^+)$	$S^2(W^-)$	**S(C)**	C_s
0 - 14	137223	0.129731	5400	0.040816	-1.2498	0.1120	-1.3618	0.1738	0.0080	0.4263	-3.1947
15 - 24	261701	0.247412	18900	0.142857	-0.6079	0.1501	-0.7580	0.0556	0.0050	0.2461	-3.0797
25 - 33	321808	0.304237	44100	0.333333	0.1051	-0.0487	0.1538	0.0306	0.0046	0.1877	0.8192
34 - 45	241211	0.228041	49500	0.374150	0.5912	-0.2365	0.8277	0.0291	0.0059	0.1870	4.4260
> 45	95810	0.090579	14400	0.108844	0.2129	-0.0232	0.2361	0.0701	0.0121	0.2868	0.8232

Table 5.4 WofE computation results (*continued*)

					Weight of Evidence (WofE)					
Aspect	**Class pixels**	**% Class pixels**	**Landslide pixels**	**% Landslide pixels**	**W^+**	**W**	**C**	**$S^2(W^+)$**	**$S^2(W)$**	**S(C)**	**C_s**
Flat	87	0.000082	0	0	0	9.4E-05	-9.4E-05	0	10.3458	3.2165	-2.9E-05
North	64632	0.061112	8100	0.061224	0.0021	-0.0001	0.0022	0.1184	0.0170	0.3679	0.0061
Northeast	125781	0.118930	17100	0.129252	0.0957	-0.0135	0.1092	0.0604	0.0094	0.2642	0.4131
East	132831	0.125597	20700	0.156463	0.2555	-0.0410	0.2965	0.0515	0.0091	0.2463	1.2036
Southeast	121512	0.114894	19800	0.149660	0.3086	-0.0457	0.3543	0.0535	0.0099	0.2518	1.4070
South	121944	0.115302	29700	0.224490	0.8118	-0.1492	0.9610	0.0391	0.0108	0.2234	4.3014
Southwest	121435	0.114821	14400	0.108844	-0.0609	0.0077	-0.0686	0.0701	0.0095	0.2822	-0.2430
West	156412	0.147893	14400	0.108844	-0.3436	0.0514	-0.3950	0.0701	0.0075	0.2786	-1.4179
Northwest	146739	0.138747	4500	0.034014	-1.5084	0.1323	-1.6407	0.2070	0.0075	0.4632	-3.5424
North	66228	0.062621	3600	0.027211	-0.9112	0.0425	-0.9537	0.2570	0.0154	0.5219	-1.8273
Profile Curvature	**Class pixels**	**% Class pixels**	**Landslide pixels**	**% Landslide pixels**	**W^+**	**W**	**C**	**$S^2(W^+)$**	**$S^2(W)$**	**S(C)**	**C_s**
Convex	113351	0.105552	16200	0.122449	0.1712	-0.0217	0.1930	0.0633	0.0103	0.2714	0.7111
Flat	669252	0.623202	72900	0.551020	-0.1392	0.2026	-0.3418	0.0275	0.0041	0.1778	-1.9224
Concave	291289	0.271246	43200	0.326531	0.2146	-0.0895	0.3040	0.0309	0.0049	0.1894	1.6056
LITHOLOGIC GROUP	**Class pixels**	**% Class pixels**	**Landslide pixels**	**% Landslide pixels**	**W^+**	**W**	**C**	**$S^2(W^+)$**	**$S^2(W)$**	**S(C)**	**C_s**
SCHIST AND QUARTZITE	159066	0.157237	8100	0.061224	-1.0311	0.1252	-1.1563	0.1184	0.0072	0.3543	-3.2632
CARBONACEOUS SLATE, PHYLLITE, LIMESTONE, QUARTZITE	74580	0.073722	1800	0.013605	-1.8056	0.0727	-1.8783	0.5069	0.0135	0.7214	-2.6037
CARBONACEOUS SLATE, PHYLLITE, QUARTZITE	13122	0.012971	0	0	0	0.0150	-0.0150	0	0.0696	0.2639	-0.0570
DIAMICTITE, SHALE, SLATE, SANDSTONE, LIMESTONE	4463	0.004412	0	0	0	0.0051	-0.0051	0	0.2027	0.4502	-0.0113
SILLIMANITE - KYANIE BEARING SCHIST, QUARTZITE	204013	0.201667	60300	0.455782	1.0256	-0.4300	1.4556	0.0274	0.0075	0.1868	7.7902
WHITE-GREEN QUARTZITE, PHYLLITE, BASIC FLOWS	197575	0.195303	18900	0.142857	-0.3523	0.0730	-0.4253	0.0556	0.0063	0.2488	-1.7098
STREAKY AND BANDED GNEISS	23534	0.023263	3600	0.027211	0.1826	-0.0047	0.1873	0.2570	0.0462	0.5506	0.3401
PHYLLITE, QUARTZITE WITH BASIC FLOWS	13721	0.013563	0	0	0	0.0157	-0.0157	0	0.0666	0.2581	-0.0609
SCHIST, GNEISS, MIGMATITE, QUARTZITE, MARBLE	116964	0.115619	2700	0.020408	-1.8512	0.1186	-1.9697	0.3403	0.0091	0.5910	-3.3327
SCHIST, PHYLLITE, QUARTZITE	57587	0.056925	4500	0.034014	-0.5738	0.0277	-0.6014	0.2070	0.0180	0.4744	-1.2677
SLATE, PHYLLITE, QUARTZARENITE, LIMESTONE, METABASICS	87693	0.086685	28800	0.217687	1.1787	-0.1762	1.3549	0.0399	0.0164	0.2373	5.7091
GRANITOID, GNEISS, MIGMATITE	5695	0.005630	0	0	0	0.0065	-0.0065	0	0.1591	0.3988	-0.0163
GRAVEL, PEBBLE, SAND, SILT AND CLAY	53620	0.053003	3600	0.027211	-0.7374	0.0310	-0.7684	0.2570	0.0191	0.5254	-1.4624
Elevation (m)	**Class pixels**	**% Class pixels**	**Landslide pixels**	**% Landslide pixels**	**W^+**	**W**	**C**	**$S^2(W^+)$**	**$S^2(W)$**	**S(C)**	**C_s**
1,050 - 2,000	264717	0.260303	101700	0.768707	1.4283	-1.2604	2.6887	0.0383	0.0068	0.2122	12.6705
2,000 - 3,000	430533	0.423354	28800	0.217687	-0.7353	0.3598	-1.0951	0.0399	0.0041	0.2099	-5.2179
3,000 - 4,000	281431	0.276738	1800	0.013605	-3.1456	0.3662	-3.5118	0.5069	0.0047	0.7153	-4.9098
4,000 - 4,900	40277	0.039605	0	0	0	0.0466	-0.0466	0	0.0234	0.1530	-0.3045

5.3 Spatial relationships interpretation

The relationship between each class of each causative factor to landslide occurrence gives an insight on the mechanisms of the slides in the research area. Despite the extensive literature available on the different underlying causes of slope failures, these cause-effect relationships vary according to the study area's characteristics, different types of failures prevalent as well as the other external triggering factors involved.

Therefore, it is an important aspect of any landslide susceptibility studies to try to understand the implication/effect that the selected causative factors have on past slope failures. This interpretation can be done from the results obtained from the four different probabilistic methods FR, SE, IV and WofE. The different weights assigned to every parameter through the different methods enabled the author to better figure out the patterns behind the past slides in the region as well as compare the observations with other susceptibility studies for similarity or contrast.

This interpretation will in turn help in choosing more reliable factors to describe mass movement mechanisms in the study region to build more robust models in the future.

5.3.1 Frequency Ratio (FR) and Information Value (IV) results

Despite being different methods altogether, the results from the frequency ratio model show a rather similar pattern to that from the information value model. Therefore, the idea of presenting and discussing about the results from these two models simultaneously was found relevant for a better perception.

5.3.1.1 Effect of slope

The variations in the results for the slope factor from the FR and IV methods have been presented in Fig. 5.1 and 5.2 respectively below. In terms of percentage class pixel distribution of the slope angle classes, the 25° – 33° category occupies most of the study area with a percentage of around 30% followed by the 15° – 24° and 34° – 45° categories occupying 25% and 23% respectively. The 0° – 14° class occupies the lower

valley areas and riverbeds (≈13%) whereas the steepest slopes (> 45°) class occupies the least area (≈9%) as seen in Table 5.1 above.

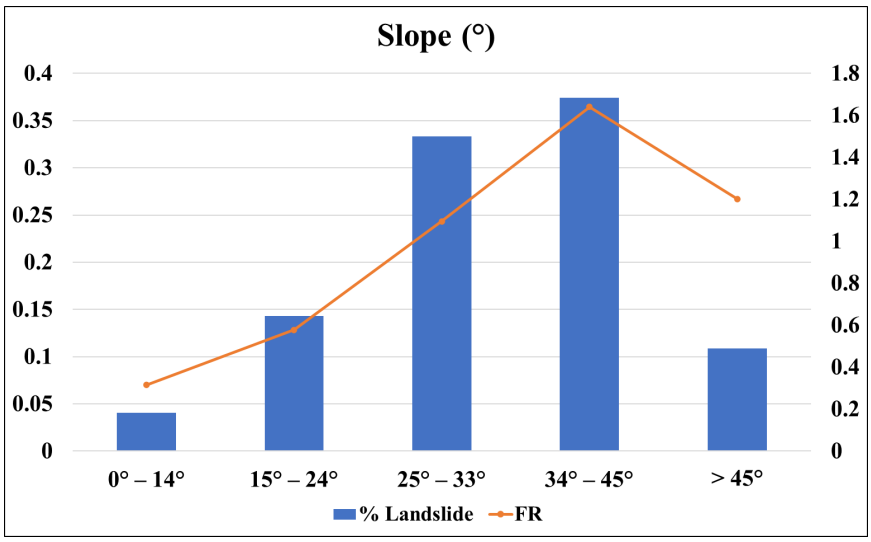

Fig. 5.1 FR variation in slope factor

For the percentage landslide distribution as seen from Fig. 5.1 above, the highest was in the category 34° – 45° followed by the categories 25° – 33°, 15° – 24°, > 45° with the least being in the 0° – 14° class. The FR distribution followed the same pattern as that of the landslide distribution with the highest being in the 34° – 45° slope class. Also, an increasing trend in both prospects and FR values is observed with the increasing order of slope classes ending with a decline in the last category (> 45°).

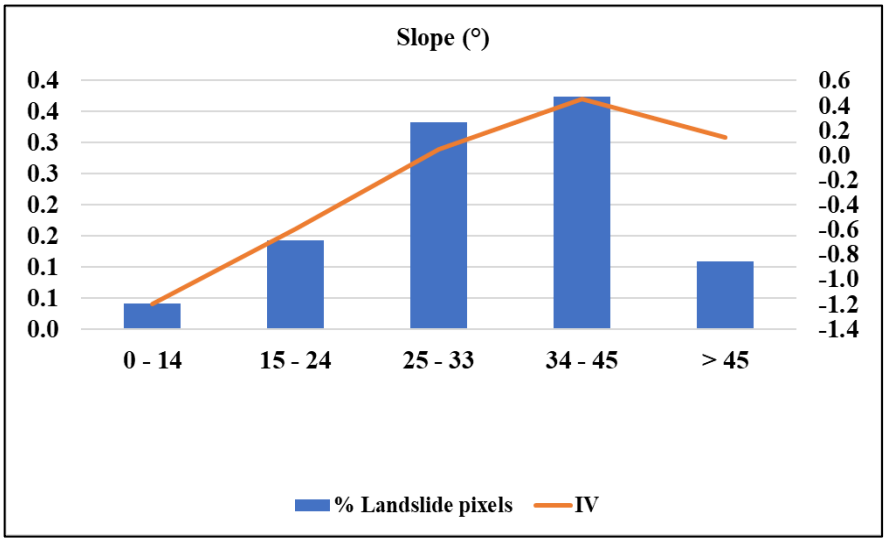

Fig. 5.2 IV variation in slope factor

The information values and percentage landslide distribution for the slope classes, as seen from Fig. 5.2, show a similar pattern to that of the FR method; an increasing trend in the first four slope categories ending with a decline in the last class (> 45°). However, as seen from Table 5.3, negative informative values were found in the 0° – 14° and 15° – 24° slope classes thereby expressing contrasting correlation to landslide occurrences as compared to the other slope classes having positive information values.

This increasing trend in slope was already predicted since slopes become more and more unstable with increasing slope angle. However, the extent of soil cover also decreases with increasing soil angle, and the presence of mature stable topography also increases, explaining the decrease in both landslide occurrences and FR/IV value. The '34° - 45°' class contributed to both the maximum percentage of landslide distribution and FR/IV value.

5.3.1.2 Effect of aspect

The variations in the results for the aspect factor from the FR and IV methods have been presented in Fig. 5.3 and 5.4 respectively below. In terms of area coverage of the different slope orientation classes, the contribution of every class is almost equal (≈11-15%) except for flat surfaces with an almost insignificant contribution in the hilly and mountainous region investigated.

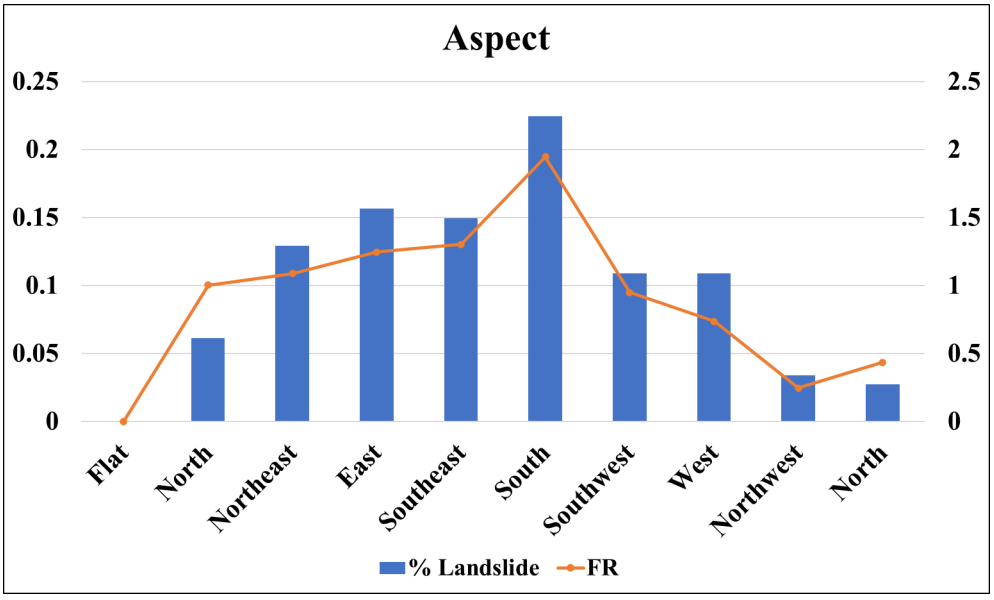

Fig. 5.3 FR variation in aspect factor

In terms of slope orientations, it can be deduced from the observed trend in Fig. 5.3 that the southern, south-eastern, eastern and north-eastern aspects contributed to more landslide pixels than all the other categories. Least affected by mass movements were the western, northern, north-western orientations. One confirmation of the credibility of the input data was the observed zero FR value obtained in flat slopes (no orientation) in the area which experienced zero slope failures.

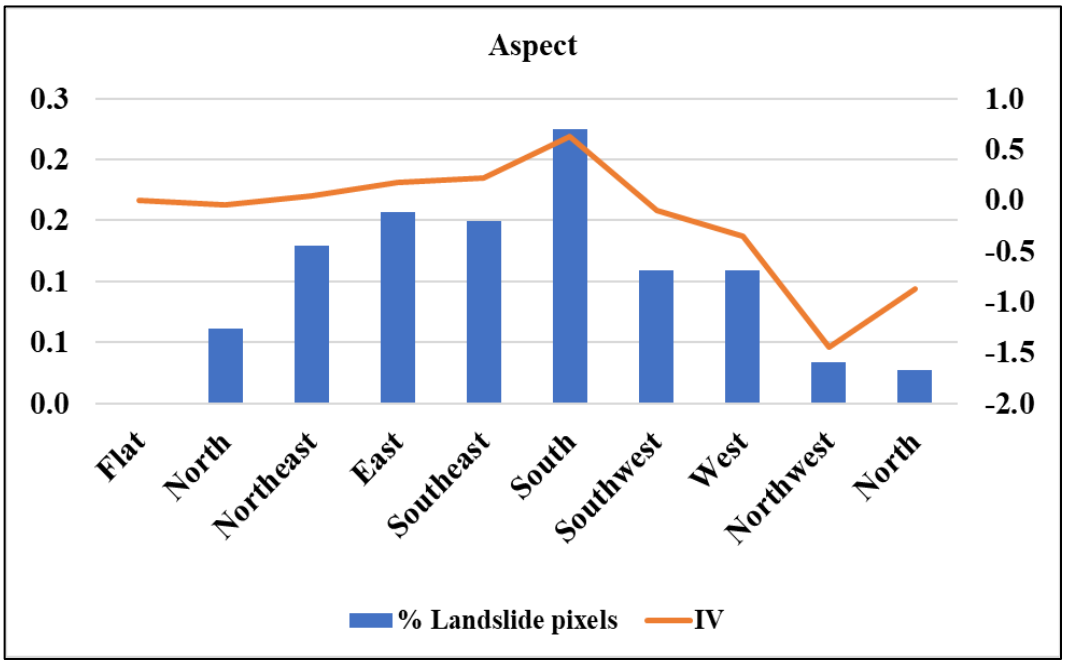

Fig. 5.4 IV variation in aspect factor

A similar trend was observed for the variation of the information values of the slope orientation classes as seen from Fig. 5.4 above. Positive information values were found in the southern, south-eastern, eastern and north-eastern aspects as seen from Table 5.3 justifying their positive contribution to landslide occurrences in the study area. The contrary can be said for the south-western, western, northern and north-western orientations which had negative information values denoting contrasting correlation to sliding. Another justification for the IV method can be seen for the flat orientations which has zero IV hence denoting no correlation with landslide occurrences.

5.3.1.3 Effect of curvature

The variations in the results for the aspect factor from the FR and IV methods have been presented in Fig. 5.5 and 5.6 respectively below.

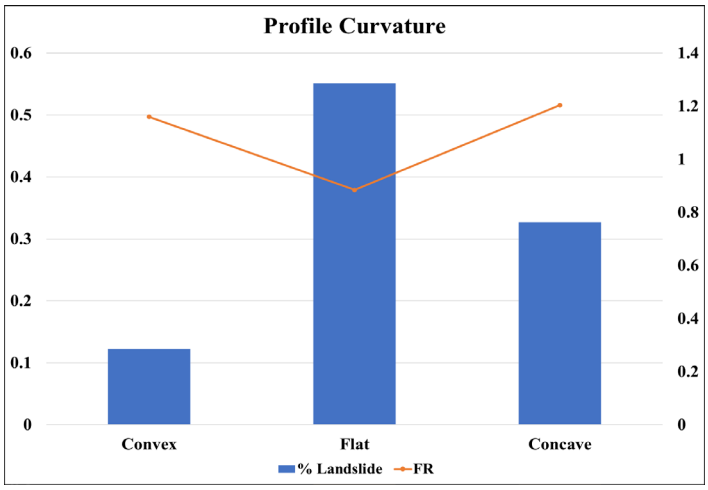

Fig. 5.5 FR variation in profile curvature factor

The percentage class pixel distribution of the area's profile curvature as seen from Table 5.1 shows a domination of recti-linear/flat surfaces which are the most occurring profile curvature type in the region with highest class pixel distribution (≈62%), followed by concave (≈27%) and convex surfaces (≈11%). The percentage landslide distribution shows a similar pattern to the percentage class pixel distribution in the respective surfaces.

However, the FR values computed shows higher correlation for concave and convex surfaces with FR > 1 respectively compared to rectilinear surfaces with FR<1 as seen from Fig. 5.5 above.

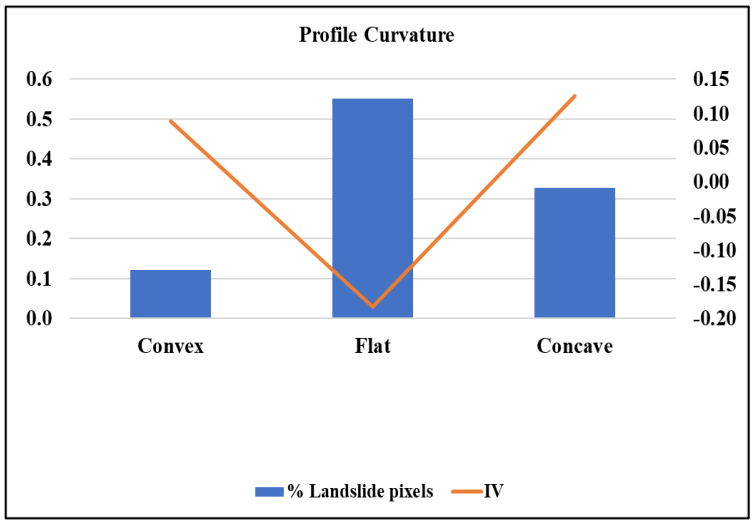

Fig. 5.6 IV variation in profile curvature factor

A similar trend is again observed for the variation of information values in the different curvature types as seen from Fig. 5.6 below. Similar to the FR results, concave faces showed better correlation to landslide occurrences with higher IV compared to convex faces while the recti-linear faces had negative IV, thereby signifying adverse correlation to slope failures.

5.3.1.4 Effect of elevation

The analysis results for the FR and IV variation in elevation parameter is presented in Fig 5.7 and 5.8 respectively. The percentage class pixel distribution of the area's elevation as processed from Table 5.1 shows that the maximum area of the research region lies in the 2,000 – 3,000 metres class followed by an almost equal contribution of areas in 1,050 – 2,000 metres and 3,000 – 4,900 metres with the least being in the 4,000 – 4,900 metres elevation category which is restricted to a hostile environment characterised by snow/glaciers all year round with bare human intervention.

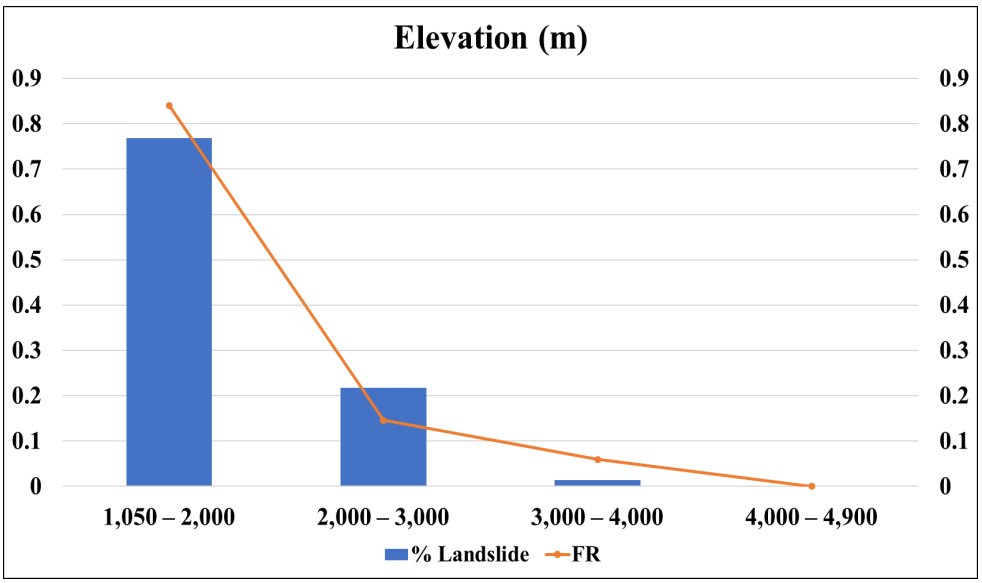

Fig. 5.7 FR variation in elevation factor

Most villages/towns in the study area are restricted to a maximum altitude of 3,000 metres, with Malana (≈2,800 metres) and Khirganga (≈2,960 metres) being the highest places. Though elevation does affect many land processes and activities, the main contribution in this study, is believed to be presence of human settlement and activities. As seen from Fig. 5.7, the highest correlation to landslide occurrences was found in the

first two categories (1,050 – 2,000 and 2,000 – 3,000 metres) with the highest being in the least elevated area, implying the possibility of other factors such as the presence of most agricultural/grass land and road networks in this class. The lowest correlation was observed in the most elevated areas which is mostly characterised by mature topography and presence of snow/glaciers nearly all year round. To summarise, a decrease in both landslide distribution and FR value is observed with increasing altitude in the study region.

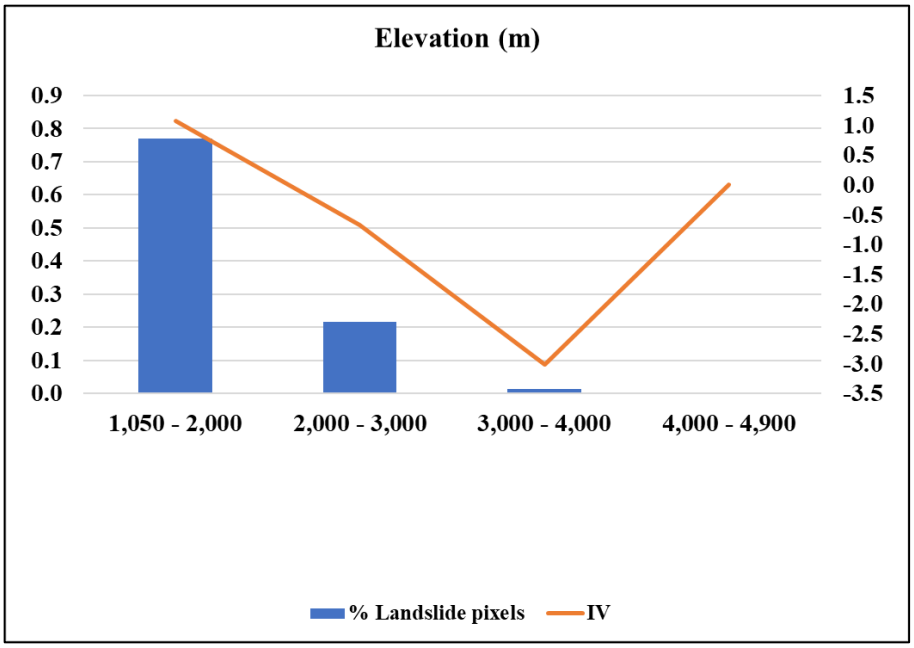

Fig. 5.8 IV variation in elevation factor

The variation of IV in the different elevation classes, as seen from Fig. 5.8 below, follow a declining trend similar to that of the FR variation in the first three classes. The information value of only the lowest elevated class signifying a positive correlation to landslide occurrences while negative correlation is observed in the next two elevation classes. The highest elevated category (4,000 – 4,900 m) has zero information value implying zero correlation to past slope failures in the area.

5.3.1.5 Effect of distance to drainage

From Table 5.1, it can be inferred that the percentage class pixel contribution of each buffered zone of 200 metres intervals from the drainage networks in the area shows an almost equal distribution with the highest being in the last zone (> 400 m) since

it encompasses the rest of the study area's pixels (≈71%). The variation for the FR and IV variation in the distance to drainage parameter is presented in Fig. 5.9 and Fig. 5.10 respectively.

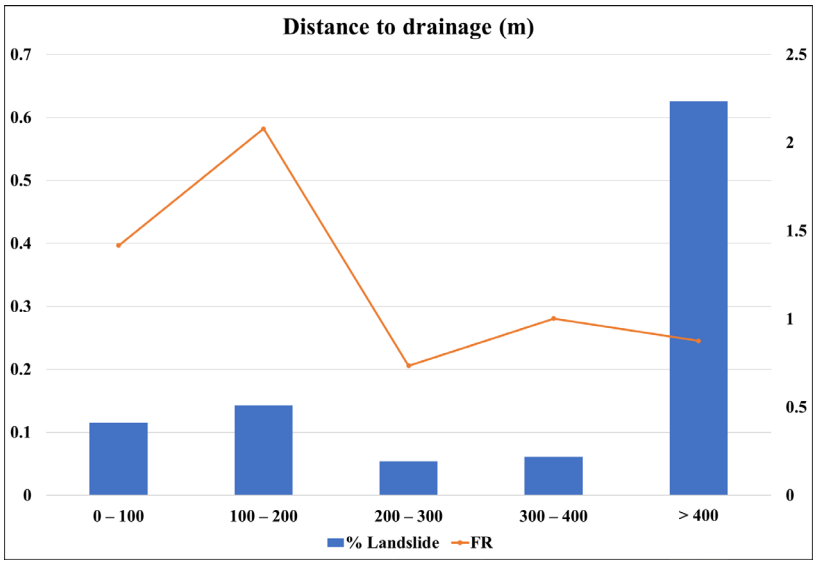

Fig. 5.9 FR variation in distance to drainage factor

As observed in Fig. 5.9, the first two categories (0 – 100 and 100 – 200 metres) depicted the highest correlations to landslide occurrences with the highest FR value being in the 100 – 200 metres class. However, since the last category englobes the rest of the area's pixel, it had the highest percentage of landslide pixel distribution but showed lesser contribution (FR <1) in terms of correlation to mass movements compared to the first two classes (FR >1).

Referring to Fig. 5.10, a similar pattern in the IV variation can be observed as that of the variation in FR values. The only two classes showing positive contribution to occurrences of landslides are the 0 – 100 and 100 – 200 metres categories with positive IV values. the remaining classes demonstrated little significance to landslide occurrence. It can be therefore concluded that distance to drainage do play a role in slope instability in the region.

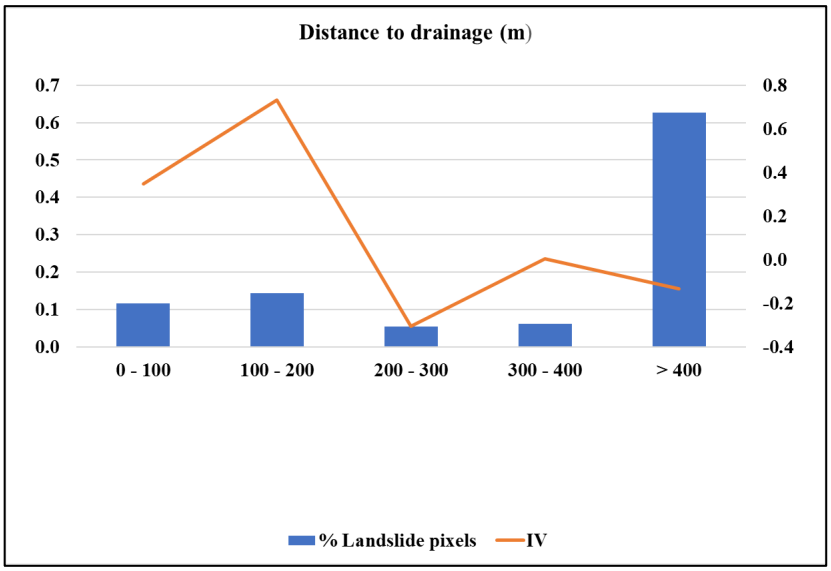

Fig. 5.10 IV variation in distance to drainage factor

5.3.1.6 Effect of distance to roads

The buffered zones of 200 metres from the road network shows an almost equal contribution of class pixels between the 200 – 400, 400 – 600, 600 – 800 and 800 – 1,000 metres categories as seen from Table 5.1. The most significant contributors are the 0 – 200 metres class covering approximately 14%, and the > 1,000 metres class covering approximately 59% of the area. The variation of FR and IV for the distance to roads parameter has been outlined in Fig. 5.11 and 5.12 respectively.

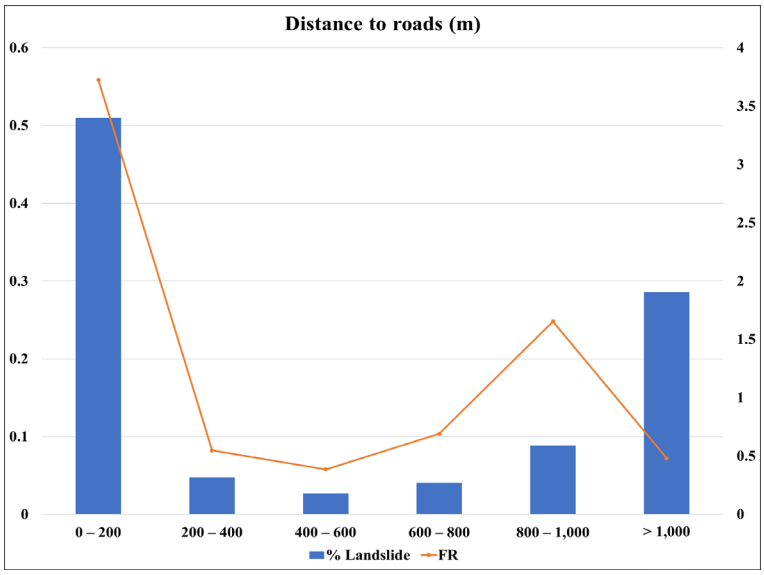

Fig. 5.11 FR variation in distance to roads factor

The distance to road map overlayed with compiled landslide distribution data in the area gave insight on the effect of road construction and widening in the region. The increase in slope instability due to road-related activities can be justified with the highest landslide distribution and highest FR value (3.72347) obtained in the first buffered zone from the road networks (0 – 200 m) as seen from Fig. 5.11. A decreasing trend in both percentage landslide and FR was observed in the next two classes, then again, a rise in landslide distribution and FR in the 800 – 1,000 metres class, which might be better justified by the other causative factors chosen. The decline in FR value for the '> 1000m' category can be justified by the huge percentage class pixel contribution of this class which englobes the rest of the study area.

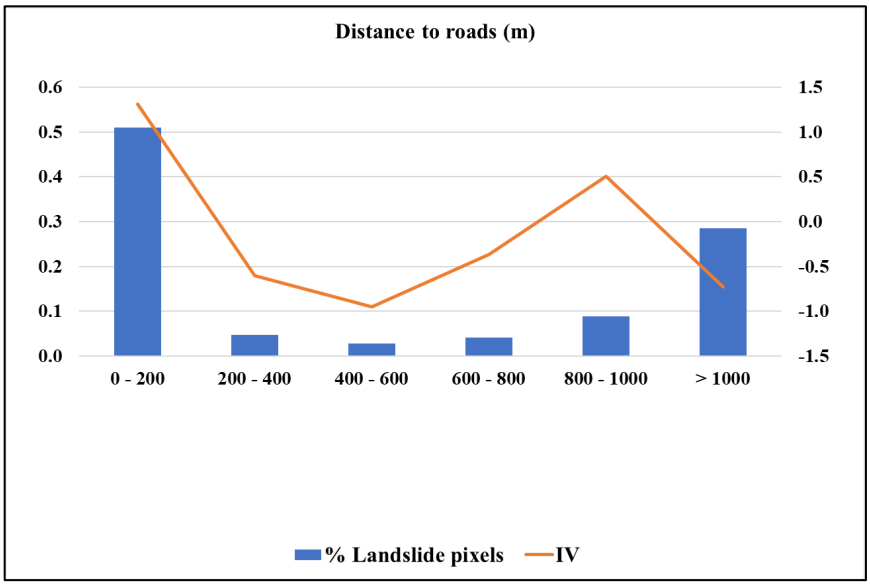

Fig. 5.12 IV variation for distance to roads factor

The variation in the information values was found similar to that of the frequency ratio model with the only two classes showing correlation to landslide occurrences being the first (0 – 200 m) with the most positive IV (1.3147) and the fifth (800 – 1,000 m) category with the second most positive IV (0.5034).

5.3.1.7 Effect of lithology

The three predominating lithostratigraphic units in the region in terms of pixel contribution are the 'Sillimanite-Kyanie bearing Schist, Quartzite', 'White-green Quartzite Phyllite, Basic flows' and 'Schist and quartzite' respectively with a contribution

of more than 15% as seen from Table 5.1. The variation in FR and IV for the effect of lithology on landslide occurrences can be observed in Fig. 5.13 and 5.14 respectively.

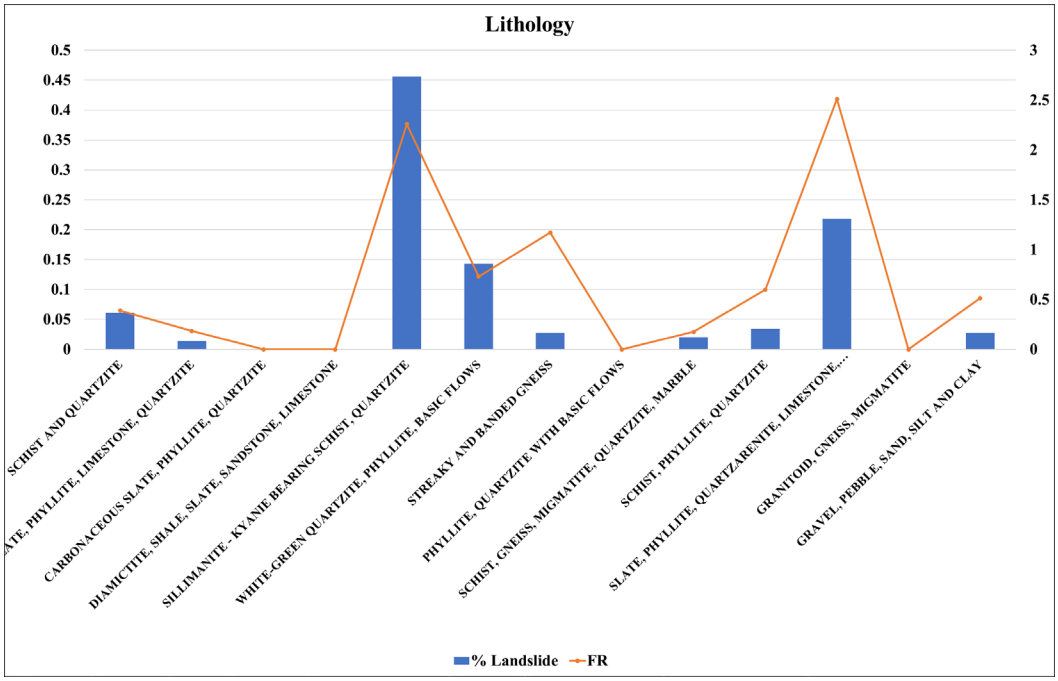

Fig. 5.13 FR variation in lithology factor

The three litho-stratigraphic units 'Sillimanite-kyanie bearing schist, quartzite', 'white-green quartzite, phyllite, basic flows' and 'slate, phyllite, quartzarenite, limestone, metabasics' had the highest landslide distribution and FR values, including the 'streaky and banded gneiss' lithologic unit that also showed high correlation to slope instability (FR > 1) as seen from Fig. 5.13 above. Positive information values (IV >0) were observed in the same three lithologic groups confirming their relationship with past landslides in the region as seen from Fig. 5.14 below.

The categories that had no landslide occurrences, hence zero FR and Information values (IV=0), thereby depicting no correlation were the 'carbonaceous slate, phyllite, quartzite', 'diamicite, shale, slate, sandstone, limestone', 'phyllite, quartzite with basic flows' and 'granitoid, gneiss, migmatite' lithologic groups.

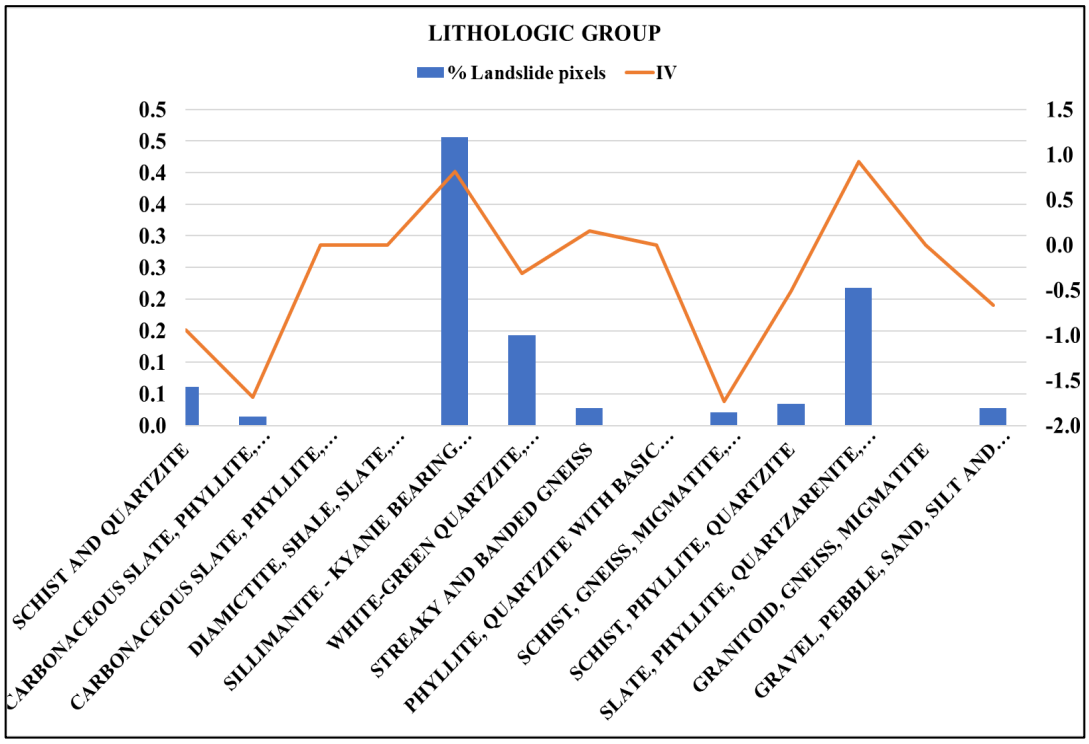

Fig. 5.14 IV variation in lithology factor

5.3.1.8 Effect of distance to faults/lineaments

As seen from Table 5.1, a similar trend was observed as that of the distance to drainage map in terms of an almost equal percentage class distribution in the first four classes and with the highest contributor being the >1,000 metres class (≈60%) englobing most of the study area.

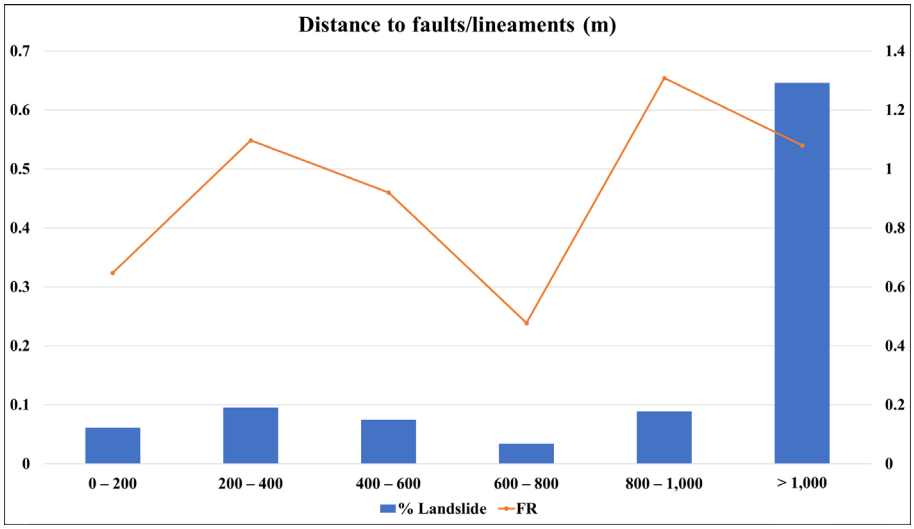

Fig. 5.15 FR variation in distance to faults/lineaments factor

For better interpretation of the results from this parameter, it has been studied along with the lithology map since the last two categories (800 – 1,000 and > 1,000 metres) of the fault buffer map are mostly covered by the three litho-stratigraphic units ('Sillimanite-kyanie bearing schist', quartzite; 'white-green quartzite, phyllite, basic flows' and 'slate, phyllite, quartzarenite, limestone, metabasics') that had the highest landslide distribution thereby contributing to the high FR value obtained for these two categories as seen above in Fig. 5.15. Additionally, the presence of 'streaky and banded gneiss' lithologic units in the 200-400 m 'distance to faults/lineaments' range shows the higher correlation value to landslide events.

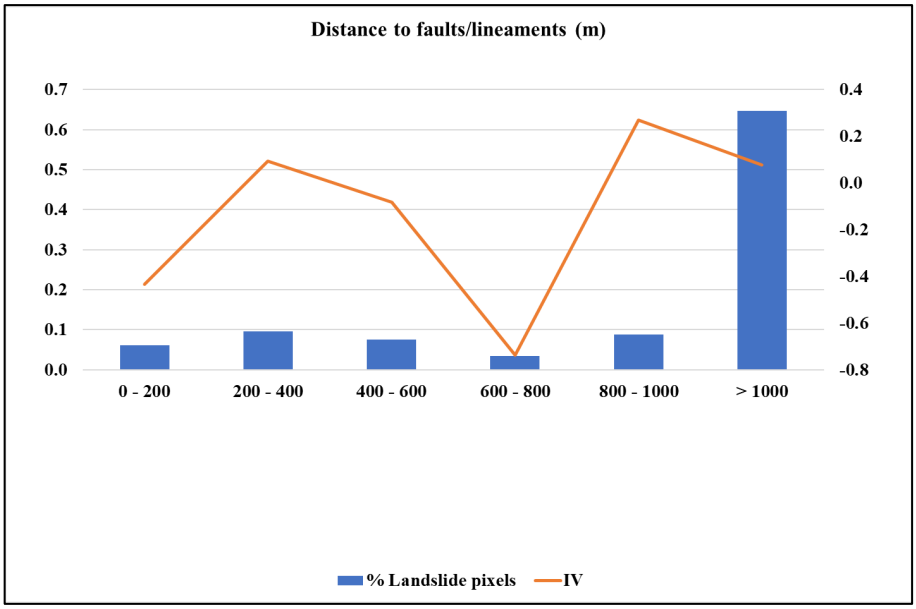

Fig. 5.16 IV variation in distance to faults/lineaments factor

The same process of referring to the lithological units has been repeated for studying the variation of information values in this parameter. However, the variation of information values for lithology has been considered instead of the FR variation. From Fig. 5.16 above, it can be inferred that the same three classes (200 – 400, 800 – 1,000 and > 1,000 m) that had highest FR, depicted positive information values (IV>0), implying positive influence on slope instability. However, among the lithological units present in the last two classes (800 – 1,000 and > 1,000 m), more specifically, the 'white-green quartzite, phyllite, basic flows' had shown negative influence on land sliding as seen above from Fig. 5.14.

5.3.1.9 Effect of land use/land cover (LULC)

As noted above from Table 5.1, the most predominant land use/land cover classes in the region are forested areas (≈30%), followed by agricultural (≈22%), barren land (≈20%) and built-up areas (≈14%) respectively. Snow/glaciers and water bodies constituted the least prevalent land use/land cover classes in terms of area coverage.

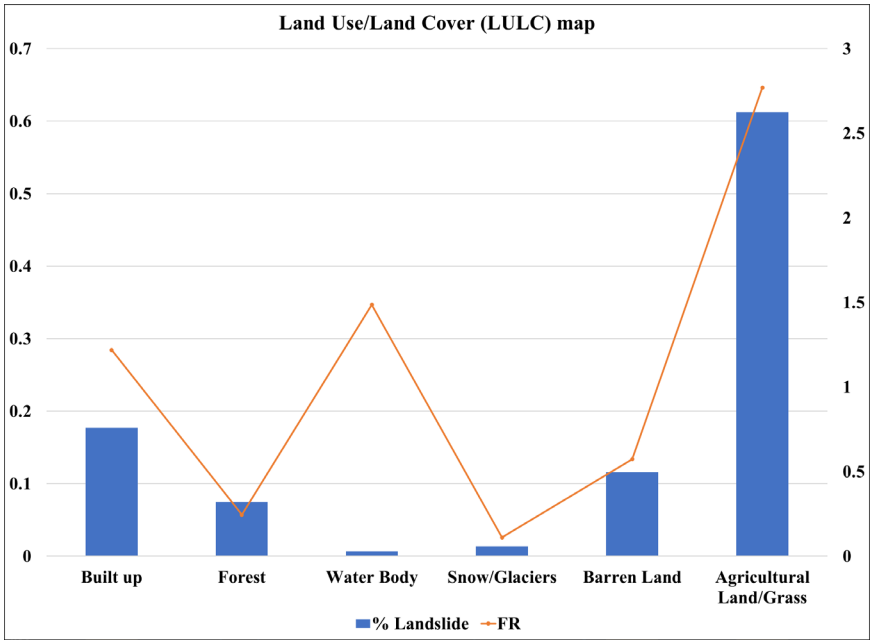

Fig. 5.17 FR variation in land use/land cover factor

The land use/land cover types having the highest landslide distribution are the Agricultural Land/Grass, Built-up and Barren Land as observed in Fig. 5.17 above. Agricultural Land/Grass Land contributed to the most landslide occurrences and FR value than any other class. Some of the possible reasons are deforestation practices to create agricultural areas over the years, change in agricultural crop patterns, drainage pattern changes in the cultivated region or increasing human intervention. While water bodies, mainly present as rivers/streams in the study area, show high correlation to landslide occurrences as shown by the FR value due to plausible causes such as bank toe erosion, lowest correlation was observed in the Forest and Snow/Glaciers categories.

The reason for low occurrences in forested areas is probably due to the root strength contribution of evergreen, deciduous pine trees which holds the soil firmly together, decreasing the probability of slope failures. The region of low landslide

distribution in the Snow/Glaciers class is most certainly due to lesser human intervention coupled with lesser extent of soil cover, but also remoteness of the region and presence of nearly all year snow/glaciers make landslide mapping an arduous task, explaining the lack of landslide data as well.

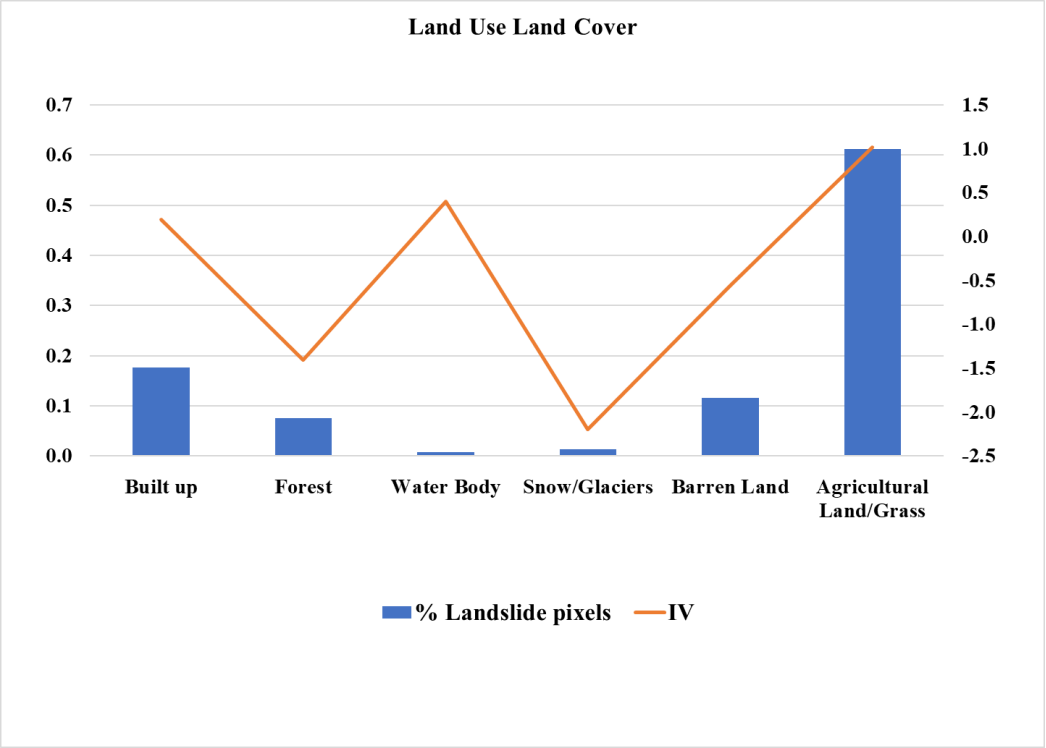

Fig. 5.18 IV variation in land use/land cover factor

The same tendency from the FR variation was noted in the variation of the information values, as seen from Fig. 5.18, with the three classes (Built-up, Water Body and Agricultural Land/Grass) showing positive association (IV>0) to landslide incidence in the study area. The rest of the classes portrayed negative association.

5.3.2 Weight-of-Evidence (WofE) results

The positive, negative and contrast weights computed through the Weight of Evidence probabilistic method for every parameter class along with their variances have been outlined in Table 5.4 above. The contribution of each class to landslide incidence has been evaluated in the sections below on the basis of the computed weights.

5.3.2.1 Effect of slope

The variation of positive (W^+) and contrast (C) weights, as noticed in Fig. 5.19, resembles the variation in the information value (IV) of the slope factor seen from Fig. 5.2 above. The negative values of both W^+ and C in the 0° – 14° and 15° – 24° slope classes correspond to the negative information values obtained earlier, thereby expressing contrasting association to landslide occurrences.

The other slope classes showed positive connection to slope instability with positive W^+ and C weights. The 34° – 45° category was found to be the most susceptible class with the most negative W^- and most positive W^+ and C values, tallying with the results from FR and IV models.

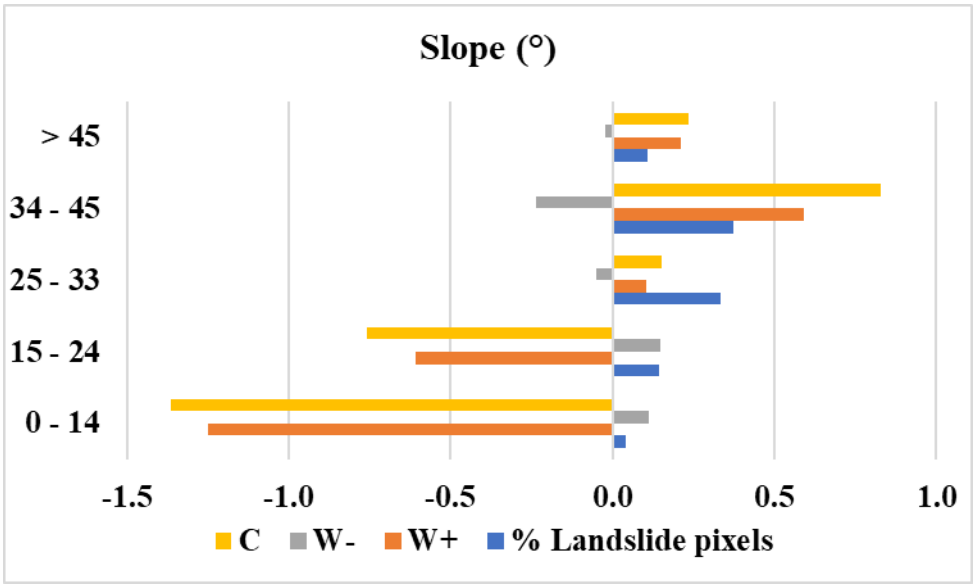

Fig. 5.19 WofE weights variation in slope factor

5.3.2.2 Effect of aspect

As seen from Fig. 5.20, negative W^+ and C values were obtained in the northern, north-western, western and south-western slope orientations depicting negative association while negative W^+ and C values were achieved in the south, south-eastern, eastern and north-eastern slope aspects symbolising affirmative correlation to landslide incidences. The same interpretations were made from the results obtained in the frequency ratio and information value models. The reverse positive and negative values of W^- compared to W^+ values in each class confirm the above-made observation.

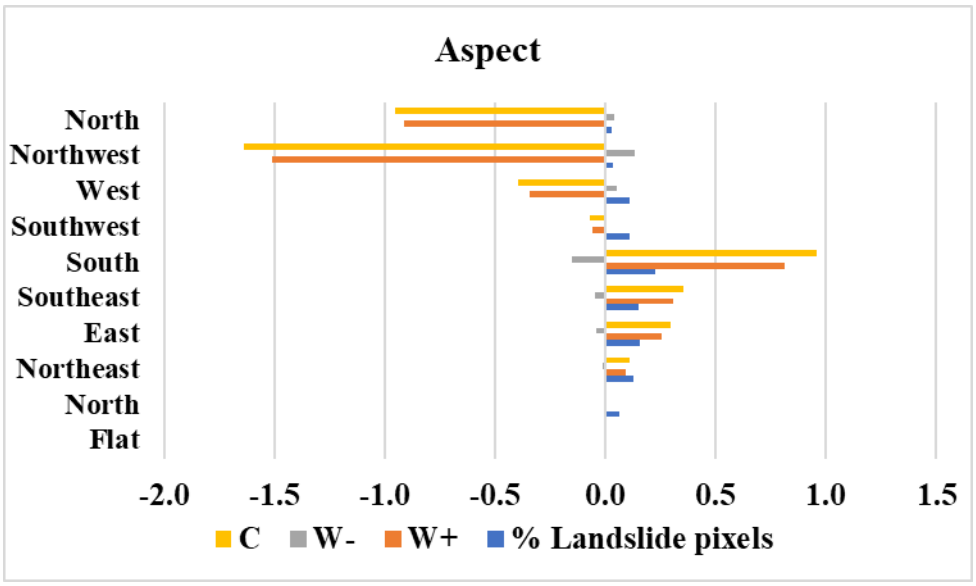

Fig. 5.20 WofE weights variation in aspect factor

5.3.2.3 Effect of curvature

Both concave and convex surfaces show positive correlation to land sliding in the area with the highest positive weight (W^+) and contrast (C) values compared to flat/linear surfaces (having negative W^+ and C values as well as positive W^- value) despite having the highest percentage landslide pixel contribution as observed from Fig. 5.21. Concave surfaces, as confirmed by the FR and IV methods previously, is found to share the most significant association to slide occurrences.

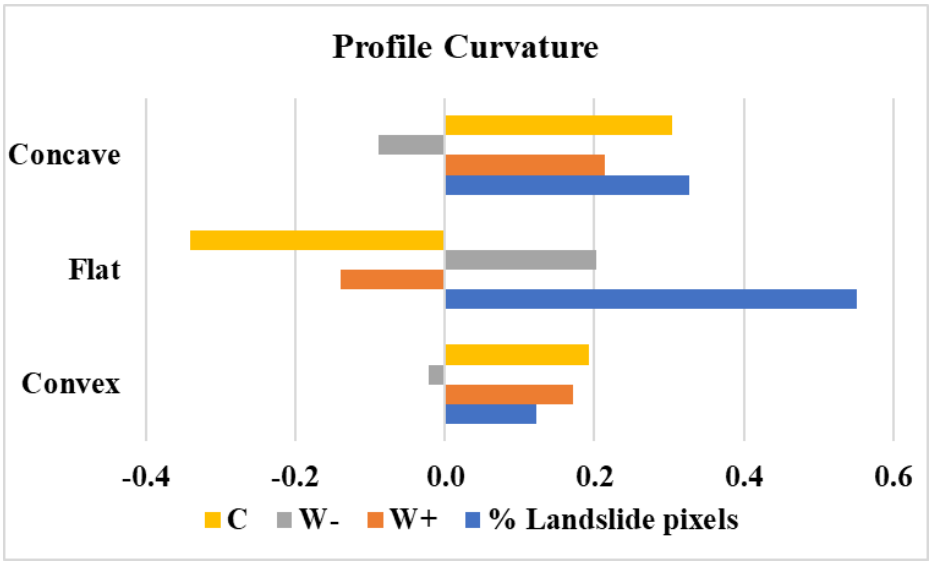

Fig. 5.21 WofE weights variation in curvature factor

5.3.2.4 Effect of elevation

It can be deduced from Fig. 5.22 that only the first elevation class (1,050 - 2,000) showed significant correlation with landslide occurrences with the class having the highest and only positive W^+ and C values compared to the two following classes (2,000 - 3,000 and 3,000 - 4,000) which had increasingly negative W^+ and C values. It is to be noted that the first class also recorded the highest W^- value confirming its strong influence.

The last category had less human intervention and lesser soil cover with snow/glaciers present almost all year round and therefore, was the least affected with zero W^+ value.

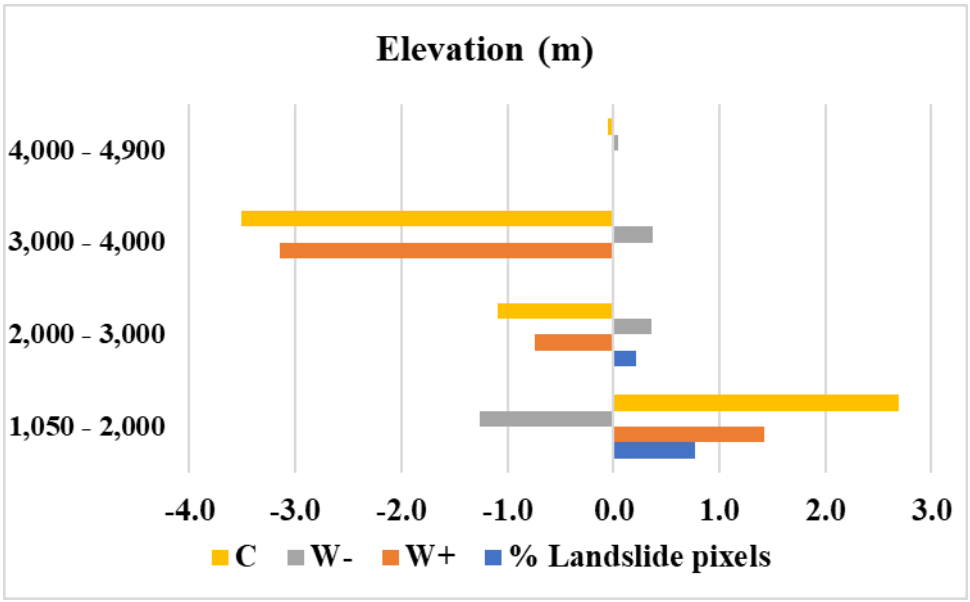

Fig. 5.22 WofE weights variation in elevation factor

5.3.2.5 Effect of distance to drainage

Only the first two categories within a 200m buffer distance from river networks demonstrated correlation to slope instability in the region due to their high contrast (C) values as well as positive weights (W^+), as seen from Fig. 5.23. This relationship between drainage and landslide happenings has been confirmed by several researchers.

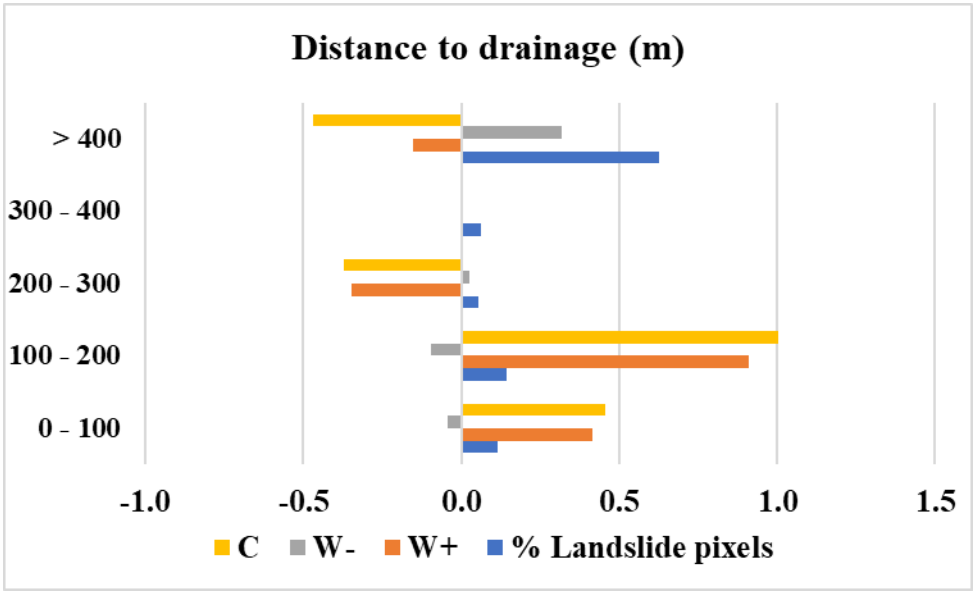

Fig. 5.23 WofE weights variation in distance to drainage factor

5.3.2.6 Effect of distance to roads

For the distance to roads parameter, only the first category was identified as the highest contributor to instability of slope faces in this region with the most positive W^+ and C values. The decreasing weight (W^+) and contrast (C) values in the next two categories signify a decrease in the probability of occurrences as one goes further away from the road networks in the area. The 800 – 1,000 metres category also received positive weights, the reasons behind which could better be explained by other factors in this class.

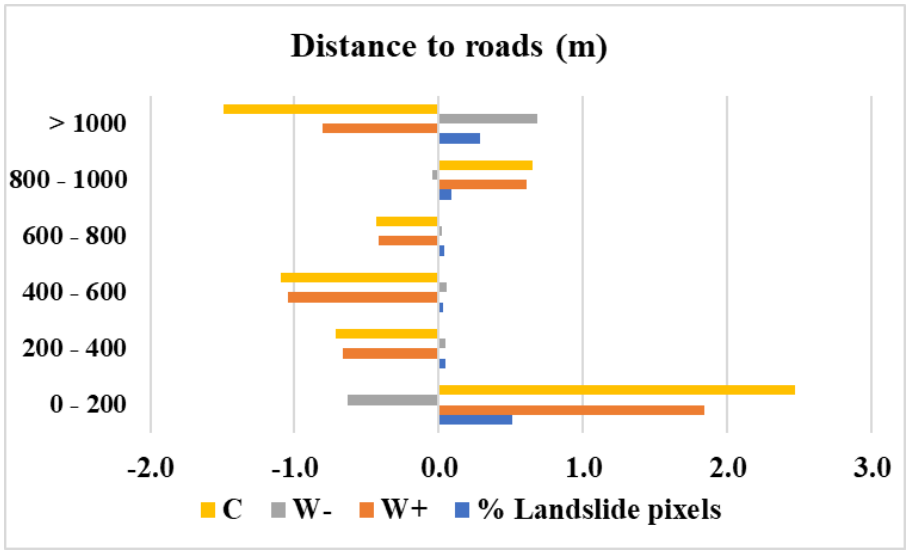

Fig. 5.24 WofE weights variation in distance to roads factor

5.3.2.7 Effect of lithology

The three lithologic groups 'Sillimanite-kyanie bearing schist, quartzite', 'Slate, phyllite, quartzarenite, limestone, metabasics' and 'streaky and banded gneiss' had the highest positive weights (W^+) as well as the highest contrast (C) values.

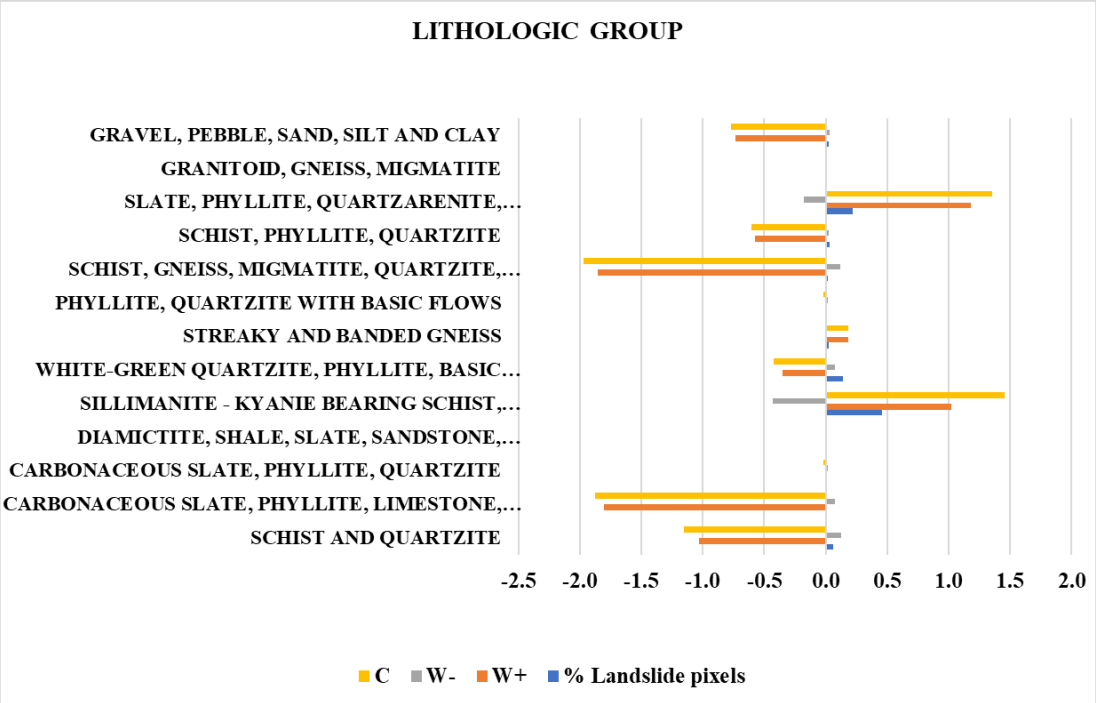

Fig. 5.25 WofE weights variation in lithology factor

The negative W^+ and C values in five categories as seen from Fig. 5.25 (reading from top to bottom; the first, fourth, fifth, eighth, twelfth and thirteenth lithologic groups) depict their contrasting association to slope instability. To conclude, the second, sixth, tenth and eleventh litho-stratigraphic units demonstrated zero correlation, since they had zero W^+ value.

5.3.2.8 Effect of distance to faults/lineaments

As seen from the distance to faults/lineaments WofE weights distribution in Fig. 5.26 below, the closest buffered zone (0 – 200m) as well as the third and fourth ones showed negative contribution in terms of negative weight (W^+) and contrast (C) values. On the opposite hand, the second (200 – 400m) class and the last two classes (800 – 1,000m and > 1,000m) demonstrated positive correlation to slope instability. The last and

largest buffered zone (> 1,000 m) even had the most negative W^- value validating its strong association.

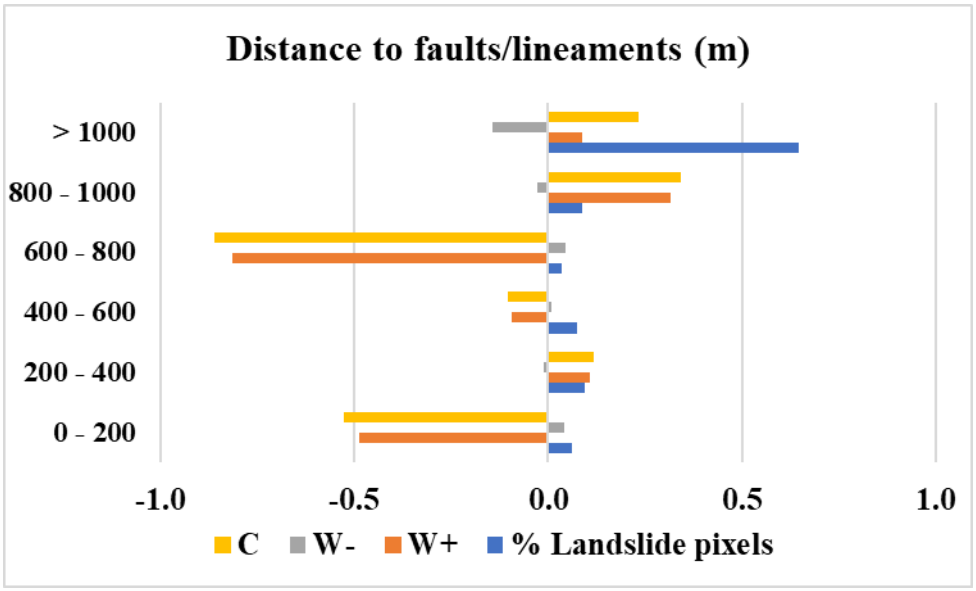

Fig. 5.26 WofE weights variation in distance to faults/lineaments factor

It is to be noted that the same pattern has been previously observed in the FR and IV variation of the same parameter.

5.3.2.9 Effect of land use/land cover

For the purpose of investigating the contribution of the different land use/land cover classes, Fig. 5.27 was consulted. It can be hence observed that the three classes having highest landslide occurrences as well as being the most significant contributors of positive weight (W^+) and contrast (C) values were Agricultural Land/Grass, Water body followed by Built-up area. Besides, the high negative W^- value in the Agricultural Land/Grass category further supplemented its strong association to instability in the area.

Snow/Glaciers and Forested areas had the highest negative contrast (C) values confirming their negative relationship with landslide happenings in the region as observed previously from the results of the FR and IV methods. This contrasting relationship of forested areas was further validated by the noted positive W^- value.

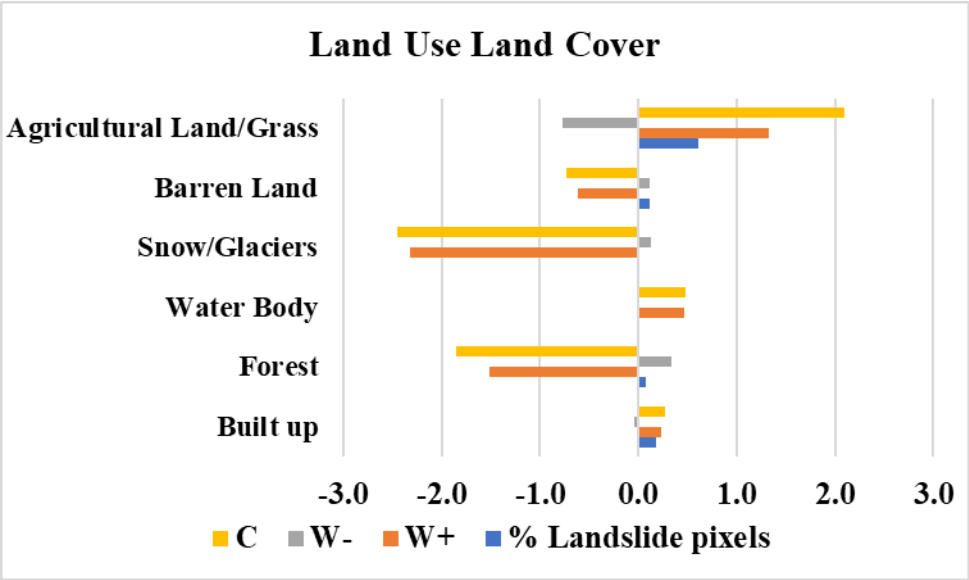

Fig. 5.27 WofE weights variation in land use/land cover factor

5.3.3 Shannon Entropy (SE) results

The factors that had the highest computed weights were Elevation (0.46), Lithologic group (0.39), Distance to roads (0.26) and Land Use/Land Cover (0.22) respectively signifying their strong association to past landslide occurrences in the area.

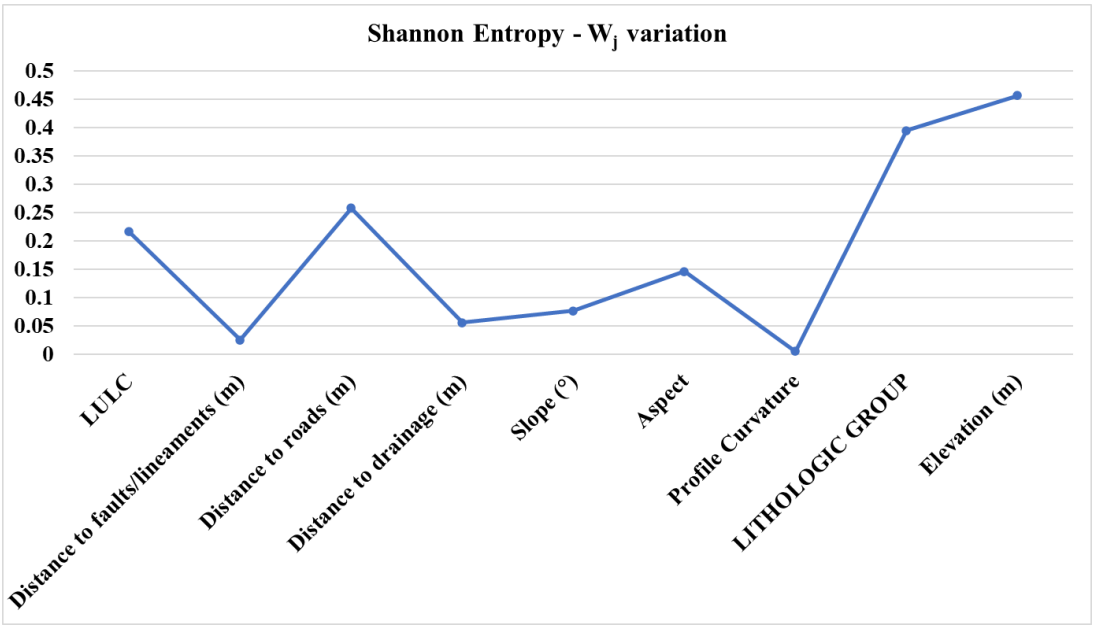

Fig. 5.28 Shannon Entropy (W_j) variation for all parameters

However, Profile curvature and Distance to faults/lineaments gained negligible weights according to Shannon's entropy method results while Slope, Aspect and Distance to drainage factors gained small weights signifying little contribution to slope instability in the area.

CHAPTER 6
LANDSLIDE SUSCEPTIBILITY ANALYSIS: RESULTS AND DISCUSSIONS

6.1 Landslide Susceptibility Map (LSM) Generation and classification

For the generation of the final susceptibility maps for each adopted model, the integration of the nine weighted conditioning factors needs to be carried out. This process involved using the Raster Calculator tool in a GIS environment to overlay the classified thematic maps as per user's requirements to compute Landslide Susceptibility Index (LSI) values, which is then classified into different susceptibility zones for the study. The classification algorithm adopted for the preparation of the final maps was Natural Jenks Break algorithm which was found to have a better representation of the landslide distribution for each susceptibility class.

6.1.1 FR

The weight calculation and interpretation phases are followed by reclassification of each parameter map as per their computed frequency ratio values. Landslide Susceptibility Index (LSI_{FR}) for the FR model was computed as per Equation 6.1 by overlaying the classified parameter maps.

$$LSI_{FR} = \left(FR_{Slope} + FR_{Aspect} + FR_{Curvature} + FR_{LULC} + FR_{Lithology} + FR_{Elevation} + FR_{D_{Road}} + FR_{D_{Drainage}} + FR_{D_{Faults\ /lineaments}}\right) \quad (6.1)$$

This evaluation was carried out through the Raster Calculator tool. The computed LSI_{FR} values were then re-classified into five susceptibility classes (Very Low, Low, Moderate, High and Very High) as shown below in Fig. 6.1. The classification of the LSM has been done using the Natural Jenks Break algorithm, which was found to be the best classification algorithm for this study.

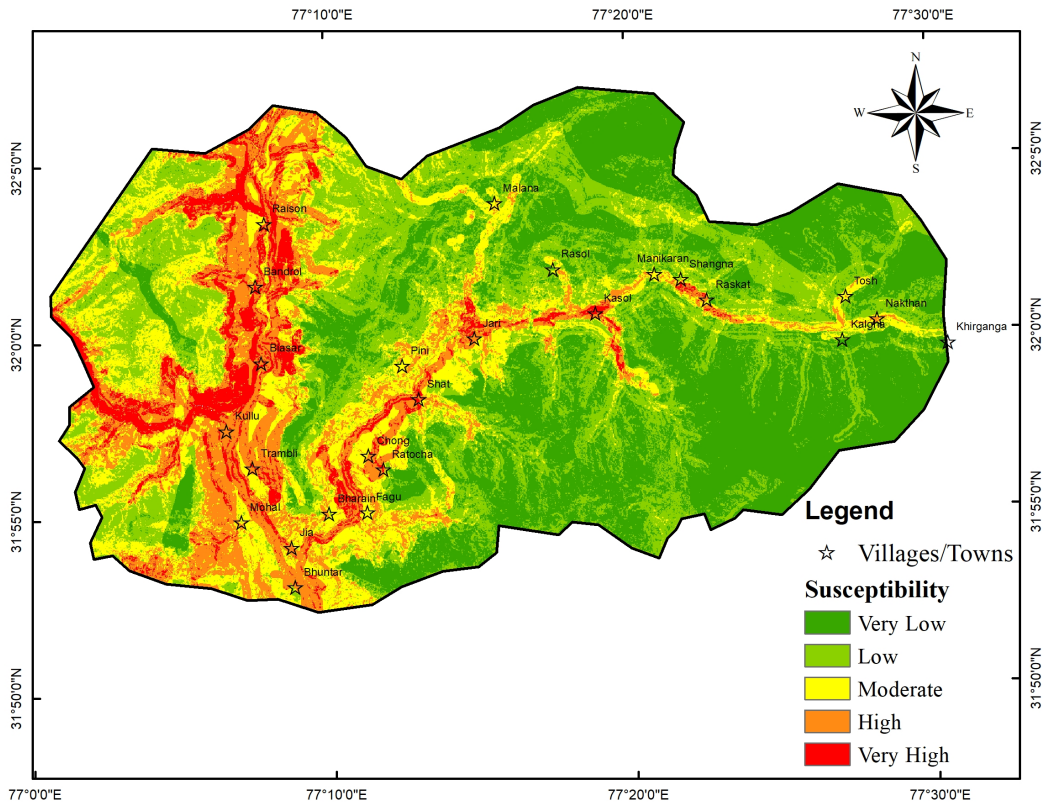

Fig. 6.1 Landslide Susceptibility Map for Frequency Ratio (FR) model

6.1.2 SE

The weights resulting from the SE model were used in combination with the re-classified thematic layers from the FR model for the evaluation of LSI as per Equation 6.2.

$$LSI_{SE} = \left(P_{ij} * W_{Slope} + P_{ij} * W_{Aspect} + P_{ij} * W_{Curvature} + P_{ij} * W_{LULC} + P_{ij} * W_{Lithology} + P_{ij} * W_{Elevation} + P_{ij} * W_{D_{Road}} + P_{ij} * W_{D_{Drainage}} + P_{ij} * W_{D_{Faults\ /lineaments}}\right) \quad (6.2)$$

The resulting Landslide Susceptibility Indexes (LSI_{SE}) were reclassified into five susceptibility classes (Very Low, Low, Moderate, High and Very High) using Natural Jenks Break algorithm as shown in Fig. 6.2.

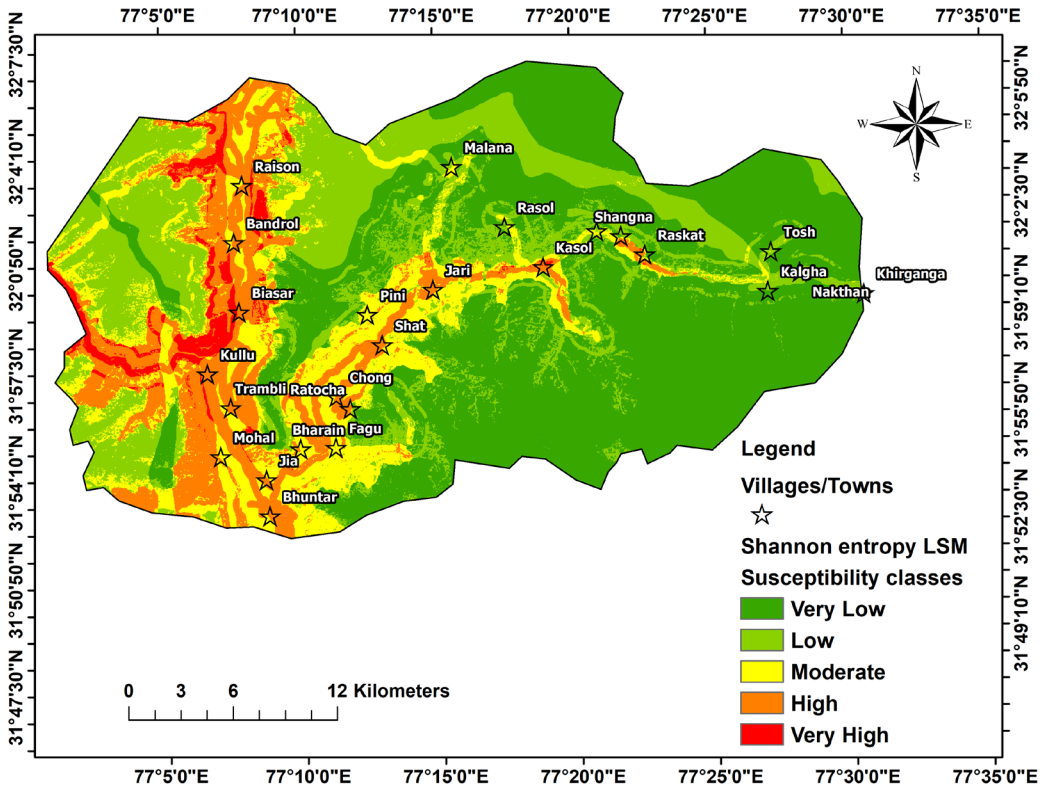

Fig. 6.2 Landslide Susceptibility Map (LSM) for Shannon Entropy (SE) model

6.1.3 IV

The integration of the nine thematic layers reclassified as per their evaluated Information Values was carried out as per Equation 6.3 for the computation of Landslide Susceptibility Indexes (LSI).

$$LSI_{IV} = \left(IV_{Slope} + IV_{Aspect} + IV_{Curvature} + IV_{LULC} + IV_{Lithology} + IV_{Elevation} + IV_{D_{Road}} + IV_{D_{Drainage}} + IV_{D_{Faults\ /lineaments}}\right) \quad (6.3)$$

The final Landslide Susceptibility Map (LSM_{IV}) was prepared by re-classifying the computed susceptibility indexes into five susceptibility classes namely, Very Low, Low, Moderate, High and Very High as shown in Fig. 6.3.

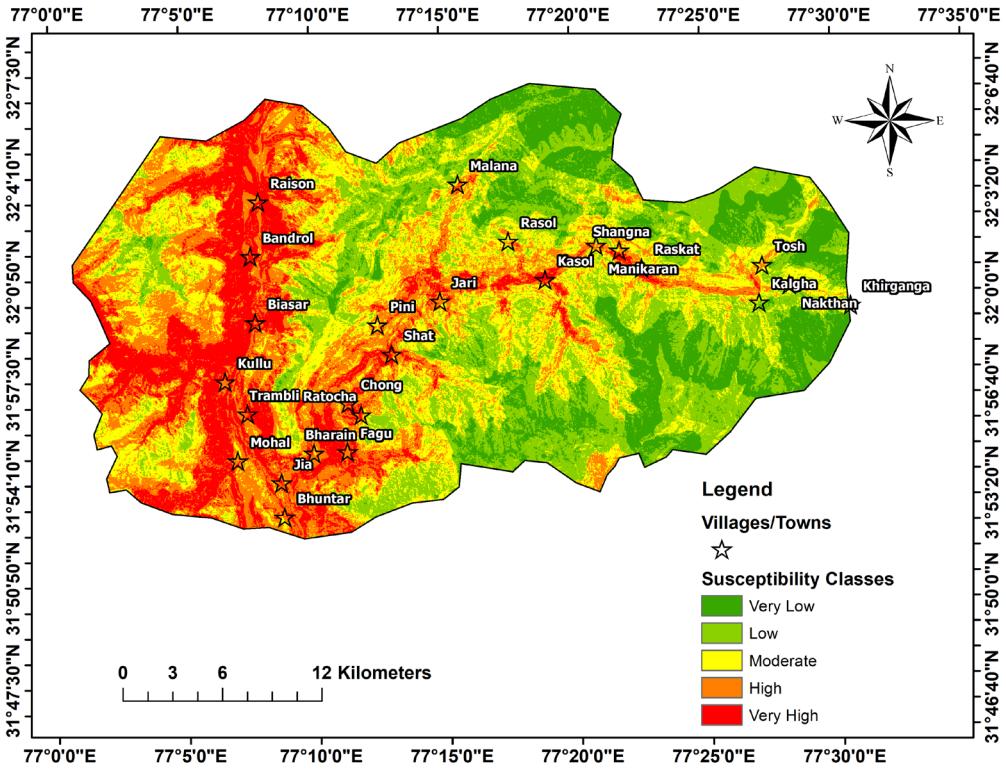

Fig. 6.3 Landslide Susceptibility Map (LSM) for Information Value (IV) model

6.1.4 WofE

After carefully analysing the different weights and contrast values calculated using the WofE approach, the contrast values, C were used to re-classify every class of the nine prepared parameter maps. The final integration was then carried out using Equation 6.4 for the LSI_{WofE} evaluation.

$$LSI_{WofE} = \left(C_{Slope} + C_{Aspect} + C_{Curvature} + C_{LULC} + C_{Lithology} + C_{Elevation} + C_{D_{Road}} + C_{D_{Drainage}} + C_{D_{Faults\ /lineaments}}\right) \quad (6.4)$$

The resulting layer was reclassified using Jenks Break algorithm into five susceptibility classes as depicted below in Fig. 6.4.

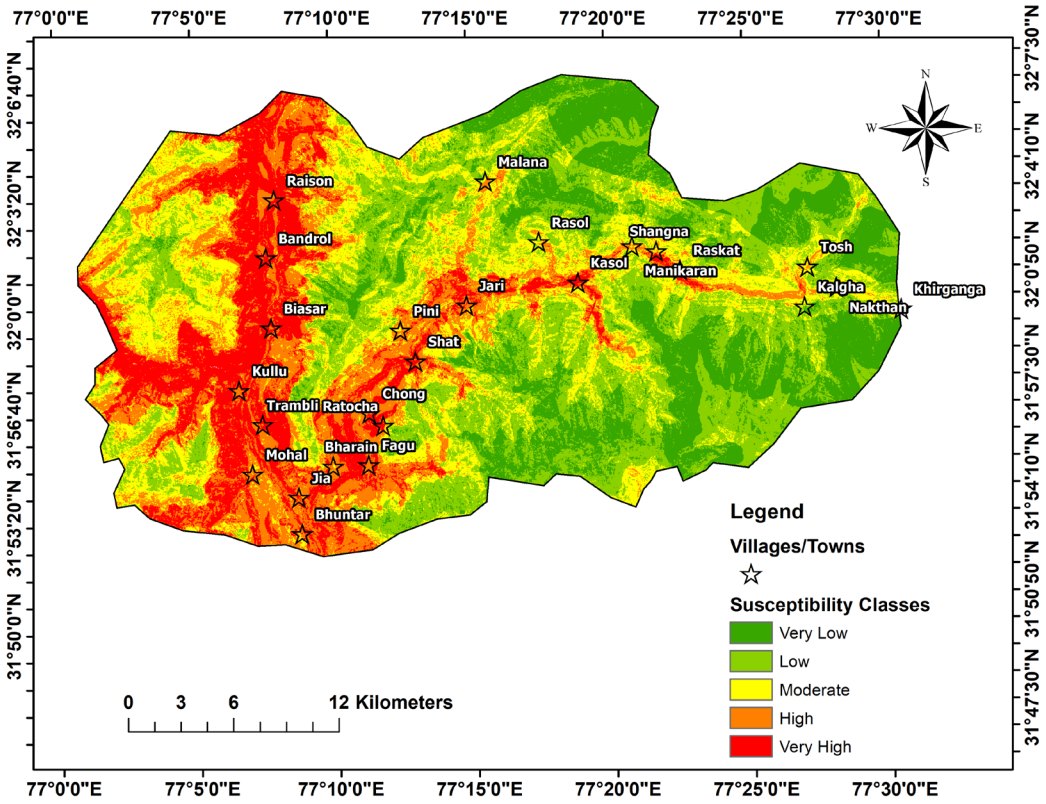

Fig. 6.4 Landslide Susceptibility Map (LSM) for Weight of Evidence (WofE) model

6.2 Validation results

The validation procedure is considered one of the essential constituents of any predictive modelling studies [66], providing scientific significance to the obtained statistical results. Several researchers have developed various validation approaches ranging from simple, straight-forward to complex ones [67].

How the validation results can be interpreted and what they truly assess are the two main concerns of the researcher. For this study, three different approaches have been adopted to carry out this task namely:

- Landslide Density Index (LDI)
- Relative Landslide Density (R) Variation
- Area Under the Curve (AUC) of the Receiver Operator Characteristics (ROC).

For the testing component of this study, the past landslide inventory dataset which was previously randomly sampled into training datasets (75%), used for model

fitness evaluation and testing datasets (25%), used for predictive capability evaluation of the models.

6.2.1 Landslide Density Index (LDI)

The Landslide Density Index (LDI), used to evaluate the quality of the produced landslide susceptibility map [68] is computed for each susceptibility class of every model as per Equation 6.5.

$$LDI = \frac{\%\ landslide\ pixels\ in\ susceptibility\ class}{\%\ class\ pixels\ in\ susceptibility\ class} \tag{6.5}$$

The computed indexes for each class of all four models has been presented in Table 6.1 below.

Table 6.1 Computed LDI values for all models

Models	Susceptibility classes	Class pixels	% Class pixels	Landslide pixels	% Landslide pixels	LDI
FR	Very Low	335136	0.3319	4500	0.0781	0.24
	Low	300859	0.2980	9000	0.1563	0.52
	Moderate	183862	0.1821	6300	0.1094	0.60
	High	136632	0.1353	16200	0.2813	2.08
	Very High	53205	0.0527	21600	0.3750	7.12
SE	Very Low	439917	0.4355	8100	0.0612	0.14
	Low	256934	0.2544	14400	0.1088	0.43
	Moderate	152711	0.1512	16200	0.1224	0.81
	High	136129	0.1348	43200	0.3265	2.42
	Very High	24360	0.0241	50400	0.3810	15.80
IV	Very Low	142075	0.1407	0	0.0000	0.00
	Low	252239	0.2498	2700	0.0204	0.08
	Moderate	253994	0.2515	15300	0.1156	0.46
	High	212441	0.2104	20700	0.1565	0.74
	Very High	149073	0.1476	93600	0.7075	4.79
WofE	Very Low	179612	0.1779	0	0.0000	0.00
	Low	294914	0.2920	9000	0.0680	0.23
	Moderate	229213	0.2270	11700	0.0884	0.39
	High	166412	0.1648	22500	0.1701	1.03
	Very High	139671	0.1383	89100	0.6735	4.87

From Table 6.1, it can be observed that approximately 18% of the study area fall under High to Very High susceptibility zones as per the FR model containing approximately 65% of the past landslides. As for the SE model, 16% of the study area fall under High to Very High susceptibility zones explaining about 70% of the past slides.

The High to Very High susceptibility zones of the final landslide susceptibility map generated through the IV method occupied approximately 17% of the study area containing over about 86% of slides while the two highest susceptible zones of the WofE model received about 84% of past landslides in approximately 30% of the study area.

A clear picture of the variation of the LDI for each model in each susceptible zone can be seen in Fig. 6.5 below.

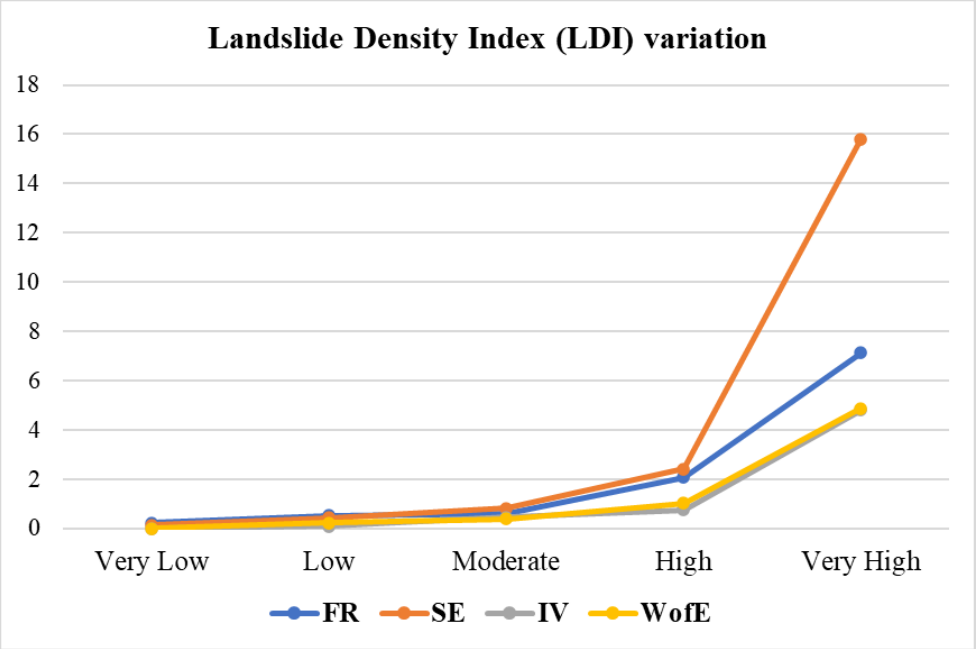

Fig. 6.5 LDI variation for all models

6.2.2 Relative Landslide Density Index (R_{index}) variation

The landslide density indexes computed in the previous section do not give an idea about the ratio of landslide distribution compared to the other susceptibility classes, rather give an idea about the variation of landslide distribution for each class separately.

Another indicative test for the goodness of fit is through the derivation of the Relative landslide density index (R_{index}) [69] as per Equation 6.6.

$$R_{index} = \frac{{n_i}/{N_i}}{\sum {n_i}/{N_i}} \tag{6.6}$$

Where,

n_i = Landslide pixels in each susceptibility class

N_i = Class pixels in each susceptibility class

The computation of R_{index} values for the four adopted probabilistic models has been outlined in Table 6.2.

Table 6.2 Computed R_{index} values for all four models

Models	Susceptibility classes	Class pixels	% Class pixels	Landslide pixels	% Landslide pixels	n_i/N_i	R_{index}
FR	Very Low	335136	0.3319	4500	0.0781	0.01	2.23
	Low	300859	0.2980	9000	0.1563	0.03	4.97
	Moderate	183862	0.1821	6300	0.1094	0.03	5.69
	High	136632	0.1353	16200	0.2813	0.12	19.69
	Very High	53205	0.0527	21600	0.3750	0.41	67.42
SE	Very Low	439917	0.4355	8100	0.0612	0.02	0.72
	Low	256934	0.2544	14400	0.1088	0.06	2.18
	Moderate	152711	0.1512	16200	0.1224	0.11	4.13
	High	136129	0.1348	43200	0.3265	0.32	12.36
	Very High	24360	0.0241	50400	0.3810	2.07	80.60
IV	Very Low	142075	0.1407	0	0.0000	0.00	0.00
	Low	252239	0.2498	2700	0.0204	0.01	1.34
	Moderate	253994	0.2515	15300	0.1156	0.06	7.57
	High	212441	0.2104	20700	0.1565	0.10	12.24
	Very High	149073	0.1476	93600	0.7075	0.63	78.85
WofE	Very Low	179612	0.1779	0	0.0000	0.00	0.00
	Low	294914	0.2920	9000	0.0680	0.03	3.57
	Moderate	229213	0.2270	11700	0.0884	0.05	5.97
	High	166412	0.1648	22500	0.1701	0.14	15.82
	Very High	139671	0.1383	89100	0.6735	0.64	74.64

The variation of R_{index} for all the models can be clearly seen from Fig. 6.6 below.

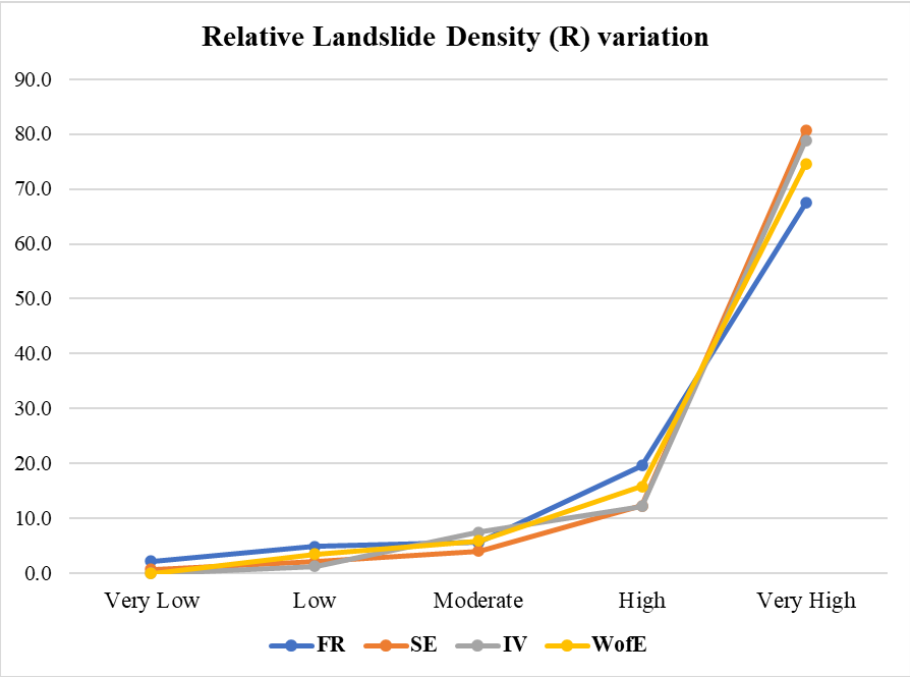

Fig. 6.6 R_{index} variation for all models

The landslide susceptibility map (LSM) for the SE model had the highest R_{index} values for the Very High susceptibility zone (≈81%) followed by the IV (≈79%), WofE (≈75%) and FR (≈68%) models respectively. The combined R_{index} values for the two highest susceptible classes also were highest for the SE model (≈92%) followed by IV (≈91%), WofE (≈90%) and FR (≈87%) models respectively. It can thus be speculated that the Shannon Entropy based LSM had the highest model fitness among the other models from the results of this metric.

6.2.3 Area Under the Curve (AUC) of Receiver Operator Characteristics (ROC) curve

Originally developed for performance evaluation of radar receivers, the Receiver Operator Characteristics (ROC) analysis is a cut-off independent accuracy metric that has been successfully applied to many fields for quality and predictive capability evaluation [26].

The ROC curve is a plot of True Positive Rate (TPR) against False Positive Rate (FPR) determined from Equation 6.7 and 6.8 respectively, and the area under ROC

curve (AUC) is used as a performance evaluation metric with an AUC=1 being a perfect fit and an AUC=0.5 being referred to as a random fit [48].

$$TPR = \frac{True\ Positives\ (TP)}{(TP + False\ Negatives(FN))} \tag{6.7}$$

$$FPR = \frac{True\ Negatives\ (TN)}{(TN + False\ Positives(FP))} \tag{6.8}$$

Where,

TP & TN = pixels correctly classified as slide and not-slide

FP & FN = pixels in-correctly classified as slide and not-slide

For this purpose, the compiled landslide inventory was randomly split into training (75%) and validation (25%) datasets with the former used to generate the Success Rate Curve (SRC) while the latter used to generate the Prediction Rate Curve (PRC).

SRC gives a measure of model fitness between the prepared landslide susceptibility map and the training datasets while the PRC gives an indication of the predictive ability of the model using the validation datasets [66], which was not previously used in the modelling procedure. This is one of the main reasons that many researchers reported higher AUC values obtained by the SRC than the PRC.

The different success rate and prediction rate curves for the four adopted models can be seen in Fig. 6.7 and 6.8 respectively.

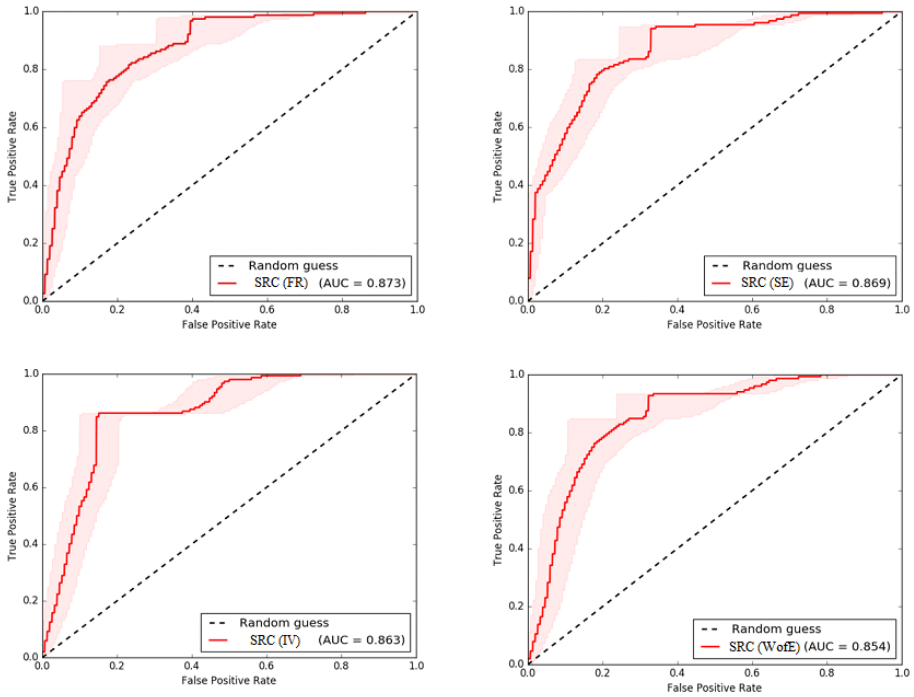

Fig. 6.7 Success rate curves for the FR, SE, IV and WofE models

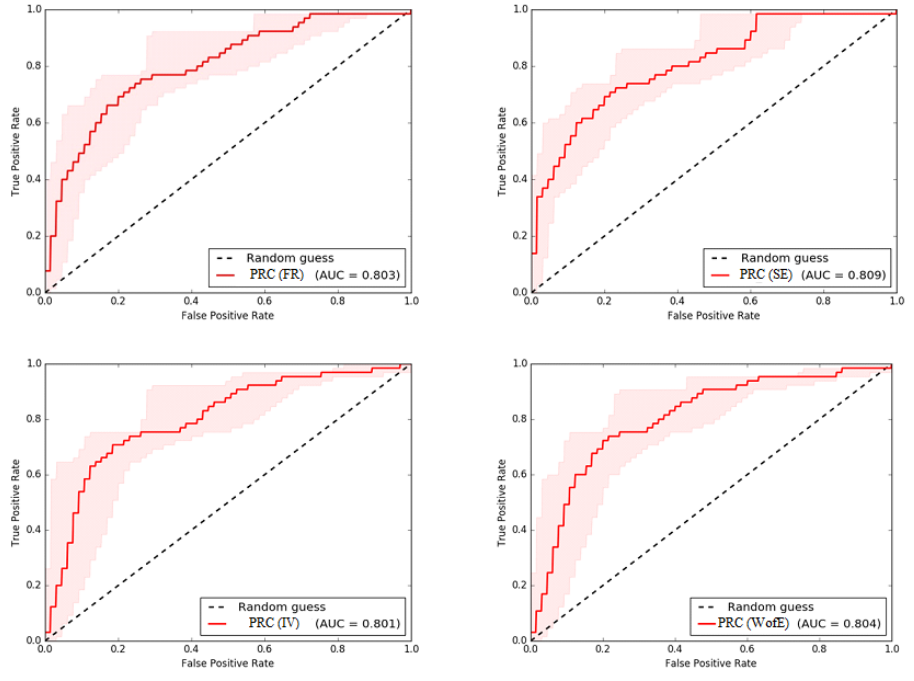

Fig. 6.8 Prediction rate curves for the FR, SE, IV and WofE models

The results from ROC analysis of all the models have been summarised in Table 6.3 below.

Table 6.3 Summary of ROC results for FR, SE, IV and WofE models

Models used in this study	Model fitness (%)	Prediction accuracy (%)
Frequency Ratio (FR)	87.3	80.3
Shannon Entropy (SE)	86.9	80.9
Information Value (IV)	86.3	80.1
Weight of Evidence (WofE)	85.4	80.4

It can be clearly observed that the Frequency Ratio (FR) model depicted the highest model fitness (87.3%) accuracy followed by the Shannon Entropy (86.9%), Information Value (86.3%) and the Weight-of-Evidence (85.4%) models respectively. This high fitness accuracy of the FR approach in hilly and mountainous areas has been noticed by several other researchers.

In case of the prediction accuracy, the prediction rate curve from the Shannon Entropy (SE) model showed highest accuracy (80.9%) followed by Weight-of Evidence (80.4%), Frequency Ratio (80.3%) and the Information Value (80.1%) models respectively.

It can be inferred from the validation results that the Frequency Ratio model had the highest fitness accuracy (87.3%) while the Shannon Entropy model had the highest prediction accuracy (80.9%). However, the results of all the four models were found to be reasonably accurate, thereby, confirming the applicability of probabilistic methods for modelling landslide susceptibility in the study area.

CHAPTER 7
CONCLUSION, LIMITATION AND RECOMMENDATION

This research work has made use of four probabilistic approaches for landslide susceptibility zonation of a portion of the Kullu tehsil in order to find out the most accurate and reliable model for the study area. This chapter outlines the conclusion reached by the researcher along with a listing of some major limitations of the study. This work ends with recommendations made by the author for future scopes of study in the area.

7.1 Conclusion

The main objectives of this research work have been met and the various research questions asked in the beginning have been answered by the author. Landslide susceptibility mapping is one of the most important tools available to disaster experts today to aid in delineating the region's susceptibility to slope failures, and in turn avoiding huge cost of field investigation as well as providing the local authorities with prepared susceptibility maps for better and more detailed landslide management and mitigation works.

Landslides are such complex events that despite much advancement, no 'unique' or 'unified' or 'definite' solution exists. All this progress is being made with the sole purpose of better understanding the mechanisms of slope failures, the different processes linked directly or indirectly to those failures as well as evaluating different methods to more accurate map landslide susceptibility.

This research work has made use of probabilistic methods to map the regions susceptible to landslides in part of the Kullu tehsil of Himachal Pradesh, a region characterised by high rise in tourism and development activities since the past decade. A careful study of literature and articles about the characteristics of the study area and about the methods employed previously, four probabilistic methods were selected for landslide susceptibility evaluation namely, Frequency Ratio (FR), Shannon Entropy (SE),

Information Value (IV) and Weight-of-Evidence (WofE). A comparison between the application of these four models for this study area had not been performed previously.

A total of 47 mapped landslide polygons along with 164 acquired ones constituted the compiled landslide inventory of 211 slide polygons which was then randomly separated into training (75% = 147 nos.) and testing (25% = 64 nos.) datasets.

This work delved into understanding the relevancy and importance of the nine selected causative factors and their classes to landslide occurrences for the area namely, slope, aspect, lithology, land use/land cover, distance to roads, distance to drainage, distance to faults/lineaments, elevation and profile curvature using the four methods. The nine parameters were also selected based on data availability and reliability.

The four landslide susceptibility maps resulting from the four probabilistic models were validated based on their fitness accuracy and predictive capability using different methods. All the four models passed with reasonable fitness accuracy (> 85%) and predictive accuracy (>80%) as per the ROC analysis. However, the Frequency Ratio model depicted highest fitness accuracy (87.3%) and the Shannon Entropy model depicted highest predictive accuracy (80.9%) while the Weight-of-Evidence model had the lowest fitness (85.4%) accuracy, and the Information Value model had the lowest predictive accuracy (80.1%).

The final landslide susceptibility maps were generated based on probabilistic analysis, hence involving very less subjectivity compared to expert-based methods. This concludes that the models developed in this study can be successfully applied to other mountainous regions having similar conditions, bearing in mind their fitness and prediction accuracy as depicted by the validation results of this study.

7.2 Limitations

Some of the limitations outlined in this study are:

- Due to travel restriction/limitation, field visits could not be carried out for detailed geotechnical tests nor for field verification of mapped areas. However, the cost of

geotechnical testing in the hilly and mountainous areas of the Parvati valley would cost a fortune.

- The restriction for higher resolution data is one of the main constraints for this study. LiDAR data could have been the best data for mapping landslide due to their higher resolution compared to other satellite datasets. However, LiDAR-based surveys are expensive to conduct, difficult to acquire and require specialised equipment.
- GIS-based landslide studies rely on association of different factors to landslide occurrences in an area. The more input data available for the model would result in better selection of data for landslide studies. The inaccessibility of the terrain in the area is one of the reasons for lesser availability of accurate data.
- After consultation of temporal landslide studies, the importance of triggering factors such as rainfall and earthquake have been highlighted by several authors. However, this study did not include multi-temporal factors due to unavailability of data.
- This work incorporated only bi-variate statistical approaches for landslide susceptibility analysis. However, landslide are multi-variate complex problems and the inter-relationship between selected factors and landslide occurrences can be evaluated to bring out any inter-dependency or any underlying collinearity.

7.3 Recommendations and future scope of study

Some of the suggestions made by the author have been presented below:

- One of the main components of any landslide susceptibility study is the landslide inventory which is used both for modelling and validation. Hence, an updated landslide inventory is imperative for an accurate representation of the real scenario. This entails building and consolidating a database for recording all local landslide occurrences, even the smallest ones both by local authorities and by local residents.
- As an extension of the methods in practice for landslide susceptibility mapping in the Kullu area, models like the Artificial Neural Network (ANN), Support Vector Machine (SVM), Multiple Logistic Regression and other machine learning

algorithms can be applied to find out the most applicable landslide susceptibility modelling approach.

- Only nine landslide causative factors have been considered in this research work based on data availability. Other researchers may investigate in the effects and relevancy of other causative factors such as the Normalised Difference Vegetation Index (NDVI), Stream Power Index (SPI), Sediment Transport Index (STI), relative relief, soil type, soil depth, agricultural crop patterns, etc. to occurrence of landslides in the study area.
- The usage of better resolution DEM is recommended for better landslide identification and mapping as well as derivation of more accurate DEM-related parameters such as slope, aspect and curvature.
- Multi-temporal aspects such as the effect of rainfall and earthquake intensities on landslide occurrences have not been considered in this study. Multi-temporal landslide inventories can be prepared for better validation purposes as well as accurate representation of landslide distribution for multi-temporal studies.

REFERENCES

[1] K. Terzaghi, “Mechanism of landslides,” in *Application of geology to engineering practice*, Geological Society of America, 1950, pp. 83-123.

[2] D. M. Cruden and D. J. Varnes, “Landslide types and processes,” in *Landslides: Investigation and Mitigation*, Transportation Research Board Special Report, 1996, pp. 36-75.

[3] E. M. Lee and D. K. Jones, Landslide risk assessment, London: Thomas Telford, 2004.

[4] G. G. Wilkinson, “A review of current issues in the integration of GIS and remote sensing data,” *International Journal of Geographical Information Science,* vol. 10, no. 1, pp. 85-101, 1996.

[5] A. Carrara, F. Guzzetti, M. Cardinali and P. Reichenbach, “Use of GIS technology in the predicction and monitoring of landslide hazard,” *Natural hazards,* vol. 20, no. 2, pp. 117-135, 1999.

[6] H. J. Oh, N. W. Park, S. S. Lee and S. Lee, “Extraction of landslide-related factors from ASTER imagery and its application to landslide susceptibility mapping,” *International Journal of Remote Sensing,* vol. 33, no. 10, pp. 3211-3231, 2012.

[7] C. Zhong, Y. Liu, P. Gao, W. Chen, H. Li, Y. Hou, T. Nuremanguli and H. Ma, "Landslide mapping with remote sensing: challenged and opportunities," *International Journal of Remote Sensing,* vol. 41, no. 4, pp. 1555-1581, 2020.

[8] F. Guzzetti, A. C. Mondini, M. Cardinally, F. Fiorucci, M. Santangelo and K. T. Chang, "Landslide inventory maps: New tools for an old problem," *Earth-Science Reviews,* vol. 112, no. 1-2, pp. 42-66, 2012.

[9] M. Cardinali, P. Reichenbach, F. Guzzetti, F. Ardizzone, G. Antonini, M. Galli, M. Cacciano, M. Castellani and P. Salvati, "A geomorphological approach to estimation of landslide hazards and risks in Umbria, Central Italy," *Natural Hazards and Earth System Sciences,* vol. 2, no. 1-2, pp. 57-72, 2002.

[10] J. Gao, "Identification of topographic settings conducive to landsliding from DEM in Nelson County, Virginia, USA," *Earth surface processes and landforms,* vol. 18, no. 7, pp. 579-591, 1993.

[11] A. Mohammadi, H. Shahabi and B. Bin Ahmad, "Integration of insartechnique, google earth images and extensive field survey for landslide inventory in a part of Cameron highlands, Pahang, Malaysia," *Applied Ecology and Environmental Research,* vol. 16, pp. 8075-8091, 2018.

[12] T. R. Martha, C. J. van Westen, N. Kerle, V. Jetten and K. V. Kumar, "Landslide hazard and risk assessment using semi-automatically created landslide inventories," *Geomorphology,* vol. 184, pp. 139-150, 2013.

[13] Y. W. Rabby and Y. Li, “An integrated approach to map landslides in Chittagong Hilly Areas, Bangladesh, using Google Earth and field mapping,” *Landslides,* vol. 16, no. 3, pp. 633-645, 2019.

[14] A. Mohammadi, H. Shahabi and B. Bin Ahmad, “Integration of insartechnique, google earth images and extensive field survey for landslide inventory in a part of Cameron highlands, Pahang, Malaysia,” *Applied Ecology and Environmental Research,* vol. 16, pp. 8075-8091, 2018.

[15] C. Zhao and Z. Lu, “Remote sensing of landslides - A review,” *Remote Sensing,* vol. 10, no. 2, p. 279, 2018.

[16] E. Psomiadis, A. Papazachariou, K. X. Soulis, D. S. Alexiou and I. Charalampopoulous, “Landslide mapping and susceptibility assessment using geospatial analysis and earth observation data,” *Land,* vol. 9, no. 5, p. 133, 2020.

[17] M. D. Bunn, B. A. Leshchinsky, M. J. Olsen and A. Booth, “A simplified, object-based framework for efficient landslide inventorying using LIDAR digital elevation model derivatives,” *Remote Sensing,* vol. 11, no. 3, p. 303, 2019.

[18] “National Landslide RIsk Management Strategy,” National Disaster Management Authority, Government of India, New Delhi, September 2019.

[19] C. J. van Westen, S. Ghosh, P. Jaiswal, T. R. Martha and S. L. Kuriakose, “From landslide inventories to landslide risk assessment; an attempt to support

methodological development in India," *Landslide science and practice,* pp. 3-20, 2013.

[20] "Vulnerability Atlas of India," Building Materials and Technology Promotion Council (BMPTC), 2019.

[21] L. Fayez, D. Pazhman, B. T. Pham, M. B. Dholakia, H. A. Solanki, M. Khalid and I. Prakash, "Application of frequency ratio model for the development of landslide susceptibility mapping at part of Uttarakhand State, India," *International Journal of Applied Engineering Research,* vol. 13, no. 9, pp. 6846-6854, 2018.

[22] S. Lee, "Current and future status of GIS-based landslide susceptibility mapping: a litterature review," *Korean Journal of Remote Sensing,* vol. 35, no. 1, pp. 179-193, 2019.

[23] P. Reichenbach, M. Rossi, B. D. Malamud, M. Mihir and F. Guzzetti, "A review of statistically-based landslide susceptibility models," *Earth-Science Reviews,* vol. 180, pp. 60-91, 2018.

[24] C. J. van Westen, T. W. Van Asch and R. Soeters, "Landslide hazard and risk zonation - why is it too difficult?," *Bulletin of Engineering geology and the Environment,* vol. 65, no. 2, pp. 167-184, 2006.

[25] E. A. C. Abella and C. J. van Westen, "Qualitative landslide susceptibility assessment by multicriteria analysis: a case study from San Antonio del Sur, Guantanamo, Cuba," *Geomorphology,* vol. 94, no. 3-4, pp. 453-466, 2008.

[26] J. Corominas, C. J. van Westen, P. Frattini, L. Cascini, J. P. Malet, S. Fotopoulou, F. Catani, M. Van Den Eeckhaut, O. Mavroulli, F. Agliardi, K. Pitilakis, M. G. Winter, M. Pastor, S. Ferlisi, V. Tofani, J. Hervas and J. T. Smith, "Recommendations for the quantitative analysis of landslide risk," *Bulletin of Engineering geology and Enironment,* vol. 73, no. 2, pp. 209-263, 2014.

[27] S. Panchal and A. K. Shrivastava, "Application of analytic hierarchy process in landslide susceptibility mapping at regional scale in GIS environment," *Journal of Statistics and Management Systems,* vol. 23, no. 2, pp. 199-206, 2020.

[28] S. R. Meena, B. K. Mishra and S. Tavakkoli Piralillou, "A hybrid spatial multi-criteria evaluation method for mapping landslide susceptible areas in kullu valley, himalayas," *Geosciences,* vol. 9, no. 4, p. 156, 2019.

[29] R. Veerappan, A. Negi and A. Siddan, "Landslide susceptibility mapping and comparison using frequency ratio and analytical hierarchy process in part of NH-58, Uttarakhand, India," in *Workshop on World Landslide Forum*, 2017.

[30] S. C. Pal and I. Chowdhuri, "GIS-based spatial prediction of landslide susceptibility using frequency ratio model of Lachung River basin, North Sikkim, India," *SN Applied Sciences,* vol. 1, no. 5, p. 416, 2019.

[31] C. J. F. Chung and A. G. Fabbri, "Probabilistic prediction models for landslide hazard mapping," *Photogrammetric engineering and remote sensing,* vol. 65, no. 12, pp. 1389-1399, 1999.

[32] B. Pradhan, “Landslide susceptibility mapping of a catchment area using frequency ratio, fuzzy logic and multivariate logistic regression approaches,” *Journal of the Indian Society of Remote Sensing,* vol. 38, no. 2, pp. 301-320, 2010.

[33] H. Kaur, S. Gupta and S. Parkash, “Comparative evaluation of various approaches for landslide hazard zoning: a critical review in Indian perspectives,” *Spatial Information Research,* vol. 25, no. 3, pp. 389-398, 2017.

[34] E. R. Sujatha, G. V. Rajamanickam and P. Kumaravel, “Landslide susceptibility analysis using Probabilistic Certainty Factor Approach: A case study on Tevankarai stream watershed, India,” *Journal of earth system science,* vol. 121, no. 5, pp. 1337-1350, 2012.

[35] R. S. Banshtu, L. D. Versain and D. D. Pandey, “Risk assessment using quantative approach: Central Himalaya, Kullu, Himachal Pradesh, India,” *Arabian Journal of Geosciences,* vol. 13, no. 5, pp. 1-11, 2020.

[36] S. Mondal and S. Mandal, “Landslide susceptibility mappin of Darjeeling Himalaya, India using index of entropy (IOE) model,” *Applied Geomatics,* vol. 11, no. 2, pp. 129-146, 2019.

[37] A. Kumar, R. K. Sharma and V. K. Bansal, “GIS-based comparative study of information value and frequency ratio method for landslide hazard zonation in part of mid-Himalaya in Himachal Pradesh,” *Innovative Infrastructure Solutions,* vol. 4, no. 1, pp. 1-17, 2019.

[38] J. S. Gardner, “Natural hazards risk in the Kullu district, Himachal Pradesh,” *Geographical Review,* vol. 92, no. 2, pp. 282-306, 2002.

[39] “Kullu district Ground Water Information Booklet,” Central Ground Water Board, 2013.

[40] G. S. Sidhu and J. N. Surya, “Soils of North-Western Himalayan eco-system and their land use, constraints, productivity potentials and future strategies,” *Agropedology,* vol. 24, no. 1, pp. 1-19, 2014.

[41] S. R. Meena and T. Gudiyangada Nachappa, “Impact of spatial resolution of digital elevation model on landslide susceptibility mapping: A case study in Kullu valley, Himalayas,” *Geosciences,* vol. 9, no. 8, p. 360, 2019.

[42] V. B. Chandel, “Geo-Physical Disasters In Himachal Pradesh, India: A Spatial Perspective,” *International Journal of Multidisciplinary Approach & Studies,* vol. 2, no. 5, 2015.

[43] M. P. Sah and R. K. Mazari, “Anthropogenically accelerated mass movement, Kulu Valley, Himachal Pradesh, India,” *Geomorphology,* vol. 26, no. 1-3, pp. 123-138, 1998.

[44] P. Vaidya, S. K. Bhardwaj and S. Sood, “Land use and land cover changes in Kullu valley of Himachal Pradesh,” *Indian Journal of Agricultural Sciences,* vol. 88, no. 6, pp. 902-906, 2018.

[45] A. S. Prasad, B. W. Pandey, W. Leimgruber and R. M. Kunwar, “Mountain hazard susceptibility and livelihood security in the upper catchment area of the river Beas, Kullu Valley, Himachal Pradesh, India,” *Geoenvironmental Disasters,* vol. 3, no. 1, pp. 1-17, 2016.

[46] B. K. Mishra, D. Bhattacharjee, A. Chattopadhyay and G. Prusty, “Tectonic and lithologic control over landslide activity within the Lajri-Kullu Tectonic Window in the Higher Himalayas of India,” *Natural Hazards,* vol. 92, no. 2, pp. 673-697, 2018.

[47] F. Guzzetti, M. Galli, P. Reichenbach, F. Ardizzone and M. J. N. H. Cardinali, “Probabilistic landslide hazard assessment at the basin scale,” *Geomorphology,* vol. 72, no. 1-4, pp. 272-299, 2005.

[48] E. Nohani, M. Moharrami, S. Sharafi, K. Khosravi, B. Pradhan, B. T. Pham, S. Lee and A. M. Melesse, “Landslide susceptibility mapping using different GIS-based bivariate models,” *Water,* vol. 11, no. 7, p. 1402, 2019.

[49] J. Mathew, V. K. Jha and G. S. Rawat, “Application of binary logistic regression analysis and its validation for landslide susceptibility mapping in part of Garhwal Himalaya, India,” *International Journal of Remote Sensing,* vol. 28, no. 10, pp. 2257-2275, 2007.

[50] S. Lee and J. A. Talib, “Probabilistic landslide susceptibility and factor effect analysis,” *Environmental Geology,* vol. 47, no. 7, pp. 982-990, 2005.

[51] K. C. Devkota, A. D. Regmi, H. R. Pourghasemi, K. Yoshida, B. Pradhan, I. C. Ryu, M. R. Dhital and O. F. Althuwaynee, "Landslide susceptibility mapping using certainty factor, index of entropy and logistic regression models in GIS and their comparison at Mugling–Narayanghat road section in Nepal Himalaya," *Natural hazards,* vol. 65, no. 1, pp. 135-165, 2013.

[52] R. Dikau, "The recognition of landslides," in *Floods and Landslides: Integrated Risk Assessment*, Berlin, Heidelberg, Springer, 1999, pp. 39-44.

[53] A. K. G. and A. K. G., "A GIS and frequency ratio-based landslide susceptibility mapping: Aghnashini river catchment, Uttara Kannada, India," *International journal of geomatics and geosciences,* vol. 1, no. 3, p. 343, 2010.

[54] H. R. Pourghasemi, M. Mohammady and B. Pradhan, "Landslide susceptibility mapping using index of entropy and conditional probability models in GIS: Safarood Basin, Iran.," *Catena,* vol. 97, pp. 71-84, 2012.

[55] P. Singh, A. Sharma, U. Sur and P. K. Rai, "Comparative landslide susceptibility assessment using statistical information value and index of entropy model in Bhanupali-Beri region, Himachal Pradesh, India," *Environment, Development and Sustainability,* vol. 23, no. 4, pp. 5233-5250, 2021.

[56] A. Haghizadeh, S. Siahkamari, A. H. Haghiabi and O. Rahmati, "Forecasting flood-prone areas using Shannon's entropy model," *Journal of Earth System Science,* vol. 126, no. 3, p. 39, 2017.

[57] L. D. Versain, "Bi-variate Statistical Approach in Landslide Hazard Zonation: Central Himalayas of Himachal Pradesh, India," *International Journal of Applied Engineering Research,* vol. 14, no. 2, pp. 415-428, 2019.

[58] S. Sharma and A. K. Mahajan, "A comparative assessment of information value, frequency ratio and analytical hierarchy process models for landslide susceptibility mapping of a Himaloayan watershed, India," *Bulletin of Engineering Geology and the Environment,* vol. 78, no. 4, pp. 2431-2448, 2019.

[59] M. Shafapour Tehrany, L. Kumar, M. Neamah Jebur and F. Shabani, "Evaluating the application of the statistical index method in flood susceptibility mapping and its comparison with frequency ratio and logistic refression methods," *Geomatics,* vol. 10, no. 1, pp. 79-101, 2019.

[60] G. F. Bonham-Carter, F. P. Agterberg and D. F. Wright, "Integration of geological datasets for gold exploration in Nova Scotia," *Photogrammetric Engineering and Remote Sensing,* vol. 54, no. 11, pp. 1585-1592, 1988.

[61] F. P. Agterberg, G. F. Bonham-Carter, Q. Cheng and D. F. Wright, "Weights of evidence modelling and weighted logistic regression for mineral potential mapping," in *Computers in geology---25 years of progress*, USA, Oxford University Press, Inc., 1993, pp. 13-32.

[62] T. Mezughi, J. M. Akhir, A. G. Rafek and I. Abdullah, "A multi-class weight of evidence approach for landslide susceptibility mapping applied to an area along the EW Highway (Gerik-Jeli), Malaysia," *Electronic Journal of Geotechnical Engineering,* vol. 16, pp. 1259-1273, 2011.

[63] A. Gadtaula and S. Dhakal, “Landslide susceptibility mapping using Weight of Evidence Method in Haku, Rasuwa District, Nepal,” *Journal of Nepal Geological Society,* vol. 58, pp. 163-171, 2019.

[64] E. J. M. Carranza, “Weights of evidence modeling of mineral potential: a case study using small number of prospects, Abra, Philippines,” *Natural Resources Research,* vol. 13, no. 3, pp. 173-187, 2004.

[65] S. Lee, J. Choi and K. Min, “Landslide susceptibility analysis and verification using the Bayesian probability model,” *Environmental Geology,* vol. 43, no. 1-2, pp. 120-131, 2002.

[66] C. J. F. Chung and A. G. Fabbri, “Validation of spatial prediction models for landslide hazard mapping,” *Natural Hazards,* vol. 30, no. 3, pp. 451-472, 2003.

[67] X. Deng, L. Li and Y. Tan, “Validation of spatial prediction models for landslide susceptibility mapping by considering structural similarity,” *ISPRS International Journal of Geo-Information,* vol. 6, no. 4, p. 103, 2017.

[68] S. Sarkar and D. P. Kanungo, “An integrated approach for landslide susceptibility mapping using remote sensing and GIS,” *Photogrammetric Engineering & Remote Sensing,* vol. 70, no. 5, pp. 617-625, 2004.

[69] N. Santacana, B. Baeza, J. Corominas, A. De Paz and J. Marturia, “A GIS-based multivariate statistical analysis for shallow landslide susceptibility mapping in La

Pobla de Lillet area (Eastern Pyrenees, Spain),” *Natural hazards,* vol. 30, no. 3, pp. 281-295, 2003.